DISSERTATIONS IN
FORESTRY AND
NATURAL SCIENCES

Antti Aula né Kallioniemi

Computed Tomography and Ultrasound Methods for Simultaneous Evaluation of Articular Cartilage and Subchondral Bone

Publications of the University of Eastern Finland
Dissertations in Forestry and Natural Sciences

UNIVERSITY OF
EASTERN FINLAND

ANTTI AULA NÉ KALLIONIEMI

Computed Tomography and Ultrasound Methods for Simultaneous Evaluation of Articular Cartilage and Subchondral Bone

Publications of the University of Eastern Finland
Dissertations in Forestry and Natural Sciences
No 27

Academic Dissertation
To be presented by permission of the Faculty of Science and Forestry for public examination in the Auditorium L22 in Snellmania Building at the University of Eastern Finland, Kuopio, on March, 18, 2011,
at 12 o'clock noon.

Department of Applied Physics

Kopijyvä
Kuopio, 2011
Editors: Prof. Pertti Pasanen
Ph.D. Sinikka Parkkinen, Prof. Kai-Erik Peiponen

Distribution:
University of Eastern Finland Library / Sales of publications
P.O. Box 107, FI-80101 Joensuu, Finland
tel. +358-50-3058396
http://www.uef.fi/kirjasto

ISBN: 978-952-61-0366-2 (Print)
ISSNL: 1798-5668
ISSN: 1798-5668

ISBN: 978-952-61-0367-9 (PDF)
ISSNL: 1798-5668
ISSN: 1798-5676

Author's address: University of Eastern Finland
Department of Applied Physics
P.O.Box 1627
70211 KUOPIO
FINLAND
email: antti.aula@uef.fi

Supervisors: Professor Jukka Jurvelin, Ph.D.
University of Eastern Finland
Department of Applied Physics
P.O.Box 1627
70211 KUOPIO
FINLAND
email: jukka.jurvelin@uef.fi

Professor Juha Töyräs, Ph.D.
University of Eastern Finland
Department of Applied Physics
P.O.Box 1627
70211 KUOPIO
FINLAND
email: juha.toyras@uef.fi

Reviewers: Associate Professor Marc Levenston, Ph.D.
Stanford University
Soft Tissue Biomechanics Laboratory
Stanford, CA, U.S.A.
email: levenston@stanford.edu

Patrick H.F. Nicholson, Ph.D.
University of Jyväskylä
Department of Health Sciences
Jyväskylä, Finland
email: patrick_nicholson@hotmail.com

Opponent: Professor Harrie Weinans, Ph.D.
Erasmus MC
Orthopaedic Research Laboratory
Rotterdam, The Netherlands
email: h.weinans@erasmusmc.nl

ABSTRACT

Current diagnostic techniques are not able to detect the earliest degenerative changes related to osteoarthritis and osteoporosis. Quantitative ultrasound (QUS) and contrast agent enhanced computed tomography (CECT) are potential techniques for the simultaneous assessment of the health of cartilage and bone.

The ability of gadolinium and iodine-based contrast agents to detect enzymatic cartilage degradation was evaluated in this study. Moreover, the optimal contrast agent concentrations and diffusion times were estimated. The feasibility of using CECT and QUS (5 MHz) methods for the simultaneous measurement of articular cartilage and subchondral bone was tested with osteochondral samples from visually healthy bovine knees. Furthermore, the effect of bone marrow composition on ultrasound propagation was studied numerically at 1 MHz frequency.

The CECT technique enabled simultaneous analysis of the contrast agent content in cartilage, bone mineral density and thicknesses of cartilage and subchondral plate. The contrast agent intake increased significantly after enzymatic (trypsin) degradation of cartilage. However, there were no major changes in the contrast agent partition profiles. The contrast agent content in the superficial cartilage correlated significantly with the dynamic modulus of cartilage. Both contrast agents required over 8 hours to reach the diffusion equilibrium. QUS was found to be feasible for the simultaneous measurement of the acoustic properties of articular cartilage and subchondral bone. The relationships between the ultrasound parameters and the properties of cartilage and bone were statistically significant. Numerical simulations demonstrated a significant effect of bone marrow composition on the QUS parameters, especially for samples with low bone volume fractions.

In conclusion, when further developed, the CECT and QUS methods may become sensitive quantitative *in vivo* methods to simultaneously assess the status of articular cartilage and subchondral bone.

PACS Classification: 43.35.+d, 87.57.Q-, 87.63.D-, 87.85.Pq

National Library of Medicine Classification: QT 34, QT 36, WE 200, WE 250, WE 300, WE 348, WN 206, WN 208

Medical Subject Headings: Bone and Bones; Bone Density; Cartilage, Articular; Osteoarthritis/diagnosis; Osteoporosis/diagnosis; Bone Marrow; Tomography, X-Ray Computed; Contrast Media; Gadolinium; Iodine; Ultrasonography; Ultrasonics; Computer Simulation

Yleinen suomalainen asiasanasto: luu; luuntiheys; rusto - - nivelet; nivelrikko - - diagnoosi; osteoporoosi - - diagnoosi; luuydin; tietokonetomografia; ultraäänitutkimus; simulointi; numeeriset menetelmät

To my dearest
Hanna, Niilo and Olivia

Acknowledgments

This study was carried out during the years 2005-2010 in the Department of Applied Physics, University of Eastern Finland.

To begin with, I would like to express my gratitude to the supervisors of my thesis for their guidance during the thesis work and for sharing their expertise. I am grateful to my principal supervisor, Professor Jukka Jurvelin, Ph.D., for giving me the privilege to work in his inspiring and renowned research group, Biophysics of Bone and Cartilage. His devotion to science and ability to find hope in the most desperate situations are truly amazing. I thank my second supervisor, Professor Juha Töyräs, Ph.D., for encouragement and for sharing his endless supply of ideas and overwhelming enthusiasm towards science.

I would like to thank the official reviewers of this thesis, Associate Professor Marc Levenston, Ph.D. and Dr. Patrick H.F. Nicholson, Ph.D., for their constructive criticism and expert comments. I am grateful to Ewen MacDonald, D.Pharm., for the linguistic review.

I acknowledge my other co-authors, Professor Miika Nieminen, Ph.D., Professor Mikko Lammi, Ph.D., Adjunct Professor Mikko Hakulinen, Ph.D. and Assistant Professor Virpi Tiitu, Ph.D. for their contributions during the measurements and the preparation of the manuscripts.

It has been an honor to work with the intelligent and spirited people working in or collaborating with our research group. The cheerful atmosphere and friendly hard working people have helped me finish the thesis. Particularly, I would like to thank Mikko Nissi, Petro Julkunen, Eveliina Lammentausta, Heikki Nieminen and Ossi Riekkinen for introducing me to the fascinating world of bone and cartilage and the related methodology. Moreover, I wish to thank Janne Karjalainen and Erna Kaleva, not only for the profound discussions concerning science and life in general, but also for their in-

valuable friendship and moments outside the working hours. The present and past members of our research group and other people with whom I have worked with deserve my gratitude. It has truly been an honor.

I would like to thank the staff of the Department of Applied Physics, Institute of Biomedicine, Anatomy and the BioMater Centre, for their efforts and help during this thesis project.

This thesis work was financially supported by the Emil Aaltonen Foundation, Finnish Cultural Foundation, Finnish Foundation for Technology Promotion, Finnish Ministry of Education, Finnish Funding Agency for Technology and Innovation (Tekes 70015/05), Kuopio University Hospital (EVO grants 5041715, 5231 and 5221), Academy of Finland (grant 205886) and National Graduate School of Musculoskeletal Disorders and Biomaterials. Atria Lihakunta Oyj, Kuopio, is acknowledged for providing the bovine joints necessary for this study.

I would like to thank all the friends and relatives who have believed in me, supported me and kept my feet on the ground. Especially I would like to thank my parents, Tuulikki and Jaakko Kallioniemi for encouraging me in my studies and supporting my choices throughout my life.

Finally, I would like to express my deepest gratitude to my wife Hanna for her endless love and understanding, and our two little miracles, Niilo and Olivia, for bringing a smile on my face even in the direst moments.

Kuopio, 10th February 2011

Antti Aula

ABBREVIATIONS

3D	three-dimensional
A/D	analog to digital
A-mode	one-dimensional amplitude representation of a reflected ultrasound wave
CCD	charge-coupled device
CECT	contrast agent enhanced computed tomography
CT	computed tomography
dGEMRIC	delayed gadolinium-enhanced magnetic resonance imaging of cartilage
DNA	deoxyribonucleic acid
DXA	dual-energy X-ray absorptiometry
ECM	extracellular matrix
FCD	fixed charge density
FD	finite difference
FDA	Food and Drug Administration
FDM	finite difference method
FDTD	finite difference time domain
FEM	finite element method
GAG	glycosaminoglycan
Gd-DTPA^{2-}	gadolinium diethylenetriamine pentaacetic acid, gadopentetate
Hypro	hydroxyproline
IVUS	intravascular ultrasound
microCT	X-ray microtomography
MRI	magnetic resonance imaging
OA	osteoarthrosis, osteoarthritis
OP	osteoporosis
PBS	phosphate-buffered saline
PE	pulse-echo
PG	proteoglycan
pQCT	peripheral quantitative computed tomography
QCT	quantitative computed tomography
QUS	quantitative ultrasound
TT	through-transmission
UA	uronic acid
US	ultrasound

SYMBOLS AND NOTATIONS

$A(f)$	amplitude spectrum
AA	average attenuation
AIB	apparent integrated backscatter
$\alpha(f)$	frequency-dependent ultrasound attenuation coefficient
BMD	bone mineral density
BS	bone surface area
BS/BV	bone-specific surface
BUA	broadband ultrasound attenuation
BUB	broadband ultrasound backscatter
BV	bone volume
BV/TV	bone volume fraction
c	speed of sound
C	concentration
d	diameter or distance between US transducer and sample
D	diffusion coefficient
DA	degree of anisotropy
Δf	frequency range
$\Delta f(x)$	forward difference form
$\nabla f(x)$	backward difference form
$\delta f(x)$	central difference form
E_{Young}	Young's (elastic) modulus
E_{Dyn}	dynamic (elastic) modulus
f	frequency
F	Faraday's constant
ϕ	bulk viscosity or concentration
h	depth
η	shear viscosity
i	imaginary unit
I	intensity of the ultrasound signal
IRC	integrated reflection coefficient
J	diffusion flux
k	wave number
λ	wavelength or the first Lamé constant
m	number of A-mode ultrasound signals
μ	linear attenuation coefficient or the second Lamé constant

n	number of samples or datapoints
$nBUA$	normalized broadband ultrasound attenuation
ν	Poisson's ratio
ω	angular temporal frequency
p	statistical significance
r	correlation coefficient
R	reflection coefficient or the gas law constant
SMI	structural model index
ρ	density
SOS	speed of sound
t	time
T	refraction coefficient or absolute temperature
$Tb.N$	trabecular number
$Tb.Sp$	trabecular separation
$Tb.Th$	trabecular thickness
TV	total sample volume
θ_i	angle of incidence
θ_r	angle of refraction
u	particle displacement
URI	ultrasound roughness index
x	distance or thickness
ψ	membrane potential
z	valence of an ion
Z	acoustic impedance
$\langle \cdots \rangle$	spatial average
$\lvert \cdots \rvert$	absolute value
$[\cdots]$	concentration
∂	partial difference operator
∇	gradient operator
$\nabla \cdot$	divergence operator

LIST OF PUBLICATIONS

This thesis consists of the present review of the author's work in the field of medical physics and the following selection of the author's publications referred to in the text by their Roman numerals:

I Kallioniemi A. S., Jurvelin J. S., Nieminen M. T., Lammi M. J. and Töyräs J.: Contrast agent enhanced pQCT of articular cartilage, *Physics in Medicine and Biology*, 52(4):1209-1219 (2007).

II Aula A. S., Jurvelin J. S. and Töyräs J.: Simultaneous computed tomography of articular cartilage and subchondral bone, *Osteoarthritis and Cartilage*, 17(12):1583-1588 (2009).

III Aula A. S., Töyräs J., Hakulinen M. A. and Jurvelin J. S.: Effect of bone marrow on acoustic properties of trabecular bone - 3D finite difference modeling study, *Ultrasound in Medicine and Biology*, 35(2):308-318 (2009).

IV Aula A. S., Töyräs J., Tiitu V. and Jurvelin J. S.: Simultaneous ultrasound measurement of articular cartilage and subchondral bone, *Osteoarthritis and Cartilage*, 18(12):1570-1576 (2010).

 The author of this thesis is the principal author in all of the above mentioned papers. The thesis also includes previously unpublished data.

Contents

1 Introduction

Articular cartilage is highly specialized connective tissue covering the ends of bones in diarthrodial joints. Good health of articular cartilage is essential for normal function of the joint, because it is a major contributor to the distribution of forces and the low friction movement of articulating bones during joint loading. The complex mechanical behavior of articular cartilage is a result of specialized composition and structural organization. Under the articular cartilage, there is a layer of solid cortical bone, *i.e.* subchondral plate, and beneath it is subchondral trabecular bone. In general, bones provide mechanical support and transform muscle contractions into bodily motions. Trabecular bone can be found, for example, at the ends of long bones. It forms a complex three-dimensional network that constantly adapts itself to optimally endure the stresses to which it is exposed. Trabecular bone aims to maximize mechanical strength with minimal weight.

Osteoarthritis, also known as osteoarthrosis, (OA) is the most common degenerative joint disease. It disturbs normal functionality of the joint, causes pain, makes daily activities more difficult and impairs the overall quality of life. OA is also a major economic burden to society as it decreases the working ability of individuals and is responsible for considerable medical and social costs [32, 77, 93, 228]. OA is associated with joint injuries, excessive loading, obesity and aging [181,194]. In cartilage, OA leads to a progressive disruption of collagen network, depletion of proteoglycans and an increase in the water content [7, 31, 185]. Subchondral sclerosis and osteophyte formation are known to occur simultaneously with the cartilage degeneration [32]. In subchondral bone, the number of trabeculae decreases but the remaining ones thicken and the overall bone volume fraction increases [24, 60]. Early degenerative changes in cartilage impair its mechanical properties and accelerate the deterioration of the tissue. Typical symptoms of OA, for

example pain, limited mobility and deformity of the joint, appear during the late stages of the disease when cartilage can be almost completely worn out [29].

Traditional diagnostic techniques, such as radiography, magnetic resonance imaging (MRI) and arthroscopy, are able to detect OA when it has reached its late stage, *i.e.* when spontaneous regeneration of the tissue is no longer possible. At present, there is no cure for OA and it is impossible to restore degenerated tissue to its original state. Even though they cause no symptoms, detection of early changes would be essential if one wished to make a possible intervention and would help in understanding the disease. These early changes include, for example, PG loss, surface fibrillation and local cartilage injuries. Moreover, sensitive quantitative techniques will be needed for the investigation of the efficacy of new drugs and treatments [222].

Osteoporosis (OP) is the most common metabolic bone disease in the developed countries [273]. In OP, the bone mineral density (BMD) decreases and the microstructure of bone tissue deteriorates. These changes lead to brittle bones and increased fracture risk [134]. OP is also an important disease in a socio-economic sense, because it increases the risk of fractures and chronic disability [46]. Conventionally, OP is diagnosed as reduced BMD, as measured with dual energy X-ray absorptiometry (DXA). The risk of fracture, however, is not only related to bone density, but also to the internal structure and organic composition of bone [34, 214, 269]. It is important to notice that the bone is not the only determinant of fracture risk. For example, the type of fall, the surface on which the fall occurs and the amount of overlying soft tissue significantly affect the risk of fracture [269].

Advances in imaging modalities like MRI, computed tomography (CT) and ultrasound (US) have triggered the development of new quantitative methods for early detection of OA. Most of these techniques are still at the pre-clinical stage, but are being continually developed toward clinical approval. In principle, All three modalities allow simultaneous analysis of articular cartilage and

subchondral bone, which might provide additional diagnostic information about the health of the joint and allow detection of OA at an early stage. MRI and CT methods may be enhanced by the use of ionic contrast agents that are hypothesized to diffuse into the cartilage depending on the fixed negative charge attributable to proteoglycan (PG) distribution [17,35,50,213,219,242]. Contrast agent enhanced computed tomography (CECT) of cartilage was introduced by Cockman *et al.* (2006), but Palmer *et al.* (2006) were the first to use an iodine-based ionic contrast agent in CECT of articular cartilage. Study I of this thesis was the first attempt to investigate the suitability of a clinical CT device for CECT imaging of articular cartilage degradation.

Ultrasound reflection from cartilage surface has been reported to detect changes due to OA, maturation, enzymatical degradation and spontaneous healing of cartilage [44,154,232]. Furthermore, the backscattered signal from the internal cartilage structures has been postulated to relate to the integrity of the tissue [217,265,271]. Recently, arthroscopic ultrasound imaging of cartilage was proposed as a novel tool for detection of articular cartilage injury and signs of early OA [103,145,266].

Quantitative ultrasound (QUS), CT and MRI methods have also been applied for detection of the properties of calcified tissues. Ultrasound speed, attenuation, reflection and backscatter are related to the structure, density, composition and mechanical properties of bone [39,96,110,112,137,158,224]. CT enables measurement of the mineral density, bone volume fraction as well as three-dimensional structure of the tissue. Though the MRI signal from the bone is very weak, the signal from bone marrow is strong and can, in principle, be utilized for estimation of bone mineral density, volume fraction and trabecular structure [47,133,157]. Clinical CT and MRI devices, however, lack the resolution to reveal the microstructure of the trabecular matrix [121,156,157], which is a significant contributor to the mechanical properties and fracture risk of the bone [108,214].

The present thesis introduces three studies which aim to investigate and improve the potential of CT and US methods in diag-

nostics of OA. The fourth study addresses the effect of bone marrow composition on the propagation of US in trabecular bone, a problem which affects not only US diagnostics of OP but also the simultaneous measurement of articular cartilage and subchondral bone. In study I, two anionic contrast agents are compared, and the effect of enzymatic cartilage degradation on the distributions of the contrast agents is examined. In studies II and III, the feasibility of using CECT and US methods for the simultaneous measurement of articular cartilage and subchondral bone is assessed. The composition and mechanical properties of the tissues are measured with state-of-the-art reference techniques and compared with the CECT and US results. The studies also consider possible sources of error related to the clinical use of the methods. Taken together, this thesis aims to develop and refine the CECT and US techniques for simultaneous measurements of articular cartilage and subchondral bone.

2 Articular cartilage and subchondral bone

Articular cartilage is a highly specialized aneural and avascular connective tissue which covers the ends of articulating bones in the diarthrodial joints [31]. The inner surface of a joint capsule is covered by synovium, which excretes synovial fluid [74]. Articular cartilage, together with synovial fluid, provides nearly frictionless, wear resistant sliding surfaces for articulating bones [189]. In a knee joint, articular cartilage, menisci and subchondral bone together absorb and distribute mechanical loads and enable smooth locomotion [3, 223]. These three tissues have a trinitarian relationship where changes in one tissue lead to adaptive changes in the other two tissues [209].

2.1 ARTICULAR CARTILAGE

Articular cartilage can be divided into fluid and solid phases. The fluid phase, interstitial water, makes up 65 - 80% of the total mass of the tissue and contains solutes such as ions and nutrients. The solid phase comprises the remaining 20-35% of the total mass and consists mainly of collagen fibrils, proteoglycans and chondrocytes (Figure 2.1). The solid matrix outside the cells is called the extracellular matrix (ECM). The pore size and density of articular cartilage have been estimated to be 25-75 Å and 1050 kg/m^3, respectively. [127, 190, 220]

Collagen network

Collagen molecules account for 60-80% of the dry weight of articular cartilage. Most of the collagen, about 90%, is type II but also types I, III, V, VI, IX, X and XI, are known to be present in cartilage

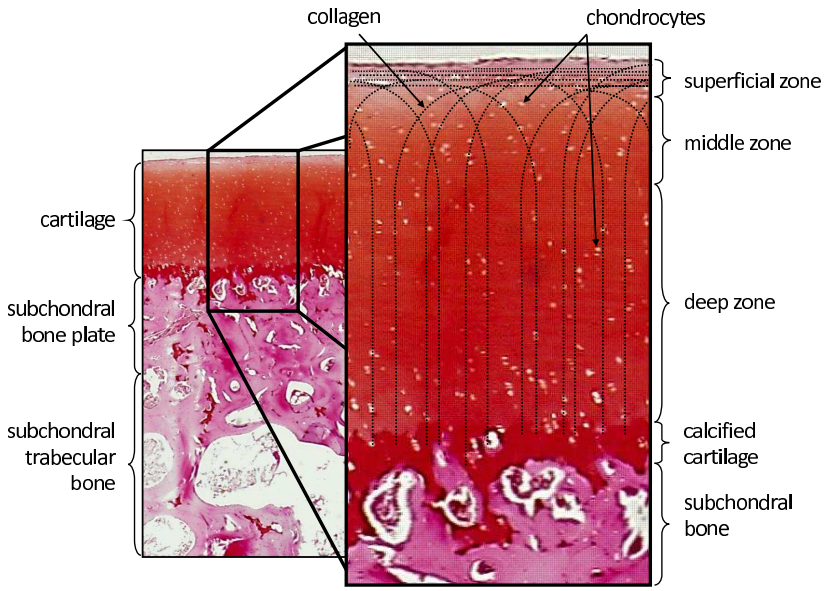

Figure 2.1: The layered structure of articular cartilage tissue, depicted in a safranin O stained light microscopy section. Collagen fibers are illustrated with dotted lines, chondrocytes are visualized as bright spots in cartilage and the tone of the cartilage indicates the proteoglycan content (darker tone indicates more PGs). A layer of calcified cartilage connects the cartilage to the subchondral bone plate, below which the trabecular bone begins.

matrix [71, 73, 117]. The menisci, on the other hand, are fibrocartilage, which consists mainly of type I collagen [190]. The collagen network in mature articular cartilage is highly anisotropic and can be divided into three zones according to its orientation [20]. The superficial zone contains thin, 20-50 nm thick collagen fibers that are oriented in parallel to the cartilage surface [102]. In the middle zone, the collagen fibers become thicker and bend towards the cartilage-bone interface. In the deep zone, the collagen fibers have reached full thickness (200-300 nm) and orientate perpendicular to the cartilage surface [102]. The collagen network is stabilized by crosslinks between collagen fibers and it is attached to the subchondral bone through the calcified cartilage layer, sometimes referred

to as the fourth zone [72,188,286].

Proteoglycans

Proteoglycans are negatively charged hydrophilic macromolecules that constitute 20-40% of the cartilage dry weight (4-7% of the total weight) [185,189]. Proteoglycans consist of negatively charged glycosaminoglycan (GAG) chains covalently attached to a chondroitin sulfate core protein [38,128]. Further, large PG aggregans are formed by hundreds of PGs linked noncovalently to hyaluronic acid with the complex kept stable by link proteins [81,100]. The PG concentration is lowest in the superficial zone, rises towards the deep zone and decreases again near the calcified zone [176,186]. Large PG aggregates are chemically or mechanically bound within the collagen matrix, which prevents their free distribution [30]. The negative charge of PGs attracts cations, which creates the Donnan effect, *i.e.* which increases the osmolarity of the tissue and attracts water [30]. The Donnan osmotic pressure depends on the amount of ions which, in turn, is dependent on the amount of PG. The negative net charge, caused by immobile PGs, is quantified as the fixed charge density (FCD) [173].

Chondrocytes

Chondrocytes, the only cells present in articular cartilage, synthesize the cartilage matrix [30,128]. Human articular cartilage is relatively acellular, chondrocytes comprise only about 1% of the tissue volume [30]. The cell density and shape vary across the depth of the tissue. The number of chondrocytes is largest and their shape flattened in the superficial zone, but their number decreases and the shape becomes more spherical towards the deep zone [102,191]. In the superficial zone, chondrocytes tend to arrange themselves in parallel to, whereas in the deep zone they tend to be perpendicular to the cartilage surface [30]. Even though chondrocytes maintain ECM by synthesizing collagen and PG, they cannot repair major damage in mature cartilage [189].

Interstitial water

The amount of water in articular cartilage is controlled by the PG content, the organization of the collagen network and the material properties of the solid matrix. Electronegative PGs cause swelling, which is restricted by the solid matrix, especially the collagen network [189]. A small percentage of interstitial water is intracellular, about 30% is attached to the collagen fibers and the rest is bound to proteoglycans as a solute [190]. Most of the interstitial water is freely exchangeable by diffusion [178]. Since cartilage has no vasculature, chondrocyte metabolism functions by diffusion between synovial fluid and interstitial water [81]. The water content of articular cartilage decreases as a function of tissue depth, being about 74% in superficial layers and 67% in deep cartilage [262].

Mechanical function

Joint loading causes compressive, tensional and shear stresses in articular cartilage. Articular cartilage is specialized to minimize and withstand these loads and decrease stresses on the subchondral bone. The friction between articulating surfaces is minimized by two main mechanisms. Synovial fluid contains macromolecules, for example lubricin, that lubricate the joint surfaces [84, 122]. The second mechanism is activated by dynamic joint loading, which pressurizes the interstitial fluid. Pressurized fluid supports the load and forms a thin fluid film between articulating surfaces, hence diminishing the friction [8]. The coefficient of friction between articular cartilage surfaces can be as low as 0.01 [42,78,179]. For perspective, the coefficient of friction between two teflon surfaces is 0.04. The fine collagen network running parallel to the surface creates a smooth (roughness < 1 μm) and wear resistant surface, which is a prerequisite for effective lubrication [79, 115].

Articular cartilage, together with muscles and other structures in the joint, functions as a cushion between the articulating bones [30, 185]. Its unique layered structure and composition mean that it can be considered as a fibril-reinforced poroviscoelastic material

with anisotropic and nonlinear mechanical properties [270]. Proteoglycans attract water into the cartilage and create a swelling pressure, which is restricted by the collagen network [185]. Mechanical loading increases the pressure in cartilage and causes the interstitial fluid to flow to less pressurized areas, while the collagen network resists the deformation of the tissue [185]. The flow of the interstitial water is restricted by the relatively low permeability of the tissue, which depends on its PG and collagen contents [147, 177, 192] and this increases the stiffness of articular cartilage under high-rate loading [185, 187]. However, collagen is known to dominate the dynamic behavior when interstitial water has no time to flow out of the tissue, and proteoglycans are mainly responsible of the static compressive stiffness of articular cartilage [148, 167]. The measure of cartilage stiffness at equilibrium, *i.e.* after the fluid flow and deformation have stopped, is called the Young's modulus or equilibrium modulus. The dynamic modulus, also known as instant modulus, indicates the stiffness of the tissue during high-rate loading. Poisson's ratio, a measure of the compressibility of the tissue, is dominated by the collagen network which resists the lateral expansion of the tissue under axial loading [144]. The composition, structure and mechanical properties of articular cartilage depend on the anatomical location and reflect the loading conditions [239, 240]. Even small changes in cartilage composition or structure can significantly affect its mechanical characteristics. In this respect, the measurement of mechanical properties can represent a good measure of cartilage health [186].

2.2 SUBCHONDRAL BONE

Bone is highly specialized and metabolically dynamic tissue which constantly adapts its shape and structure in response to the forces applied on it. Bone is a composite material of a mineralized extracellular matrix, cells and a non-mineral matrix of collagen and proteoglycans. Osteoblasts are the cells responsible for manufacturing bone, while bone is resorbed by the osteoclasts. Both of these bone-

reforming cells inhabit the surfaces of bones, constantly remodeling the tissue. When osteoblasts become trapped into the mineralized matrix they produce, they become osteocytes. Osteocytes and osteoblasts are suggested to sense mechanical stresses and regulate the remodeling of the bone structure [67]. The mineralized phase, about 65% of the dry weight, consists mostly of hydroxyapatite crystals which provide bone with hardness and resistance to compression. The rest of the dry weight is the organic matrix, mainly type I collagen fibers that contribute to tensile strength and toughness [272]. The solid rigid surface of the bones is called cortical bone. To the naked eye it seems solid, but microscopically an organized structure of Haversian canals can be seen. Haversian canals are surrounded by concentric layers of lamellar bone, forming structures parallel to the bone axis. These structures are called Haversian systems or osteons, and they form a fine network of canals containing blood vessels, nerves and lymphatic canals. In diarthrodial joints, a layer of cortical bone called the subchondral plate can be found under the articular cartilage. The subchondral trabecular bone is connected to the inner surface of the subchondral plate. [22,81,245,285]

Trabecular bone

The matrix of trabecular bone, also known as cancellous or spongy bone, is connected to the inner surface of the cortical bone (Figure 2.2). The trabeculae form a branching three-dimensional network of fine interconnected bone structures and provide a complex internal support system of high strength [245]. Trabecular bone can be found at the ends of the long bones and in the cores of the small bones and flat bones. There are no Haversian systems in trabecular bone but both types of bone have the same basic histological structure when examined closely. Bone cells in the trabecular bone are nourished by diffusion of nutrients through the bone marrow. [22,245]

About 80% of the bone mass is cortical bone, but it covers only about 20% of the total bone surface area [135]. Since the osteoblasts

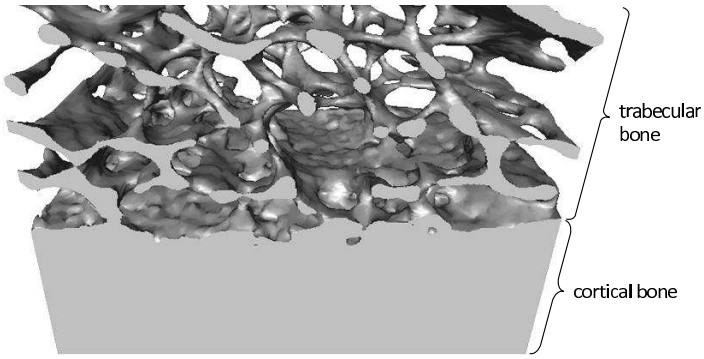

Figure 2.2: Trabecular structure is connected to the inner surface of the cortical bone and the space between the trabeculae is filled with bone marrow. Trabeculae can be rod-like or plate-like which can also be seen in this microCT reconstruction of bovine proximal tibia.

and osteoclasts inhabit the surface of the bone, the metabolism of cancellous bone is about eight times faster than that of cortical bone [62, 80]. Thus, the trabecular matrix is more active and susceptible to imbalance in bone turnover. This is the reason why the first signs of osteoporosis can be observed in the trabecular matrix [80]. After the skeletal growth is complete, remodeling results in an annual turnover of about 25 percent for cancellous bone and three percent for cortical bone [57]. The morphology of the trabecular matrix varies depending on the skeletal site, health and loading conditions (Table 2.1).

Bone marrow

Bone marrow fills the cavities of bones and can be either red or yellow. Both types of marrow contain mesenchymal stem cells that are able to produce osteoblasts, chondrocytes, myocytes and many other types of cells. Red bone marrow contains also hemopoietic stem cells that can differentiate into red blood cells, platelets and white blood cells. About 75% of red bone marrow is water; the rest being solid matter consisting of connective tissue, blood vessels and cells. On the other hand, about 96% of the yellow bone marrow is

Table 2.1: The values of morphometric parameters of human trabecular bone at different anatomical locations. The morphology of bone varies significantly between locations as well as between individuals.

Location/study	***BV/TV*** (%)	***Tb.Th*** (μm)	***Tb.Sp*** (μm)	***Tb.N*** (mm^{-1})	***DA*** (-)	***SMI*** (-)
Distal tibia						
Lai *et al.* [155]	7.6 ± 4.5	125 ± 30	979 ± 164	1.02 ± 0.15	2.01 ± 0.25	2.25 ± 0.58
Proximal femur						
Lai *et al.* [155]	9.0 ± 3.3	123 ± 17	895 ± 128	1.12 ± 0.13	1.78 ± 0.37	1.87 ± 0.45
Nägele *et al.* [196]	20.6 ± 12.8	207 ± 57	951 ± 417	1.09 ± 0.33	2.31 ± 0.61	1.01 ± 0.80
Padilla *et al.* [212]	11.5 ± 5.5	83 ± 17	723 ± 278	1.33 ± 0.40	1.50 ± 0.15	–
Distal radius						
Nägele *et al.* [196]	10.2 ± 4.1	148 ± 26	792 ± 113	1.12 ± 0.12	1.88 ± 0.45	2.01 ± 0.82

BV/TV = bone volume fraction, *Tb.Th* = trabecular thickness, *Tb.Sp* = trabecular separation, *Tb.N* = trabecular number, *DA* = degree of anisotropy, *SMI* = structural model index

fat. The remaining 4% consists of connective tissue, blood vessels and cells. At birth, all bone marrow is red. With age it is converted into yellow marrow, until by adulthood half of the marrow is yellow. At that point, red bone marrow is found mainly in flat bones and at the ends of long bones. If the body needs to increase the production of blood cells, yellow bone marrow is converted back into red bone marrow. [22, 90]

Mechanical function

The main functions of the bone tissue are to provide mechanical support, to protect organs and bone marrow, to transform muscle contractions into bodily motions and to act as a reservoir of calcium, phosphate and some other minerals [81]. The mechanical properties of bone tissue depend on its structure, composition and quantity, which in turn depend on the local loading conditions (Table 2.2). The trabecular structure rearranges itself to optimally endure the stresses to which it is exposed and this results in a highly anisotropic structure with good mechanical properties. Julius Wolff described this behavior in 1892 and defined Wolff's law: every change in form and function of a bone, or in its function alone, is followed by certain definite changes in its internal architecture [285].

Table 2.2: Ultimate strength and Young's modulus of human trabecular and cortical bone at different anatomical locations.

Location/study	Bone type	**Ultimate strength**	**Young's modulus**
Tibia			
Hakulinen *et al.* [96]	Trabecular	9.5 ± 3.9 MPa	575 ± 179 MPa
Muller *et al.* [193]	Cortical	142 ± 15 MPa	16.0 ± 1.8 GPa
Femur			
Hakulinen *et al.* [96]	Trabecular	10.9 ± 4.2 MPa	624 ± 214 MPa
Grimal *et al.* [92]	Cortical	195 ± 20 MPa	17.3 ± 1.3 GPa
Calcaneus			
Mittra *et al.* [182]	Trabecular	1.9 ± 1.0 MPa	70 ± 59 MPa

3 Osteoarthritis and osteoporosis

Osteoarthritis and osteoporosis are musculoskeletal diseases which have severe socio-economic impacts. OA is a joint disease which affects articular cartilage and subchondral bone, while OP affects the bones, making them more brittle and prone to fractures. Both diseases become more prevalent with age and are more common in women. It has been estimated that both diseases will become more common as the number of elderly people grows, and both require early intervention in order to prevent the progression of the disease. However, the relationship between OA and OP is not simple. One factor, for example obesity or smoking habits, may increase the risk of one disease but decrease the risk of the other. There is no consensus about the relationship between OA and OP but it is a topic of heated debate. [9, 58, 68, 164–166, 292]

3.1 OSTEOARTHRITIS

OA has been estimated to be the most common chronic condition to limit activity in population aged over 45 years [263]. The prevalence of OA increases with age and evidence of OA can be found in almost all individuals over 65 years old [162]. Radiographic osteoarthiritic changes can be found in the hands of almost all individuals over 70 years of age, though only one out of four experience symptoms [107,162,291]. The high prevalence and chronic nature of OA explain the high costs to society. In the United States, OA is estimated to cost between $1750 and $2800 per year per patient and the annual cost of end-stage knee or hip OA is even higher [169, 171]. If an individual develops symptomatic OA, they will suffer from it for the rest of their life [33]. Since OA causes pain and limits daily activities, it affects the patients and their families and reduces the

quality of their life [26].

Etiology and pathogenesis

Osteoarthritis is the most common degenerative joint disease and it can affect most joints. The origin of the disease is still unknown, but the degenerative changes appear in both in articular cartilage and subchondral bone [10, 41]. OA is associated with aging and obesity, and it is more common in women [32]. OA may be initiated by several factors, *e.g.* injury, inflammation, genetic susceptibility or metabolic disorders, and it causes progressive degradation of articular cartilage and subchondral sclerosis [29, 31].

The first detectable signs of OA are depletion of PGs, fibrillation of the superficial collagen network and thickening of the subchondral plate [29]. PG depletion and deterioration of the collagen network increase the permeability and water content of the tissue, and evoke fibrillation in the cartilage surface [190]. These changes impair the mechanical properties and wear resistance of the tissue, accelerate deterioration and eventually lead to delamination of cartilage [185]. The damaged tissue stimulates the chondrocytes to synthesize new ECM and the cells cluster around the new tissue due to proliferation [29]. Mature articular cartilage, however, exhibits highly limited capability for regeneration, mainly because the turnover rate of collagen has been estimated to be more than one hundred years [264]. This is also the reason why degenerative changes are considered to be irreversible after collagen fibrillation has occurred.

The origin of OA is still unresolved, partly because of the asymptomatic development of the disease. When the disease becomes symptomatic and is diagnosed, severe changes can already be found in both cartilage and subchondral bone (Table 3.1). Some studies have suggested that the origin of OA lies within subchondral bone which becomes harder and this increases the stresses on the overlying cartilage, hence initiating the degenerative processes [223]. A more common opinion, however, is that the degradation of the superficial cartilage weakens the mechanical properties of cartilage

and increases stresses on subchondral bone, which responds by thickening and hardening [75]. Cartilage and bone are traditionally investigated separately, but a simultaneous investigation of all components of the joint may be more relevant and yield additional information about the state of the disease.

Table 3.1: The composition and mechanical properties of human articular cartilage and subchondral bone in healthy and osteoarthritic joints.

Cartilage parameters	**healthy**	**OA**	
collagen (%/dw)	79	85	[230]
PG (%/dw)	21	15	[230]
water (%)	76	79	[230]
permeability (m^4/Ns)	10^{-15}	10^{-14}	[190]
roughness (μm)	7	34	[145]
E_{dyn} (MPa)	4.67	1.87	[143]
E_{Young} (MPa)	0.64	0.21	[143]
Subchondral bone parameters	**healthy**	**OA**	
Tb.Th (μm)	160	180	[60]
Tb.Sp (μm)	588	580	[60]
SMI (-)	1.31	0.96	[60]
BV/TV (%)	21	25	[60]
BMD (mg/cm^3)	670	770	[60]

PG = proteoglycan, E_{dyn} = dynamic modulus, E_{Young} = Young's modulus, *Tb.Th* = trabecular thickness, *Tb.Sp* = trabecular separation, *SMI* = structural model index, *BV/TV* = bone volume fraction, *BMD* = bone mineral density.

Diagnostics

The clinical symptoms of OA are mainly joint stiffness, pain and deformity [5, 31]. Often, when the symptoms eventually appear, the damage is beyond spontaneous healing and the disease may be diagnosed with the conventional methods. At the moment, the primary means for OA diagnostics are anamnesis, clinical exami-

nation and plain radiography which can reveal joint space narrowing, subchondral sclerosis and osteophyte formation. The Kellgren-Lawrence scaling system was introduced in 1957 to grade the severity of OA based on radiographs [141] and this is still the most widely used radiological scaling method in epidemiological and clinical studies. These conventional methods are unfortunately not sensitive enough to detect the early changes related to OA.

Other clinically used methods include magnetic resonance imaging, computed tomography, arthroscopy and external ultrasound imaging. Plain MRI can typically reveal qualitative changes in subchondral bone, ligaments, menisci as well as alterations in the morphology of cartilage [104]. Delayed gadolinium-enhanced MRI of cartilage (dGEMRIC) has been used, although not frequently, in clinical practice for evaluation of the proteoglycan content of cartilage [180, 227, 254, 283]. However, due to the high cost and low availability, MRI is not the primary modality in OA diagnostics. Plain CT yields good three-dimensional data on the bones, but it is difficult to separate articular cartilage from synovial fluid and the menisci. CT, like all X-ray methods, exposes the patient to ionizing radiation.

Cartilage fibrillation, lesions and exposed subchondral bone can be evaluated in arthroscopy. A scaling system has been developed for evaluation of the severity of the cartilage damage [25] but it relies on a subjective estimation of tissue integrity as well as the size and depth of the lesions. It must be noted that arthroscopy is a surgical operation and is not usually used as a diagnostic technique.

External, *i.e.* transcutaneous, ultrasound imaging is used in the diagnostics and treatment of rheumatoid arthritis. This technique can detect effusion and thickening of the joint capsule [48]. Transcutaneous measurements of articular cartilage have been attempted [4], but the measurements are difficult due to the location and natural curvature of the cartilage and the shadow cast by other structures like the patella. However, OA often causes synovitis, which can be diagnosed with this method [55, 140]. Intra-articular ultrasound imaging of cartilage was recently introduced [116, 266]

and the first *in vivo* trials have demonstrated the potential of the technique [132].

Therapy

At the moment there are no effective means to slow down or stop the progression of OA and the treatment focuses on relieving symptoms and pain. Operative procedures like mosaicplasty or autologous chondrocyte transplantation may be used for the treatment of traumatic cartilage lesions. Total joint replacement, in the most extreme cases, is considered when the disease has advanced and medication no longer eases the pain [126]. Cartilage repair surgery has been proven to alleviate the symptoms but the long term results of the procedure are not clear [31, 66]. Bone marrow stimulation procedures and whole-tissue transplantations have been proposed for the management of focal chondral defects of the knee, but the cell-based techniques, such as autologous chondrocyte implantation, will require additional human trials in order to validate their efficacy [18].

Even though there is no cure for OA at the moment, new sensitive methods are crucial in the development of drugs and treatments for the disease, *e.g.* to reveal the efficacy of these methods [222]. Moreover, research in the field is advancing rapidly and especially disease-modifying drugs have shown promise. Several new drugs are in pre-clinical tests and some have already advanced to clinical trials [86,222]. Although medical prevention of OA is not yet possible, it has been estimated that half of the new OA cases could be prevented with control of the known modifiable risk factors such as obesity, knee injuries and excessive joint loading [76].

3.2 OSTEOPOROSIS

Osteoporosis is the most common metabolic bone disease in the developed countries [273]. It affects over 200 million people worldwide and in Europe in the year 2000 it was responsible for costs of over 36 billion euros [64,250]. Osteoporosis is an important disease

in the socio-economic sense because it increases the risk of frequent fractures and chronic disability [46]. Osteoporotic hip fractures are known to significantly increase mortality of patients [52,221]. In osteoporosis, the bone mineral density is decreased and the trabecular microstructure becomes disrupted, resulting in more brittle bones and increased risk of fracture [134]. The World Health Organization defines osteoporosis as "A value of BMD 2.5 standard deviations or more below the young adult mean (T-score $\leq$ -2.5)" as measured by DXA. Osteoporotic fractures occur as a result of low energy impact that would not normally lead to fractures in healthy people [236]. Even though patients with low BMD have a higher fracture risk, most of fractures occur in people with normal BMD [247].

Etiology and pathogenesis

Osteoporosis is a very common disease but the majority of people are unaware of the disease until a low-impact fracture occurs [250]. The risk of osteoporotic fractures increases with age, lack of exercise and malnutrition [134]. Moreover, hormonal imbalances, smoking and genetic susceptibility are also associated with osteoporosis. The pathogenesis of osteoporosis can be traced to an imbalance between bone resorption and bone formation [267]. If bone resorption is increased or bone formation is diminished, then the bone mass will decrease and the risk of a fracture increases [51]. Since trabecular bone is more active than cortical bone, osteoporosis can first be seen as a loss of trabecular bone mass [80]. The trabeculae and the cortical layer become thinner, the density and connectivity of trabeculae decrease, and the trabecular structure becomes more isotropic [13]. This structural degradation makes trabecular bone weaker and prone to fractures [214]. The bone tissue itself, however, may be normally calcified and otherwise qualitatively normal [164].

Diagnostics and therapy

Osteoporosis is usually diagnosed when a fracture occurs. However, osteoporosis may also be diagnosed based on BMD loss, which

can be observed qualitatively in plain radiographs or measured quantitatively by DXA [134]. When compared to two-dimensional DXA, quantitative CT can provide volumetric information on bone mineral density and make it possible to visualize the three-dimensional morphology of the bones. The risk of bone fracture is not only related to bone mass but also to fine structure and organic composition of bone [214, 269]. DXA or clinical CT cannot provide information about the microstructure or the organic composition of bone, and they expose patients to ionizing radiation. Clinical ultrasound devices developed for the diagnostics of osteoporosis are typically used for measurements of peripheral locations, such as calcaneus, radius and the phalanges [15, 49, 85, 119]. Even though these locations are not amongst the primary fracture sites, for example QUS measurements of the heel have been shown to predict fractures with similar reliability as the DXA measurements [85, 119, 183, 246]. QUS systems can be constructed to be portable and cost-efficient and they do not involve ionizing radiation [139]. This makes QUS an attractive method for screening. Moreover, the development of the pulse-echo techniques could allow measurements of the important osteoporotic fracture sites, like the femoral neck and lumbar spine [225].

Early diagnosis is important in the effective management of osteoporosis, as the risk groups need to be identified before the fractures have occurred. According to the Finnish clinical guidelines, the basis in treatment and prevention of osteoporosis is exercise and adequate intake of calcium and vitamin D. More severe cases can be treated with medication, *e.g.* bisphosphonates. Osteoporotic fractures often occur in elderly people and require operational treatment, osteosynthetic treatment or endoprostheses.

4 Acoustic properties of cartilage and bone

Ultrasound can be defined as sound waves with frequencies above the normal human hearing range, *i.e.* above 20 kHz. Ultrasound, as sound in general, is a propagating mechanic oscillating motion of particles. If the particles vibrate in parallel to the direction of propagation, the wave is longitudinal. There are several other types of mechanical waves, *e.g.* shear and surface waves, but biological soft tissues behave mechanically like viscous fluids which favors the use of longitudinally vibrating ultrasound. Ultrasound is generated and received through piezoelectric crystals. When an oscillating voltage is applied over such a crystal, it begins to expand and contract along with the voltage and this generates a mechanic vibration. Conversely, if a piezoelectric crystal is exposed to mechanic vibration, a respective oscillating voltage is generated over the material. [205,279]

4.1 BASIC PHYSICS OF ULTRASOUND

The linear wave equation, derived from the Newton's second law, approximates to the simple harmonic vibration in a homogeneous, linear, isotropic material. It is a hyperbolic partial differential equation that satisfies [241]:

$$\frac{\partial^2 u}{\partial t^2} = c^2 \nabla^2 u, \tag{4.1}$$

where c is a material-specific constant, speed of sound, and u is the three-dimensional displacement vector. If the wave equation is simplified to one dimension, the solution is the wave function [241]:

$$u(x,t) = u_0 e^{i(\omega t - kx)}, \tag{4.2}$$

where particle displacement u depends on the distance x and time t. u_0 is the particle displacement when $t = 0$, ω is the angular frequency, k is the wave number and i is the imaginary unit.

An ultrasound wave that propagates in an ideal homogeneous elastic material loses no energy. In real materials, however, ultrasound attenuates due to absorption, scattering and beam spreading. Acoustic impedance Z is a material-specific constant, which represents the acoustic resistance of the material. Acoustic impedances can be used for calculation of reflection and refraction coefficients, which, together with Snell's law, describe the behavior of ultrasound at an ideal acoustic interface. If the reflecting object is of the same magnitude or smaller than the wavelength of the ultrasound, scattering becomes the dominant interaction instead of specular reflection. At scatterer sizes close to the wavelength, scattering patterns are complex and depend on the geometry and acoustic impedance of the scatterers. Rayleigh scattering is the dominant mechanism for very small scatterers ($d \ll \lambda$), spreading the energy uniformly in all directions. The propagation of ultrasound in an elastic isotropic material depends on the mechanical properties of the material. The speed of sound in a given material depends on Young's modulus, the density and Poisson's ratio of the material, while the acoustic pressure is related to Young's modulus and the particle displacement. Table 4.1 contains the basic equations describing ultrasound propagation in elastic isotropic media. [241,279,280]

4.2 MEASUREMENT TECHNIQUES

QUS parameters are usually measured in the through-transmission (TT) or pulse-echo (PE) geometries. The through-transmission geometry requires the presence of two transducers on opposite sides of the object and this allows the quantification of the speed of sound and ultrasound attenuation in the object. One transducer transmits the ultrasound and the other records the signal transmitted through the object. TT measurements have been used in clinical

Table 4.1: Basic equations governing the propagation of ultrasound pulses in elastic isotropic media.

Parameter/law	**Equation**	
Intensity of ultrasound	$I = I_0 e^{-2\alpha(f)x}$	(4.3)
Acoustic impedance	$Z = \rho c$	(4.4)
Reflection coefficient	$R = \frac{Z_2 \cos\theta_i - Z_1 \cos\theta_r}{Z_2 \cos\theta_i + Z_1 \cos\theta_r}$	(4.5)
Refraction coefficient	$T = \frac{2Z_2 \cos\theta_i}{Z_2 \cos\theta_i + Z_1 \cos\theta_r}$	(4.6)
Snell's law	$\frac{\sin\theta_i}{\sin\theta_r} = \frac{c_1}{c_2}$	(4.7)
Speed of sound	$c = \sqrt{\frac{E_{Young}(1-\nu)}{\rho(1+\nu)(1-2\nu)}}$	(4.8)
Acoustic pressure	$p = E_{Young}\frac{\partial u}{\partial x}$	(4.9)

Subscripts 1 and 2 refer to materials before and after the boundary.

$\alpha(f)$ = attenuation coefficient
E_{Young} = Young's modulus
f = frequency
$k = 2\pi/\lambda$ = wave number
λ = wavelength
ν = Poisson's ratio
ρ = density
t = time
θ_i = angle of incidence
θ_r = angle of refraction
u = particle displacement
x = distance

bone densitometry [205], but the potential of pulse-echo measurements has been growing after intense research conducted in recent years [39, 98, 112, 137, 226, 229, 277]. The pulse-echo geometry requires only one transducer and allows measurements of reflection and backscatter parameters. The ultrasound pulse is transmitted to the object and the returning signal is recorded with the same transducer. Quantitative ultrasound parameters are often normalized with reference measurements to minimize the system specific errors. The TT reference signal is acquired by measuring the signal transmitted through water only and the PE reference is the reflected signal from a known reflector, for example a polished steel

plate. Another QUS method, the axial-transmission technique requires two transducers that are placed on the same side of the sample; this technique has been used to measure the speed of sound on the surface of cortical bone [184].

There are several error sources related to all QUS measurement techniques. The TT technique, for example, requires information about the size of the bone before it can provide reliable results [160, 260]. Moreover, all of the mentioned techniques are affected by the overlying soft tissue [87, 225]. Therefore TT and axial-transmission are usually applied at peripheral sites with minimal soft tissue. In principle, the PE technique could have several benefits compared to transmission techniques. It would allow measurement of thicknesses of tissue layers at virtually any location. Moreover, it should be possible to estimate the composition of the overlying soft tissue with broadband transducers and then to use this information to correct the measured QUS parameters [137,226].

4.3 ACOUSTIC PROPERTIES OF CARTILAGE AND BONE

The equations presented in Table 4.1 are valid in elastic, homogeneous isotropic materials. However, biological tissues are often inhomogeneous, anisotropic and include structures that cause scattering. Several analytical and numerical models have been developed to describe the propagation of ultrasound in biological tissues, and the most important of these are introduced in chapter 4.4.

Ultrasound attenuation in biological tissues is known to increase significantly with frequency, due to increased scattering and absorption. The choice of the ultrasound frequency is a tradeoff between axial resolution and penetration depth; high frequency ultrasound provides better resolution but attenuates quickly. The central frequencies applied in the laboratory studies for articular cartilage are typically between 12 and 50 MHz [61,231,233,271]. On the other hand, optimal frequencies for the measurement of bone are much lower. A frequency range from 0.1 to 1 MHz has been suggested as being the most useful for the characterization of bone [158], but also

higher frequencies, up to 10 MHz, have been successfully applied in laboratory studies [97,110,112,137]. Thus, in order to simultaneously measure the properties of articular cartilage and subchondral bone, the ultrasound frequency must be chosen carefully.

Ultrasound has been used for the measurement of knee cartilage from outside the joint, but the measurement has proven to be difficult. The patella shadows the articulating surfaces of the knee, and the measurement can only be done in flexion and only on the distal part of the femoral groove [4]. Moreover, the overlying soft tissues affect the measurements and make interpretation of the results even more difficult [87,225]. Currently, there are no clinically approved instruments for intra-articular or arthroscopic ultrasound measurements of cartilage, but existing intravascular ultrasound (IVUS) catheters have been proposed as a way of accomplishing this task [116,266]. Importantly, the intra-articular PE ultrasound measurement at optimal frequency could allow simultaneous assessment of articular cartilage and the underlying bone.

Acoustic properties of articular cartilage

Articular cartilage is an inhomogeneous, anisotropic poroviscoelastic material. The acoustic properties of cartilage depend on the structure and composition of the tissue and vary with the anatomical location, maturation and the health of the tissue [45,153,257]. The speed of sound in cartilage, typically about 1650 m/s, is known to decrease with collagen degradation, PG depletion as well as with increased water content (Table 4.2). The speed of sound has been found to depend also on the collagen orientation, since the ultrasound waves travel faster along the collagen fibers than perpendicular to them [2,88,216].

The surface of healthy articular cartilage yields a clear narrow echo, but the reflection coefficient is low, about 1-6% [145,153,232]. Based on the reported speed of sound (1600-1800 m/s) and density (1050 kg/m^3), the acoustic impedance of healthy articular cartilage may be approximated to be about 1.7 - 1.9 $\times 10^6$ kg/(m^{2}s). On the other hand, the reported acoustic impedance of water (1.52

Table 4.2: Ultrasound velocities reported in the literature for articular cartilage, bone and bone marrow.

Tissue/Species	Health/treatment	c (m/s)	Study
Human			
Cartilage, femur	normal	1658 ± 185	[195]
	OA	1581 ± 148	
Cortical bone, tibia	normal	3893 ± 150	[208]
Cortical bone, radius	normal	3988 ± 85	[249]
	OP	3924 ± 88	
Trabecular bone, femur	OA	2409 ± 291	[207]
Trabecular bone, tibia	normal	1728 ± 166	[99]
Trabecular bone, calcaneus	normal	1520 ± 36	[198]
Bovine			
Cartilage, femur	normal	1638 ± 18	[257]
Cartilage, tibia	normal	1602 ± 35	
Cartilage, patella	normal	1654 ± 82	[260]
	chondroitinase ABC	1646 ± 68	
	collagenase	1567 ± 100	
Cortical bone	normal	3791 ± 205	[59]
	normal	4410 ± 28.3	[205]
Trabecular bone, femur	normal	2171 ± 148	[206]
Trabecular bone, tibia	normal	2284 ± 83	[113]
Bone marrow	normal	1372	[69]
	normal	1690 ± 71	[59]
Distilled water, 26°C		1498	[69]

$\times 10^6$ kg/(m^{2}s), [280]) and reflection values (1-6%) yield acoustic impedance values between 1.55 and 1.71 $\times 10^6$ kg/(m^{2}s). This discrepancy may be explained by the anisotropic poroviscoelastic mechanical properties and inhomogeneous composition of cartilage.

Ultrasound reflection and scattering are sensitive to both the structure and composition of the superficial cartilage layer and collagen has been postulated to be the dominant scatterer in the tissue [44, 45, 260]. Degradation of the surface widens the reflection and yields a backscatter-like signal from the internal cartilage [44, 195, 231]. Table 4.3 shows how the pulse-echo parameters depend on the health of the cartilage.

Ultrasound backscatter from internal cartilage depends on the structure and composition of the tissue. Chemical (mono-iodo-

Table 4.3: Values of pulse-echo ultrasound parameters reported in the literature for normal, osteoarthritic and repaired cartilage and in normal and low mineral density bone.

Parameter and tissue	normal	abnormal	Frequency and study
Rabbit cartilage[a]			40 MHz, [265]
R (%)	7.0 ± 1.9	1.7 ± 1.0	
IRC (dB)	-24.6 ± 2.5	-39.9 ± 2.5	
AIB (dB)	-46.0 ± 2.9	-36.8 ± 6.2	
URI (μm)	8.9 ± 3.0	29.6 ± 7.0	
Bovine cartilage[b]			20 MHz, [231]
R (%)	5.3 ± 0.9	2.4 ± 1.6	
IRC (dB)	-26.7 ± 1.6	-34.1 ± 5.5	
URI (μm)	7.4 ± 1.2	24.2 ± 15.5	
Bovine subchondral bone[b]			20 MHz, [231]
R (%)	8.3 ± 2.4	15.0 ± 5.3	
IRC (dB)	-16.9 ± 4.7	-11.0 ± 5.7	
Human trabecular bone[c]			5 MHz, [136]
IRC (dB)	-9.7 ± 1.9	-13.9 ± 2.7	
AIB (dB)	-22.4 ± 1.9	-25.0 ± 1.8	

[a] abnormal refers to repaired cartilage.

[b] abnormal refers to spontaneous OA-like changes.

[c] abnormal refers to low mineral density bone.

R = reflection coefficient, *IRC* = integrated reflection coefficient, *AIB* = apparent integrated backscatter, *URI* = ultrasound roughness index

acetic acid) cartilage degradation significantly affects ultrasound reflection at the cartilage surface and the backscatter in the tissue, whereas specific PG depletion has only a minor effect. Degradation of collagen network and increased roughness of the cartilage surface have been shown to significantly decrease surface reflection and internal scattering. The ultrasound backscatter is stronger in immature or repaired cartilage than in healthy mature cartilage. The measurement of the backscatter, however, is complicated because the signal may be very weak. [27, 44, 45, 217, 232, 260, 265, 271]

There seems to be no consensus about the roles of collagen and PGs on ultrasound attenuation [2, 125, 200, 201, 237]. Attenuation in articular cartilage, however, has been reported to depend on the degenerative state of the tissue; for example ultrasound attenuation,

measured in a frequency range from 5 to 9 MHz, decreased from 2.7 to 1.8 dB mm^{-1} with spontaneous degeneration in bovine articular cartilage [200].

Acoustic properties of bone

The acoustic properties of trabecular bone depend on its components, *i.e.* trabecular bone tissue and bone marrow (Tables 4.2 and 4.3). In acoustical terms, trabecular bone can be considered as a biphasic viscoelastic medium which consists of a solid bone matrix and viscous bone marrow. The thickness of the trabeculae is typically of the same magnitude or smaller than the wavelength of the ultrasound used in bone analyses, which results in complex scattering processes. The scattering in the internal structures and the viscous friction have been hypothesized to be the main causes of attenuation in trabecular bone [199, 248]. The reflection and backscatter parameters have been reported to correlate with structure, mechanical properties, mineral density and collagen content of trabecular bone [39, 96, 98, 111, 112, 137, 198, 277].

The ultrasound velocity in trabecular bone depends mainly on the trabecular structure, as the speed of sound is high in the bone tissue (Table 4.2). The ultrasound velocity is highest, and attenuation lowest in the samples with a high bone volume fraction or apparent BMD and along the primary axis of the trabeculae [16, 94, 210, 212]. Speed of sound has been shown to predict fractures similarly, and ultrasound attenuation even better than the BMD [14, 197].

Analytical models of wave propagation

Application of the mixture law is a simple way to estimate the propagation of an ultrasound pulse in a mixture of multiple components. The propagation velocity in a mixture is the average of the velocities of the components, weighted according to the volume fraction of each component. The mixture model can be extended to include also velocity fluctuations as a function of porosity. Stre-

litzki *et al.* studied the scattering and attenuation with this model and proposed that it could be used as a basis for more detailed studies [248].

M.A. Biot described the frequency dependence of elastic wave propagation in a fluid saturated solid, originally for application in geophysics [21]. The theory considers ultrasound-induced motion separately for solid and liquid phases. The medium is assumed to be isotropic and scattering is neglected. Biot's theory requires 14 input parameters. For example densities, mechanical moduli, porosity and pore size of the phases all must be known. Some of the input parameters are difficult to determine which complicates the application of Biot's theory. Biot's theory has been successfully applied in predicting wave propagation in trabecular bone, irrespective of the fact that it consistently underestimates ultrasound attenuation [95]. However, Biot's theory did predict the existence of fast and slow waves in trabecular bone, and this hypothesis was confirmed in experimental studies [114].

Schoenberg's theory simplifies cancellous bone and considers it as a layered structure of bone and marrow plates [235]. This assumption, however, is only valid in plate-like trabecular bone. Schoenberg's theory requires only six input parameters but no viscous losses are predicted because the fluid is assumed to be inviscid. Qualitative agreement has been reported between the experimentally-determined phase velocity and that predicted by Schoenberg's theory [118]. Schoenberg's theory has also predicted the frequency dependence of ultrasound attenuation in trabecular bone [168].

Several models have been developed for describing ultrasound scattering in trabecular bone. Wear *et al.* reviewed the limitations of frequency dependent backscatter measurements with a cylinder scattering model [276]. Autocorrelation functions and models, originally developed for soft tissue, have provided comparable results with experimental data [123,199,211]. Moreover, these studies have predicted the frequency dependency of the attenuation and the effect of bone structure on the ultrasound propagation. Analytical

models are generally applicable when the model geometry is simple. Numerical models, however, can combine physical theory and more complex realistic geometries. For example, numerical models allow investigation of ultrasound propagation in a realistic trabecular bone structure scanned with a microCT.

4.4 SIMULATION OF WAVE PROPAGATION

The finite element method (FEM) is a widely used method for solving partial differential equations with a computer. The basis of FEM is the element mesh that is created for the area of interest. The mesh is composed of nodes and the elements that are formed when the nodes are connected to each other. FEM makes it possible to describe a partial differential equation with a group of linear equations. The values at the nodes of the grid can be obtained by solving the linear equations. The numerical solution is always an approximation, and the precision of the solution depends on the size and type of the elements in the mesh. Implementation of FEM is easy for simple phenomena such as heat dissipation, but more difficult for nonlinear systems.

The finite difference method (FDM) can be considered as a special case of the finite element method. It is merely another way to solve partial differential equations. Whereas FEM approximates the solution of a partial differential equation, the finite difference method approximates the actual partial differential equation. The mesh is also created differently as it usually consists of isotropic voxels. The implementation of FDM is simple, which is the reason it is used in applications that require a large number of nodes.

Finite difference method

In the finite difference method, three finite difference forms are generally considered:

$$\text{Forward difference: } \Delta f(x) = f(x+a) - f(x) \tag{4.10}$$

$$\text{Backward difference: } \nabla f(x) = f(x) - f(x-a) \tag{4.11}$$

$$\text{Central difference: } \delta f(x) = f(x+\frac{1}{2}a) - f(x-\frac{1}{2}a) \tag{4.12}$$

The finite difference method replaces derivatives by finite difference approximations; it is a discrete analog of the derivative. The derivative of a function f at a point x is defined as

$$f'(x) = \lim_{a \to 0} \frac{f(x+a) - f(x)}{a}. \tag{4.13}$$

If difference a is finite instead of infinitesimal,

$$f'(x) = \frac{f(x+a) - f(x)}{a}. \tag{4.14}$$

When both time and space are approximated by finite differences, the method is called the finite difference time domain (FDTD) method. Different finite difference forms can be combined to produce different FDTD methods. The FDTD software used in this study, Wave 3000 Pro 2.2, utilizes the explicit method which means that time is approximated with the forward difference and space with the central difference form. The explicit method is the least accurate, and can be unstable, but it is the easiest to implement and requires the least computing resources.

Viscoelastic FDTD method

The elastic method assumes that there is no energy loss during propagation; energy is lost only at the acoustic interfaces according to the boundary conditions. The speed of sound in a medium depends on the mechanical properties of the medium. If the equations for a homogeneous isotropic elastic solid are applied to the

wave equation, this can be expressed as [89]

$$\rho \frac{\partial^2 u}{\partial t^2} = \mu \nabla^2 u + (\lambda + \mu) \nabla (\nabla \cdot u), \tag{4.15}$$

where λ and μ, the Lamé constants, are elastic constants of the medium. The Lamé constants may be expressed in terms of other elastic constants, such as Young's modulus, Poisson's ratio and the bulk modulus. The Wave 3000 Pro software is based on a local interaction formulation designed for parallel processing implementation for the lossless case [56]. It includes absorption losses as the elastic Lamé constants are replaced with viscoelastic "constants", derived from the viscous loss formulation [138]:

$$\mu \rightarrow \mu + \eta \frac{\partial}{\partial t} \text{ and } \lambda \rightarrow \lambda + \left(\phi - \frac{2}{3} \eta \right) \frac{\partial}{\partial t}. \tag{4.16}$$

Combination of equations 4.15 and 4.16 yields the following equation which applies in an isotropic region:

$$\rho \frac{\partial^2 u}{\partial t^2} = \left(\mu + \eta \frac{\partial}{\partial t} \right) \nabla^2 u + \left(\lambda + \mu + \phi \frac{\partial}{\partial t} + \frac{\eta}{3} \frac{\partial}{\partial t} \right) \nabla (\nabla \cdot u), \tag{4.17}$$

where ρ is density, λ is the first Lamé constant, μ is the second Lamé constant, η is shear viscosity, ϕ is bulk viscosity, ∇ is the gradient operator, $\nabla \cdot$ is the divergence operator, ∂ is the partial differential operator and t is time. $u(x, y, z, t)$ is a three-dimensional vector whose components are the x, y and z components of displacement of the medium at the location (x, y, z). The Wave 3000 software solves this equation for all nodes at all time points. It is noteworthy, however, that the software considers fluids as solids with a low shear bulk velocity.

5 Contrast agent enhanced CT of cartilage

The concept of computed tomography was invented by Godfrey Newbold Hounsfield in Hayes, England, in 1967 and was publicly announced in 1972. Allan McLeod Cormack discovered the same process independently at the same time at Tufts University, Medford, MA, USA. In 1979 they shared the Nobel Prize in Physiology or Medicine. CT is a procedure in which a number of X-ray projections are collected from many directions and digitally reconstructed to provide an image which contains accurate anatomical information. [278]

5.1 X-RAY COMPUTED TOMOGRAPHY

For clinical use, X-rays are generated in an X-ray tube where high velocity electrons interact with heavy atoms. X-rays attenuate due to the interactions with the atoms in the matter they penetrate:

$$I(x) = I_0 e^{-\mu x}, \tag{5.1}$$

where I is intensity at distance x, I_0 is the initial intensity and μ is the linear attenuation coefficient which depends on the density, atomic number and electron density of the material. X-ray radiation is able to ionize matter which makes it potentially harmful for living beings. Ionizing radiation can damage DNA and may cause cell death, mutations or cancer. [43, 65].

In computed tomography, a two-dimensional function is determined by its projections in number of directions [130]. The quality of the backprojected image depends on the number of projections, which obviously is related to the radiation dose on the object.

CT images contain information on the density variation in the object and can be calibrated to volumetric density maps. Quan-

titative computed tomography (QCT) can permit quantification of mineral density, cortical thickness, size and shape of bones. Peripheral quantitative tomography (pQCT) is a technique used to quantitatively analyze peripheral skeletal locations, *e.g.* radius or tibia. X-ray microtomography (microCT) is a pre-clinical method that provides high-resolution computed tomography (down to 1 μm) data on small animals or *in vitro* samples. Modern full-body, pQCT and microCT devices yield isotropic three-dimensional data and can reach voxel sizes down to about 500, 100 and 1 μm, respectively. MicroCT is the only CT method able to reliably analyze the microstructure of trabecular bone, because a reliable morphological analysis requires an isotropic voxel size smaller than 100 μm [121,243].

5.2 CONTRAST AGENT ENHANCEMENT

Articular cartilage, like most of the soft tissues in the human body, consists mostly of water and contains hardly any heavy elements. As a result, the X-ray attenuation does not vary extensively between soft tissues and it is difficult to separate articular cartilage from synovial fluid and the menisci. One solution to this problem is to use contrast agents that contain heavy atoms for contrast enhancement. A variety of contrast agents have been developed for targeting different tissues [43,65]. Heavy atoms, that are responsible for the contrast enhancement, can be attached to functional carrier molecules that target specific tissues. Contrast agents have been used in arthrographies for decades [53], but contrast agent aided estimation of the tissue composition is still a new field and new contrast agents are constantly being developed and tested. During last few years, several gadolinium- and iodine-based cationic, anionic and electroneutral contrast agents have been examined for detection of cartilage morphology and composition [12,50,150,281].

Negatively charged gadopentetate (Gd-DTPA^{2-}) was proposed as an MRI contrast agent for the estimation of the proteoglycan content of articular cartilage over a decade ago [17,35]. Delayed

gadolinium-enhanced MRI of cartilage is a gadolinium-based contrast agent enhancement technique, where anionic Gd-DTPA^{2-} is believed to diffuse into the cartilage in inverse proportion to the tissue proteoglycan distribution [17, 35, 91, 202, 254, 283]. The electronegative PGs repel the negatively charged contrast agent molecules and, when the Gibbs-Donnan diffusion equilibrium is reached, the contrast agent distribution is considered to depend only on the FCD distribution in the tissue [17, 35]. Paramagnetic gadolinium shortens the T_1 relaxation time, which is exploited in the MRI-based estimation of the gadolinium content in cartilage and called the "dGEMRIC index" [82, 251, 283, 284]. Gadolinium is a relatively heavy atom ($Z = 64$), so it can, in principle, be used as a CT contrast agent. Cockman *et al.* (2006) were the first to realize this property and apply the idea of dGEMRIC to a CT device [50]. Gadolinium-based contrast agents, however, are usually toxic and can only be administered in small amounts, which limits their use as CT contrast agents. An adequate contrast enhancement in CT requires over a hundred times higher gadolinium concentration than is usually used in MRI studies. Palmer *et al.* (2006) were the first to apply an iodine-based agent for contrast enhanced CT imaging of articular cartilage [213]. Iodine is a safer element and clinically used iodine-based contrast agents are readily available in various sizes and charges. CECT has been successfully applied for *in vivo* assessment of cartilage degeneration in a small animal model [219].

Physics of contrast agent diffusion

The diffusion of contrast agent molecules is caused by Brownian motion which transports contrast agent molecules from a higher to a lower concentration area [1]. The diffusion coefficient (D_A) describes the mobility of certain molecules (A) in a given medium. Fick's law describes the flux of molecules (J_A) in a medium, *e.g.* cartilage, over a concentration gradient [173]:

$$J_A = -D_A \frac{\partial C}{\partial x} \tag{5.2}$$

If the initial concentration of molecule A in bath is C_b and zero in cartilage,

$$J_A = D_A \frac{C_b}{h}, \tag{5.3}$$

where h is the depth of cartilage. The concentration change due to diffusion can be described with the mass balance principle and equation 5.2:

$$\frac{\partial C}{\partial t} = -\frac{\partial}{\partial x} J_A = \frac{\partial}{\partial x} D_A \frac{\partial C}{\partial x} = D_A \frac{\partial^2 C}{\partial x^2}. \tag{5.4}$$

Table 5.1: Basic equations governing the diffusion of charged particles in a semi-permeable membrane.

Parameter/law	**Equation**	
Nernst equation	$\Delta\Psi = -\frac{RT}{zF} \ln \frac{[C]_1}{[C]_2}$	(5.5)
Donnan ratio	$r = \left(\frac{[C]_1}{[C]_2} \right)^{1/z}$	(5.6)
Membrane potential	$\Delta\Psi = -\frac{RT}{F} \ln r$	(5.7)

Subscripts 1 and 2 refer to the sides of the membrane.
$[C]$ = concentration of a given ion
R = the gas law constant
F = Faraday's constant
T = absolute temperature
Ψ = Membrane potential
z = valence of the ion

The Gibbs-Donnan theory describes the behavior of charged particles at a semi-permeable membrane. It refers to the observation that impermeable charged particles on one side of a semi-permeable membrane cause an imbalance in the distribution of mobile charged particles. The mobile ions diffuse through the membrane until an equilibrium is reached. At equilibrium, the distribution of ions is governed by the Nernst equation (eq. 5.5, Table 5.1) so that the electrical potential gradient is the same for all mobile ions. This can be reduced to the Donnan ratio (eq. 5.6, Table 5.1), which is generally the same for all mobile ion species. The membrane

potential can now be written in the form presented in equation 5.7 (Table 5.1). The presence of impermeable charged particles causes an osmotic gradient across the membrane [63].

Let us consider a simple situation with concentration C_1 of immobile anions (A^-), bound to sodium on one side of the membrane and concentration C_2 of potassium chloride on the other side. Both salts dissociate completely and the solute volumes are the same. The concentration gradients force ions to diffuse to the other side of the membrane, but the electronegativity is maintained. Let x, y and z be the number of moles of Na^+, K^+ and Cl^-, respectively, transported across the membrane. Now, according to equation 5.6,

$$\frac{[\mathrm{Na}]_1}{[\mathrm{Na}]_2} = \frac{[\mathrm{K}]_1}{[\mathrm{K}]_2} = \frac{[\mathrm{Cl}]_2}{[\mathrm{Cl}]_1}, \tag{5.8}$$

$$[\mathrm{Na}]_1 = C_1 - x, [\mathrm{K}]_1 = y, [\mathrm{Cl}]_1 = z, \tag{5.9}$$

$$[\mathrm{Na}]_2 = x, [\mathrm{K}]_2 = C_2 - y, [\mathrm{Cl}]_2 = C_2 - z \tag{5.10}$$

and due to the preservation of electronegativity, $x = y - z$, the equations above yield

$$\frac{C_1 - (y - z)}{y - z} = \frac{y}{C_2 - y} = \frac{C_2 - z}{z}, \tag{5.11}$$

which reduces to $C_2 = y + z$. Now it is possible to solve x, y and z:

$$x = \frac{C_1 C_2}{C_1 + 2C_2}; y = \frac{C_1 C_2 + C_2^2}{C_1 + 2C_2}; z = \frac{C_2^2}{C_1 + 2C_2}. \tag{5.12}$$

and finally the Donnan ratio:

$$r = \frac{[\mathrm{Na}]_1}{[\mathrm{Na}]_2} = \frac{[\mathrm{K}]_1}{[\mathrm{K}]_2} = \frac{[\mathrm{Cl}]_2}{[\mathrm{Cl}]_1} = \frac{C_1 + C_2}{C_2}.$$

The previous example demonstrates how the fixed charge can affect the partition of charged mobile particles; *i.e.* it repels the same charge and attracts the opposite charge. If there were other charged particles present, for example an anionic contrast agent, they would equilibrate according to the Donnan ratio which depends on the concentration of immobile ions (C_1) and the net concentration of

mobile ions with the same valence (C_2). The effect of the charge is also evident from equation 5.6; a greater charge of a mobile particle will lead to a larger concentration gradient across the membrane. The side with immobile charged particles has higher osmolarity due to the presence of counterions, and hence it draws in water. This phenomenon, called the Donnan effect, provides the swelling pressure which is crucial for the mechanical function of articular cartilage.

Contrast agent enhanced imaging of articular cartilage

The Gibbs-Donnan theory assumes free diffusion, complete dissociation of the molecules and equal fluid volumes on both sides of the membrane. Articular cartilage, however, cannot be considered to fulfill these assumptions. In articular cartilage, negatively charged proteoglycans are fixed in the tissue, attract cations and repel anions [173]. However, cartilage is anisotropic and heterogeneous and its permeability, water content and FCD vary as a function of tissue depth [163, 186]. Nonetheless, the Gibbs-Donnan theory is still a reasonable approximation of the behavior of charged particles in articular cartilage.

The reported correlations (r^2) between the dGEMRIC index and cartilage PG content range from 0.38 up to 0.98 [17, 202, 204, 275]. The dGEMRIC index has also been reported to depend on the mechanical properties and health of the cartilage [152,203,204,234,274, 284]. This index has been used successfully to follow the changes in patients with autologous chondrocyte transplants or OA [82,151, 218, 252, 256, 275, 284]. Most of the published studies did not include measurement of pre-contrast T_1 relaxation time; this was assumed to be constant. However, considerable variation has been reported in T_1, which increases the uncertainty in the dGEMRIC results [275]. The estimation of the contrast agent concentration is based on the change in T_1 and a constant relaxivity, specific to the contrast agent and tissue [17]. However, the relaxivity of the Gd-DTPA^{2-} depends on the macromolecular content of the tissue, which may further complicate the interpretation of the results [244].

Equilibration times from 2 to 12 hours have been used for *in vitro* samples [83,202,234]. However, the *in vivo* situation is more complicated due to metabolism and relatively rapid washout of the contrast agent. *In vivo*, the optimal delay between intravenous injection and MRI imaging has been reported to be about two hours [253]. In the case of intra-articular administration of the contrast agent, vasoconstrictive drugs can be used to slow down the washout from the joint. However, it is evident that *in vivo* the contrast agent may not reach the Gibbs-Donnan equilibrium and thus it is not reliable if one wishes to quantify the PG or FCD distribution in the cartilage.

Compared to the dGEMRIC technique, CECT of articular cartilage is a novel technique. It has been studied for about five years, but its results are promising. The contrast agent enhanced X-ray attenuation in articular cartilage has been reported to enhance morphological analysis and correlate with the PG content of healthy and enzymatically degenerated tissue [11, 213, 219, 242, 288, 289]. Furthermore, contrast agent enhanced X-ray attenuation has been shown to correlate with the Young's modulus of cartilage [11].

Even though dGEMRIC and CECT are analogous techniques, they have some fundamental differences. The dGEMRIC measures the fluid phase of the tissue, and the measurement gives an indirect estimation of the contrast agent concentration in the water compartment. CECT, on the other hand, measures the whole volume, which means that the fluid volume fraction affects the results. However, the contrast agent directly attenuates the X-rays (equation 5.1), which should make estimation of the contrast agent concentration more straightforward. MRI studies are more expensive, but do not expose the patient to ionizing radiation. On the other hand, pQCT devices may be used to scan peripheral locations with low radiation doses; in fact the effective radiation dose can be negligible. MRI provides good soft tissue contrast, even without contrast agents, but obtains virtually no signal from the bone tissue. CT, on the other hand, has been widely used for estimation of bone morphology and mineral density, but its ability to visualize soft tissues is poor. Both techniques may be used for qualitative detection

of degraded or injured cartilage but, for example, the reliability of quantitative measurement of PG or FCD needs to be viewed with caution.

6 Aims of the present study

The thesis focuses on development of CT and ultrasound techniques for simultaneous evaluation of articular cartilage and subchondral bone. Especially, the work aims to establish the basis of contrast agent enhanced computed tomography of articular cartilage with a clinical pQCT instrument.

The specific aims of this thesis were:

1. to investigate the feasibility of using gadopentetate and ioxaglate enhanced pQCT to detect enzymatically induced specific proteoglycan depletion in cartilage.

2. to assess the feasibility of using contrast agent enhanced computed tomography in the simultaneous measurement of articular cartilage and subchondral bone, and to investigate the relationships between the contrast agent intake and the mechanical properties of cartilage.

3. to numerically investigate the role of bone marrow composition on the propagation of ultrasound in trabecular bone.

4. to assess the feasibility of using 5 MHz pulse-echo ultrasound in the simultaneous measurement of articular cartilage and subchondral bone, and to investigate the relationships between QUS parameters and the composition and mechanical properties of cartilage.

7 Materials and methods

This thesis consists of four independent studies (I-IV). The microCT and DXA data used in study III was obtained from an earlier study by Hakulinen *et al.* [97]. The rest of the data is original. The studies II and IV are based on the same set of samples. The materials and methods used in the studies are summarized in Table 7.1. In this thesis, all data and images were analyzed with Matlab software (v. 6.0-7.4, The Mathworks Inc. Natick, MA, USA).

Table 7.1: Summary of materials and methods used in studies I - IV. All measurements were conducted at room temperature (typically 20 - 23 °C)

Study	Tissue	Species/Location	Material	Methods
I	cartilage	bovine patella	diffusion test, n=6 CECT, n=16	CECT, biochemical and histological analyses
II	cartilage and bone	bovine tibia	n=10	CECT, pQCT, 30 MHz US, indentation
III	bone	human femur, human tibia	n=7 n=4	microCT, DXA, FDTD simulation
IV	cartilage and bone	bovine tibia	n=10	5 MHz US, biochemical, biomechanical and histological analyses

CECT=contrast enhanced computed tomography, pQCT=peripheral quantitative computed tomography, US=ultrasound, microCT=X-ray microtomography, DXA=dual-energy X-ray absorptiometry, FDTD=finite difference time domain

7.1 SAMPLE PREPARATION

This thesis work includes osteochondral samples from bovine patellae and tibiae and trabecular bone cylinders from cadaveric human knees. The bovine knees were obtained from a local abattoir (Atria Oyj, Kuopio, Finland) and prepared within a few hours *post mortem*.

The human trabecular bone samples used in study III were prepared, scanned with microCT and measured with DXA for an earlier study [96]. In that study, cylindrical subchondral bone plugs (diameter 16 mm, height 8 mm) were drilled from femoral medial condyle, tibial medial plateau and femoral groove of human cadavers (National Authority for Medicolegal Affairs, Helsinki, Finland, permission 1781/32/200/01).

For study I, cylindrical osteochondral plugs were prepared from visually intact upper lateral quadrants of bovine patellae (diameter 18 mm). The rectangular medio-lateral samples (width 30 mm, length 50 mm and height 20 mm, Figure 7.1) for studies II and IV were cut from visually intact bovine medial tibial plateaus and the samples were divided into four medio-lateral regions for the measurements. All bovine samples were kept moist during the preparation and frozen in phosphate buffered saline (PBS) containing inhibitors of proteolytic enzymes (5 mM ethylenediaminetetraacetic acid and 5 mM benzamide hydrogen chloride) until thawing prior to the experiments. During the measurements, the samples were either immersed in PBS supplemented with the enzyme inhibitors (ultrasound and biomechanical measurements) or sealed in a container with a PBS-soaked swab (computed tomography).

Study I included enzymatic degradation of cartilage for simulation of typical early osteoarthritic changes in tissue composition. Trypsin (T 0646, Sigma Chemical Company, St. Louis, MO, USA) was used to cleave PGs with slight simultaneous degradation of the collagen network [101]. Phenylmethylsulfonyl fluoride (Sigma Chemical Company) was used to stop the trypsin digestion.

7.2 CONTRAST AGENT ENHANCED CT

Two contrast agents were used for the contrast agent enhanced CT measurements. Magnevist (Schering AG, Berlin, Germany) is a gadolinium ($Z = 64$) based MRI contrast agent that dissociates into (2^-) charged gadopentetate ($C_{14}H_{20}GdN_3O_{10}$, molecular mass 548 g/mol). The X-ray contrast agent Hexabrix (Mallinckrodt Inc.,

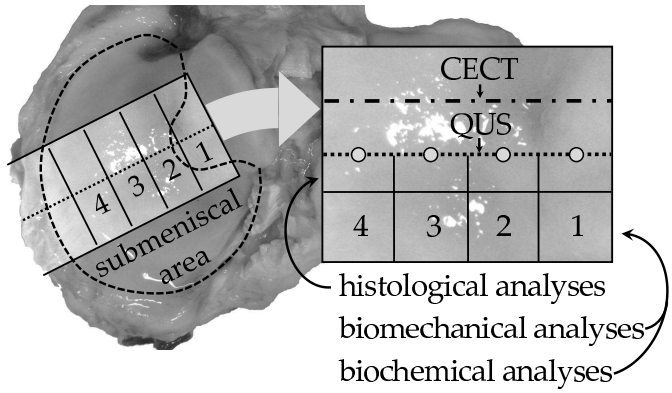

Figure 7.1: The sample preparation for the studies II and IV. The samples were cut from the medial tibial plateaus of bovine knees ($n = 10$). The ultrasound scan line is illustrated with the dotted line and the CECT slice with a dash-dot line. The edge of the meniscus is shown with the dashed line. For the biomechanical, biochemical and histological analyses, the samples were divided into four (1-4) locations in the medio-lateral direction. Circles show the sites of ArtScan measurements.

St. Louis, MO,USA) is an iodinated ($Z = 53$) dimer that consists of two salts, ioxaglate meglumine and ioxaglate sodium. Both salts dissociate into (1^-) charged ioxaglate ($C_{24}H_{21}I_6N_5O_8$, 1269 g/mol. A clinical pQCT device (XCT 2000, StraTec Medizintechnik GmbH, Pforzheim, Germany) was used for the imaging of the contrast agent enhanced samples. The thickness of the pQCT slice was 2.3 mm and the in-plane pixel size was 0.2×0.2 mm^2. The X-ray tube voltage was 58 kVp. The pQCT device has been designed for the measurement of bones and the X-ray absorption is calibrated to bone mineral density values, mg/cm^3. For the cartilage and bone samples, three frames (study I) or five frames (study II) were averaged to enhance the signal-to-noise ratio.

The interrelationships between the X-ray attenuation and concentrations of the contrast agents were investigated by measuring the absorption at four different concentrations between 0 to 210 mM for ioxaglate and 0 to 200 mM for gadopentetate. PBS was used as the solvent. The contrast agent concentrations used in the

subsequent studies were chosen based on this information so that the contrast enhancement would yield attenuation coefficient values similar to mean value of cartilage and bone. Time required for diffusion equilibrium was investigated with both contrast agents in normal and trypsin treated cartilage. The time points of the pQCT measurements were 0, 2, 4, 6, 8, 23, 25 and 27 hours of immersion in the contrast agent solution.

The effect of trypsin treatment on the distribution of the contrast agents (study I) was studied with eight osteochondral plugs per contrast agent. The samples were cut into two halves, one half was used as a control and the other was treated with trypsin. Next, the samples were immersed in the contrast agent solutions for 21 hours and scanned with the pQCT device. For the simultaneous measurement of articular cartilage and subchondral bone (study II), ten rectangular osteochondral samples were immersed in 21 mM ioxaglate solution for 35.5 hours. The pH and osmolarity of the contrast agent solution were adjusted to 7.4 and 310 mOsmol/l, respectively. After the contrast agent immersion, the samples were scanned with the pQCT device.

In study I, the contrast agent content of the cartilage was analyzed by converting the BMD values to concentration values using the calibration equation and subtracting the average pre-contrast BMD value of cartilage. The contrast agent concentration profiles were derived by averaging horizontal cartilage layers from the surface to bone interface. In study II, the sample specific X-ray absorption profiles prior to the contrast agent immersion were subtracted from the contrast agent enhanced profiles. This subtraction method is intended to leave only the signal due to the presence of the contrast agent. After the subtraction, the slope of the calibration equation was used to convert the BMD values into contrast agent concentration values. Moreover, the contrast agent concentration was normalized with the contrast agent concentration of the bath. The borderline voxels were discarded to minimize the partial volume effect. Study I investigated the contrast agent accumulation into full-thickness cartilage volume while study II focused on the

superficial layer of the cartilage.

Since the pQCT device quantifies the X-ray attenuation in bone mineral density values, analysis of the subchondral bone BMD is quite straightforward. The mineral density of the subchondral plate was analyzed from a 1 mm thick layer of bone below the articular cartilage. At each region, the subchondral bone was divided into subchondral plate and trabecular bone with a local threshold rule (75% of the maximum BMD). The BMD of the subchondral trabecular bone was calculated as the mean of a 10 mm thick region of interest immediately below the subchondral plate.

7.3 ACOUSTIC MEASUREMENTS

Acoustic properties of articular cartilage and bone were measured using an UltraPAC scanning acoustic system (Physical Acoustics Corporation, Princeton, NJ, USA). The system consists of a 0.5 to 100 MHz ultrasound pulser-receiver board and a 500 MHz 8-bit A/D board. The scanning drives allow an ultrasound transducer to be moved in 5.1 μm steps in a horizontal plane and 3.8 μm steps in a vertical direction. In study II, the UltraPAC system was used with a 30 MHz transducer to measure the thickness of cartilage at each measurement site, *i.e.* at the center of the region of interest. In study IV, a 5 MHz ultrasound transducer was used to measure the QUS parameters from cartilage and subchondral bone across the sample. In that study, the distance between the consecutive A-mode acquisitions was 150 μm. Both transducers were focused and their specifications are listed in Table 7.2.

Quantitative ultrasound parameters

Ultrasound parameters were determined using the pulse-echo technique (studies II - IV) and through-transmission technique (study III). Most of the QUS parameters applied in this work were calculated from the amplitude spectra of the signals. The amplitude spectrum provides information on the behavior of separate frequency components in the signal and can be achieved by converting

Table 7.2: Characteristics of the ultrasound transducers used in this thesis.

Transducer model (Panametrics)	V326	V307
Nominal central frequency (MHz)	30	5
Measured -6 dB frequency range (MHz)	17.8 - 40.9	3.2 - 6.7
Focal length (mm)	31.8	49.8
Focal zone (mm)	9.4	8.8
Element diameter (mm)	6.4	25.4
Confocal beam diameter (μm)	258	600
Study	II	IV

a time-domain signal into the frequency-domain using the Fourier transform.

In this study, the speed of sound (*SOS*) and ultrasound roughness index (*URI*) were the only parameters calculated in the time domain. *SOS* was determined from the through-transmission signal using the cross-correlation method [40], while *URI* was calculated from the pulse-echo signal as described by Saarakkala *et al.* (2004). The other parameters calculated from the TT measurements were the average attenuation (*AA*) and normalized broadband ultrasound attenuation (*nBUA*). The PE signal allowed calculation of the integrated reflection coefficient (*IRC*), apparent integrated backscatter (*AIB*) and broadband ultrasound backscatter (*BUB*). The mathematical definitions of the parameters are presented in Table 7.3.

7.4 ULTRASOUND SIMULATIONS

In study III, a sample-specific FDTD model was used to assess the effect of bone marrow on the propagation of ultrasound through trabecular bone. The wave propagation was simulated with the Wave 3000 Pro 2.2 software (CyberLogic Inc., New York, NY, USA), which solves the equation 4.17 within each homogenous grid element and computes the displacement vector at each time step of the simulation.

Table 7.3: Summary of the ultrasound parameters determined in the thesis.

Parameter	Equation	
$\alpha(f)$*	$10\log_{10}\left\langle \frac{\lvert A_w(f,z)\rvert^2}{\lvert A_s(f,z)\rvert^2} \right\rangle$	
SOS	$\frac{c_w \cdot x}{x-(\Delta t \cdot c_w)}$	[207]
URI	$\sqrt{\frac{1}{m}\sum_{i=1}^{m}\left(d_i - \langle d\rangle\right)^2}$	[232]
AA	$\frac{1}{\Delta f \cdot x}\int_{\Delta f}\alpha(f)df$	[225]
IRC	$\frac{1}{\Delta f}\int_{\Delta f} 10\log_{10}\left\langle \frac{\lvert A_n(f,x)\rvert^2}{\lvert A_r(f,x)\rvert^2} \right\rangle df$	[44]
AIB	$\frac{1}{\Delta f}\int_{\Delta f} 10\log_{10}\left\langle \frac{\lvert A_b(f,x)\rvert^2}{\lvert A_r(f,x)\rvert^2} \right\rangle df$	[44]
BUB	$\frac{1}{\Delta f}\int_{\Delta f}\left(10\log_{10}\left\langle \frac{\lvert A_b(f,x)\rvert^2}{\lvert A_r(f,x)\rvert^2} \right\rangle + \alpha(f)\cdot SOS \cdot t_w\right) df$	[198,229]

* Normalized broadband ultrasound attenuation (*nBUA*) is determined as the slope of the linear part of the attenuation spectrum, $\alpha(f)$, normalized according to the thickness of the sample.

c_w=the speed of sound in water, x=the thickness of the sample and Δt=time-of-flight difference through the water bath with and without the sample. m=number of measurement points, d=distance between the transducer and cartilage surface and $\langle ... \rangle$=spatial average. Δf=effective frequency range, $A(f,x)$=amplitude spectrum of a pulse recorded at distance x from the transducer and the indices s and w refer to through-transmission signals with and without the sample, respectively. Indices s and w refer to through-transmission signal through the water bath with and without the sample. Indices n, r and b refer to pulse-echo signals from the surface of the sample, surface of the perfect reflector and backscatter signal, respectively. t_w=the time difference between the echo from the sample surface and the center of the gated region.

The model geometry was constructed to simulate a realistic measurement setup applied in an earlier experimental study [96]. The simulation geometry included two focused 1 MHz transducers 10 cm apart in a water bath with the sample in the middle. This allowed calculation of both pulse-echo and through-transmission parameters. The input function was acquired by digitizing the signal of a real transducer (V302, GE Panametrics, Waltham, MA, USA) and fitting a Gaussian sine signal to it. The tissues, *i.e.* bone and bone marrow, were simplified to be homogeneous and have the acoustic properties of cortical bone and porcine fat, respectively. To simulate the effect of bone marrow composition, the simulations were repeated after substituting fat with water. The acoustic properties of the materials were acquired from the material library present in the simulation software.

The simulation job parameters were set as follows: time step scale = 0.9 and point/cycle ratio = 10. The resolving wavelength was set according to the pixel resolution of the model (*i.e.* to 0.90 and 0.72 mm). The mesh was created based on the resolving wavelength and the point/cycle ratio, resulting in 90 and 72 μm grids. The simulation time was set to 100 μs.

7.5 REFERENCE METHODS

Several reference methods were used to investigate the relationships between the contrast agent content, ultrasound parameters, structure and composition of the samples. The reference methods included biomechanical measurements, microCT imaging, DXA, biochemical and histological analyses.

Mechanical testing

The dynamic indentation stiffness of the cartilage (study II) was determined with an arthroscopic indentation instrument (ArtScan 200, ArtScan Oyj, Helsinki, Finland) optimized for the measurement of thin cartilage [170]. The diameter and length of the indenter were 0.6 mm and 0.14 mm, respectively. The instrument has been

described in more detail by Korhonen *et al.* [148]. The indenter force was recorded when the contact force of the reference plate reached 5 N and the final value for cartilage stiffness was determined as the average indenter force recorded in four consecutive measurements.

In study IV, the dynamic modulus and Young's modulus of the cartilage were determined with a custom made material testing device [258] equipped with a cylindrical plane-ended (diameter=1.13 mm) indenter. After applying a 12.5 kPa pre-strain, four stress-relaxation steps (strain 5%) were performed until equilibrium (relaxation time 900 s). The thickness of the cartilage at the indentation site was measured with the needle probe technique [129] and the information was used for calculation of the mechanical moduli. The dynamic modulus was calculated from the third stress-relaxation step and Young's modulus as the slope of equilibrium stress-strain curve fit to the last three stress-relaxation steps. The modulus values were calculated using an elastic isotropic model, according to Hayes *et al.* [105]. For calculation of the dynamic modulus of cartilage, the Poisson's ratio was assumed to be 0.5 (*i.e.* dynamically incompressible [172]), while at equilibrium the Poisson's ratio was set to 0.1 [260].

X-ray methods

In study III, the trabecular bone samples were imaged with a microCT device (SkyScan 1072, SkyScan, Aartselaar, Belgium) with an isotropic voxel size of 18 μm [97]. The stacks of cross-sectional images were segmented with the local threshold method [268]. The following morphometric parameters were determined from the 3D datasets using the software provided with the instrument: bone volume (*BV*), total sample volume (*TV*), bone surface area (*BS*), bone volume fraction (*BV/TV*), bone-specific surface (*BS/BV*), mean trabecular thickness (*Tb.Th*), mean trabecular separation (*Tb.Sp*), structural model index (*SMI*), connectivity and degree of architectural anisotropy (DA) [215]. A direct 3D analysis, without model assumptions on the trabecular structure, was used to calculate the trabecular thickness and separation [106].

Bone mineral density of the above mentioned trabecular bone samples was measured with DXA (Lunar Prodigy, GE Medical, Wessling, Germany) using the anterior-posterior spine measurement protocol. The samples were placed in a water bath, which represented soft tissue, to optimize the accuracy of the measurement. The volumetric BMD was calculated by dividing the measured areal BMD value with the sample thickness. [96]

Histological and biochemical analyses

After the measurements in studies I, II and IV, a tissue region as close to the measurement site as possible was prepared for biochemical and histological analyses. Biochemical analyses were used to determine the contents of water, proteoglycans and collagen in the cartilage. The PG content was estimated by quantifying the amount of uronic acid in the tissue [23] and normalizing it according to the wet weight of the sample. To estimate the collagen content of the samples, a spectrophotometric assay for hydroxyproline was performed after hydrolysis of the freeze-dried and papain digested tissue [28]. Hydroxyproline contents were normalized against the wet weights of the samples. Safranin-O stained microscopic sections (thickness 3 μm) were prepared for qualitative histological imaging of the spatial PG distribution [142] and imaged in an optical microscope equipped with a CCD camera (Nikon Microphot FXA and Nikon CoolSNAP, Nikon Corporation, Tokyo, Japan).

7.6 STATISTICAL ANALYSES

The Wilcoxon signed ranks test was used for statistical comparison of the contrast agent content in untreated and enzymatically degraded cartilage in study I and to study the effect of bone marrow composition on the ultrasound parameters in study III. The Pearson's correlation coefficient was used for the correlation analyses in study I. In studies II-IV, the normality of the data was examined with the Shapiro-Wilk test and the Spearman's rho was used for the

correlation analyses. The Kruskal-Wallis *post hoc* test was used in study II, and Friedman's *post hoc* test in study IV, to test the statistical significance of the differences in parameter values between the measurement sites. The statistical analyses were conducted using the SPSS software (v. 11.5-14, SPSS Inc., Chicago, IL, USA), Matlab (v. 6.0-7.4, Mathworks Inc., Natick, MA, USA) and the R Statistical Software version 2.11.1 (R Foundation for Statistical Computing, Vienna, Austria).

8 Results

This chapter summarizes the most important results of studies I - IV and contains some unpublished data. The complete results are presented in the original studies I - IV.

8.1 CONTRAST AGENT ENHANCED CT OF CARTILAGE AND BONE

Study I investigated the effect of enzymatic proteoglycan depletion on the contrast agent partitioning in articular cartilage. Additionally, the effect of contrast agent concentration on the X-ray attenuation and the time required for the contrast agent to reach the diffusion equilibrium in articular cartilage were evaluated. The X-ray attenuation was found to depend linearly on the concentration of both contrast agents ($r = 1.00$, $p < 0.01$). Appropriate contrast agent concentrations were chosen to provide attenuation coefficient values similar to the mean value of cartilage and bone, *i.e.* 21 mM and 200 mM for ioxaglate and gadopentetate, respectively. Both contrast agents required over 8 hours to reach diffusion equilibria in articular cartilage. Immersion times lasting over 20 hours were chosen to ensure that diffusion equilibrium had been attained. Trypsin treatment led to faster contrast agent intake and increased contrast agent content at equilibrium.

After 21 hours of immersion in the contrast agent, gadopentetate partitioned to $50 \pm 2\%$ and ioxaglate to $60 \pm 4\%$ of the bath concentration in healthy articular cartilage from bovine patella. Trypsin digestion cleaved 70% of the uronic acid and evoked a 4% increase in the water content. The digestion caused the equilibrium partition to rise to $66 \pm 2\%$ for gadopentetate and to $89 \pm 6\%$ for ioxaglate. The effect of trypsin treatment was statistically significant ($p = 0.012$) for uronic acid and water contents and partitions of both contrast agents. The depletion of proteoglycans caused only minor changes in the shape of the contrast agent profiles (Figure 8.1).

Statistically significant correlations were found between the equilibrium partitions of ioxaglate and gadopentetate and the uronic acid and water contents of the tissue (Table 8.1).

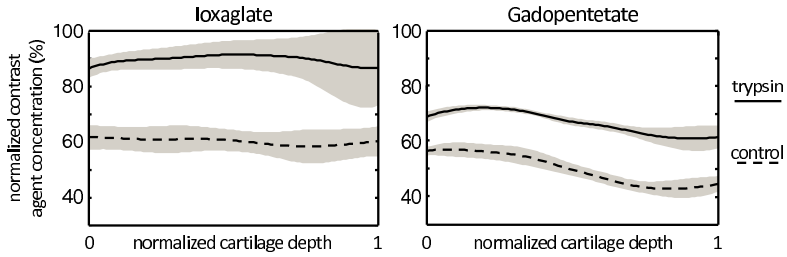

Figure 8.1: Contrast agent partitions as a function of tissue depth. Trypsin treatment increased the amount of contrast agent in the cartilage, but had only a minor effect on the depthwise distribution of the contrast agents. The gray area indicates the standard deviation.

Table 8.1: Linear correlation coefficients between the contrast agent contents and cartilage composition. In study I, the equilibrium partitions of ioxaglate and gadopentetate were found to correlate with the uronic acid and water contents in the tissue.

	***UA/ww* (μg/mg)**	***UA/dw* (μg/mg)**	**Water**
Ioxaglate			
Control ($n = 8$)	-0.75*	-0.80*	0.55
All ($n = 16$)	-0.94**	-0.97**	0.58*
Gadopentetate			
Control ($n = 8$)	-0.73*	-0.70*	0.43
All ($n = 16$)	-0.95**	-0.98**	0.65**

** $p < 0.01$, * $p < 0.05$

UA/ww = uronic acid per wet weight, *UA/dw* = uronic acid per dry weight

Study II investigated the partitioning of ioxaglate in healthy cartilage from the bovine medial tibial plateau and the interrelationships between the partition of the contrast agent and the composition and mechanical properties of the tissue. Moreover, the feasibility of the CECT method for the simultaneous analysis of artic-

ular cartilage and subchondral bone was assessed. In this study, ioxaglate partitioned to $48 \pm 2\%$ after 35.5 hours of immersion. The average contrast agent content in the full-thickness cartilage correlated significantly ($p < 0.01$) only with the uronic acid content of the tissue (Table 8.2). The superficial contrast agent content, however, displayed significant correlations ($p < 0.01$) with the uronic acid, hydroxyproline and water contents, as well as with the mechanical moduli and thickness of cartilage.

At the medial tibial plateau, the average *BMD*s of the subchondral plate and subchondral trabecular bone were 826 ± 51 mg/cm^3 and 576 ± 55 mg/cm^3, respectively. The average thickness of the subchondral plate at medial tibial plateau was 2.7 ± 1.3 mm.

8.2 SIMULTANEOUS ULTRASOUND MEASUREMENT OF CARTILAGE AND BONE

Study IV assessed the feasibility of using 5 MHz pulse-echo ultrasound for the simultaneous measurement of articular cartilage and subchondral bone. Moreover, the relationships between the QUS parameters and the composition and mechanical properties of cartilage were investigated. Pulse-echo measurements across the medial tibial plateau yielded the following average values and standard deviations for the QUS parameters. The *IRC* for the cartilage surface was -42 ± 6 dB, *AIB* for the internal cartilage was -70 ± 5 dB and the *URI* was 42 ± 33 μm. The average inclination of the cartilage surface, calculated from the time-of-flight information, was 4.6 ± 3.0 degrees. The *IRC* for the cartilage-bone interface was -25 ± 6 dB, *AIB* for the subchondral bone was -36 ± 4 dB and the inclination of the cartilage-bone interface was 5.9 ± 3.2 degrees.

AIB of the internal cartilage correlated significantly ($p < 0.01$) with the hydroxyproline and water contents as well as with the dynamic modulus and thickness of the cartilage, whereas *URI* correlated with the water content, the mechanical moduli and the thickness of the cartilage (Table 8.2). *AIB* of the subchondral bone exhibited a weak but statistically significant ($p < 0.05$) correlation with

Table 8.2: Correlation coefficients between the CECT, QUS and reference parameters. Superficial contrast agent content correlated significantly with the composition and mechanical properties of the cartilage. Ultrasound parameters did not correlate with the uronic acid content, but ultrasound backscatter from internal cartilage correlated with the hydroxyproline and water contents, dynamic modulus and thickness of the cartilage. Cartilage surface roughness, measured with ultrasound, correlated with the water content, mechanical moduli and thickness of the cartilage. Ultrasound backscatter from the subchondral bone had a weak but statistically significant correlation with the BMD *of the subchondral plate.*

	UA	***Hypro***	***Water***	$\boldsymbol{E}_{ArtScan}$	$\boldsymbol{E}_{dyn}$	$\boldsymbol{E}_{Young}$	$\boldsymbol{Th}_{cart}$	$\boldsymbol{Th}_{plate}$	$\boldsymbol{BMD}_{plate}$	$\boldsymbol{BMD}_{trab}$
$CECT_s$	-0.52**	-0.62**	0.63**	-0.80**	-0.71**	-0.67**	0.69**	0.49**	0.16	0.14
$CECT_f$	-0.41**	-0.03	0.20	-0.26	-0.10	-0.29	0.03	0.30	0.08	-0.02
$^{a}AIB_{cart}$	0.01	0.58**	-0.52**	0.46**	0.57**	0.16	-0.55**	-0.15	-0.11	-0.20
$^{a}IRC_{cart}$	-0.13	-0.16	0.16	-0.09	-0.05	-0.06	0.10	-0.30	0.14	-0.36*
^{a}URI	-0.28	-0.29	0.47**	-0.49**	-0.49**	-0.41**	0.56**	0.14	0.08	0.09
$^{b}AIB_{bone}$	0.24	0.00	-0.01	0.03	-0.06	0.04	–	0.04	-0.34*	-0.05
$^{b}IRC_{bone}$	0.02	-0.02	0.18	-0.11	-0.29	-0.21	–	0.05	0.09	-0.05

** $p < 0.01$, * $p < 0.05$

[a] Partial correlation with inclination of the cartilage surface as the controlling parameter.

[b] Partial correlation with inclinations of the cartilage and bone surfaces and the thickness of the cartilage as the controlling parameters.

$CECT_s$=superficial contrast agent content, $CECT_f$=full-thickness contrast agent content, AIB=apparent integrated backscatter, IRC=integrated reflection coefficient, URI=ultrasound roughness index, UA=uronic acid, $Hypro$=hydroxyproline, $E_{ArtScan}$=dynamic modulus measured with ArtScan, E_{dyn}=dynamic modulus, E_{Young}=Young's modulus, Th=thickness, BMD_{plate}=bone mineral density of the subchondral plate, BMD_{trab}=bone mineral density of the subchondral trabecular bone

the *BMD* of the subchondral plate. *IRC*s of the cartilage or bone surfaces were not found to correlate with the corresponding reference parameters.

8.3 THE EFFECT OF BONE MARROW COMPOSITION ON THE ACOUSTIC PROPERTIES OF TRABECULAR BONE

In study III, FDTD simulations were used to estimate the effect of bone marrow composition on the ultrasound propagation in trabecular bone. In the samples with fatty bone marrow, the simulations revealed significant correlations between the QUS parameters and the bone volume fraction ($n = 11$). Spearman's correlation was statistically significant between *BV/TV* and *SOS* ($r = 0.94$, $p < 0.01$) and *IRC* ($r = 0.91$, $p < 0.01$). *nBUA* and *AA* seemed to depend nonlinearly on the *BV/TV* (quadratic fit, $r = 0.77$, $p < 0.05$ and $r = 0.89$, $p < 0.01$, respectively). Substitution of bone marrow with water had only a minor effect on the ability of the QUS parameters to predict *BV/TV* or *BMD*.

Replacement of fatty bone marrow with water increased the speed of sound and ultrasound backscattering significantly ($p < 0.01$) while ultrasound attenuation and reflection from the sample surface were significantly ($p < 0.01$) decreased (Table 8.3). Substitution of the bone marrow with water affected the QUS parameters by 0-20%, depending on the bone volume fraction of the sample. For *SOS*, *AA* and *IRC*, the change was greater in the samples with low *BV/TV*.

The effect of bone marrow composition was studied using three-dimensional FDTD simulations. The voxel size of the FDTD mesh was found to significantly affect the fine structure of the samples and the results of the simulations ($n = 5$). In particular, *AA* and *nBUA* ($r = 1.00$, $p < 0.01$), *IRC* ($r = 0.90$, $p < 0.05$) and *AIB* ($r = 0.90$, $p < 0.05$) displayed strong associations with the voxel size.

Table 8.3: The effect of bone marrow composition on the QUS parameters. Simulations with fat or water as bone marrow demonstrated a statistically significant interaction between the bone marrow composition and the ultrasound parameters. AIB *was the only parameter that was not affected by the change in bone marrow composition.*

	fat	**water**	**change**
SOS (m/s)	1976 ± 282	1989 ± 278	0.7% **
nBUA (dB/cm/MHz)	48.7 ± 14.8	44.1 ± 11.9	8.5% **
AA (dB/cm)	30.2 ± 4.6	27.9 ± 4.6	7.8% **
IRC (dB)	-19.6 ± 4.9	-17.1 ± 3.3	11.7% **
AIB (dB)	-35.6 ± 2.7	-35.7 ± 2.8	0.5%
BUB (dB)	-29.2 ± 3.4	-29.9 ± 3.4	2.2% **

** $p < 0.01$, * $p < 0.05$

SOS=speed of sound, *nBUA*=normalized broadband ultrasound attenuation, *AA*=average attenuation, *IRC*=integrated reflection coefficient, *AIB*=apparent integrated backscatter, *BUB*=broadband ultrasound backscatter

8.4 TOPOGRAPHICAL VARIATION IN THE PROPERTIES OF CARTILAGE AND BONE

In studies II and IV, the composition, mechanical properties, contrast agent partition and QUS parameters were mapped across the medial tibial plateau of bovine knees (Figure 8.2). Cartilage near the center of the joint (lateral side, location 1) was thicker, contained less proteoglycans and collagen, had a higher water content and exhibited lower values of mechanical moduli (Table 8.4). The contrast agent content, especially in the superficial cartilage, increased towards the center of the joint. Ultrasound roughness index was higher and the backscatter lower in the lateral side of the medial tibial plateau. Moreover, ultrasound reflection from the cartilage-bone interface and backscatter from the subchondral bone were lower in the lateral side of the medial tibial plateau.

The contents of uronic acid, hydroxyproline and water, as well as the thickness, dynamic modulus and Young's modulus varied statistically significantly ($p < 0.01$) across the medial tibial plateau (Table 8.5). The concentration of contrast agent in the superficial

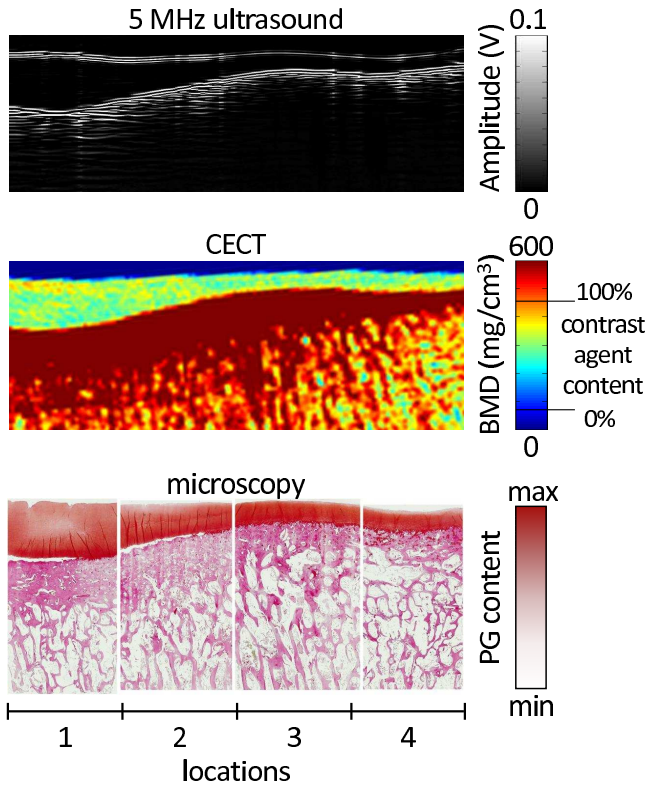

Figure 8.2: Ultrasound image, CECT image and histological sections of a medial tibial plateau. Both CECT and QUS methods reveal the shapes of the cartilage and bone surfaces and the thickness of the cartilage layer.

cartilage was more sensitive to this compositional and structural variation as compared to the mean contrast agent content in full-thickness cartilage. Ultrasound backscatter from the internal cartilage varied also significantly, while no statistically significant variation was observed for the ultrasound reflection from the surface of the cartilage. The ultrasound roughness index was significantly different only between locations 1 and 3. The bone mineral densities of the subchondral plate ($p < 0.05$) and subchondral trabecular bone ($p < 0.01$) were found to vary significantly across the medial tibial plateau.

In studies II and IV, the thickness of the cartilage was determined with four different methods; CECT, 5 MHz ultrasound, 30 MHz ultrasound and the needle probe technique. Compared to the needle probe method, CECT underestimated the thickness by 0.2 mm (9.3 %) on average. The correlation between needle probe and CECT methods was $r = 0.87$ $(p < 0.01)$. 5 MHz and 30 MHz ultrasound overestimated the thickness by 15.8% and 12.3%, respectively and their correlations with the needle probe method were $r = 0.89$ and $r = 0.88$, respectively.

Table 8.4: The mean values and standard deviations of all parameters determined in studies II and IV at locations 1-4. The variation across the medial tibial plateau was statistically significant (Table 8.5) for most of the parameters.

Location	**1**	**2**	**3**	**4**
CT parameters				
$CECT_s$ (%)	60 ± 4	57 ± 4	50 ± 3	49 ± 3
$CECT_f$ (%)	50 ± 2	49 ± 3	47 ± 2	48 ± 3
BMD_{plate} (mg/cm^3)	870 ± 53	882 ± 49	883 ± 58	820 ± 87
BMD_{trab} (mg/cm^3)	483 ± 42	534 ± 59	536 ± 47	457 ± 36
Th_{plate} (mm)	3.3 ± 0.9	3.5 ± 1.1	3.0 ± 0.5	1.8 ± 0.9
ultrasound parameters				
IRC_{cart} (dB)	-42 ± 7	-41 ± 5	-41 ± 8	-42 ± 5
AIB_{cart} (dB)	-72 ± 3	-73 ± 4	-70 ± 6	-65 ± 5
URI (μm)	70 ± 46	33 ± 20	30 ± 20	35 ± 25
IRC_{bone} (dB)	-32 ± 7	-25 ± 4	-22 ± 4	-23 ± 3
AIB_{bone} (dB)	-40 ± 4	-36 ± 3	-34 ± 2	-34 ± 2
reference parameters				
UA/ww (μg/mg)	4.5 ± 0.7	5.0 ± 0.9	6.5 ± 0.9	5.4 ± 1.4
$Hypro$ (μg/mg)	6.6 ± 1.6	7.8 ± 1.1	10.2 ± 0.9	12.1 ± 2.8
$Water$ (%)	89 ± 1	87 ± 2	84 ± 1	84 ± 1
Th_{cart} (mm)	3.1 ± 0.4	2.2 ± 0.4	1.6 ± 0.4	1.0 ± 0.2
$E_{ArtScan}$ (MPa)	4.2 ± 0.7	8.2 ± 3.1	21.5 ± 4.1	23.7 ± 2.5
E_{Dyn} (MPa)	0.4 ± 0.2	1.2 ± 0.9	4.1 ± 2.4	7.7 ± 2.8
E_{Young} (MPa)	0.2 ± 0.0	0.3 ± 0.2	0.9 ± 0.2	0.7 ± 0.3

$CECT_s$=superficial contrast agent content, $CECT_f$=full-thickness contrast agent content, BMD_{plate}=bone mineral density of the subchondral plate, BMD_{trab}=bone mineral density of the subchondral trabecular bone, Th=thickness, IRC=integrated reflection coefficient, AIB=apparent integrated backscatter, URI=ultrasound roughness index, UA/ww=uronic acid content per wet weight, $Hypro$=hydroxyproline, $E_{ArtScan}$=dynamic modulus measured with ArtScan, E_{dyn}=dynamic modulus, E_{Young}=Young's modulus

Table 8.5: Statistical significance (p-values, Friedman's post hoc *test) of the topographical variation in the properties of cartilage and subchondral bone between the measurement locations. Only p-values < 0.05 are shown.*

Parameter	**all**	**1-2**	**1-3**	**1-4**	**2-3**	**2-4**	**3-4**
CT parameters							
$CECT_s$	0.000	–	0.001	0.000	0.046	0.028	–
$CECT_f$	0.029	–	0.028	–	–	–	–
BMD_{plate}	0.029	–	–	–	–	0.028	0.046
BMD_{trab}	0.006	0.028	0.047	–	–	0.005	0.010
Th_{plate}	0.003	–	–	0.029	–	0.003	–
ultrasound parameters							
AIB_{cart}	0.000	–	–	0.017	–	0.000	0.029
IRC_{cart}	–	–	–	–	–	–	–
URI	0.046	–	0.046	–	–	–	–
AIB_{bone}	0.000	–	0.002	0.000	–	–	–
IRC_{bone}	0.000	–	0.000	0.005	0.046	–	–
reference parameters							
UA	0.001	–	0.001	–	0.046	–	–
$Hypro$	0.003	–	0.010	0.003	0.029	0.010	–
$Water$	0.000	–	0.003	0.000	–	–	–
$Thickness$	0.000	–	0.002	0.000	–	0.005	–
$E_{ArtScan}$	0.000	–	0.000	0.000	–	0.017	–
E_{Dyn}	0.000	–	0.001	0.000	–	0.006	–
E_{Young}	0.000	–	0.000	0.005	0.046	–	–

$CECT_s$=superficial contrast agent content, $CECT_f$=full-thickness contrast agent content, BMD_{plate}=bone mineral density of the subchondral plate, BMD_{trab}=bone mineral density of the subchondral trabecular bone, Th=thickness, IRC=integrated reflection coefficient, AIB=apparent integrated backscatter, URI=ultrasound roughness index, UA/ww=uronic acid content per wet weight, $Hypro$=hydroxyproline, $E_{ArtScan}$=dynamic modulus measured with ArtScan, E_{dyn}=dynamic modulus, E_{Young}=Young's modulus

9 Discussion

In this thesis, contrast agent enhanced computed tomography and quantitative ultrasound were applied to examine the properties of articular cartilage and subchondral bone. Study I investigated the ability of contrast agent enhanced computed tomography to detect enzymatically induced proteoglycan loss in articular cartilage. Two contrast agents, ioxaglate and gadopentetate, were studied and compared. Study II assessed the feasibility of using CECT in the simultaneous measurement of articular cartilage and subchondral bone. In study III, FDTD simulations were used to investigate the effect of bone marrow composition on ultrasound propagation in trabecular bone. Study IV investigated the potential of 5 MHz ultrasound for undertaking a simultaneous evaluation of articular cartilage and subchondral bone.

9.1 CONTRAST AGENT ENHANCED COMPUTED TOMOGRAPHY OF CARTILAGE AND BONE

Penetration of both ioxaglate and gadopentetate increased significantly after trypsin-induced PG loss (Table 8.1). Thus, both contrast agents were able to detect enzymatic PG loss. In healthy articular cartilage, the PG content is typically lower in the superficial cartilage and increases as one proceeds towards the deep zone. The FCD of the tissue arises from the negatively charged PG and anionic contrast agents are assumed to distribute inversely to the distribution of FCD in the tissue [17]. In study I, the equilibrium partition of gadopentetate in intact cartilage followed this assumption. However, enzymatic PG digestion had only a minor effect on the shape of the partition profiles (Figure 8.1) even though 70% of the PG was cleaved. Ioxaglate, on the other hand, distributed almost evenly in healthy cartilage and, again, PG digestion did not significantly alter the depthwise distribution of this contrast agent. These results suggest that the FCD is not the only factor controlling the distribution

of anionic contrast agents. The present results demonstrate that the contrast agent content in superficial cartilage is also related to the collagen and water contents within the tissue (Table 8.2). However, the uronic acid content was the only parameter that correlated significantly with the contrast agent concentration in the full-thickness cartilage.

In study II, only the contrast agent concentration in the superficial cartilage was found to correlate with the dynamic modulus of cartilage, which is in line with the dGEMRIC study of Samosky et al [234]. A mechanical indenter produces tensile, compressive and shear stresses in cartilage. The collagen architecture dominates the tensile behavior while the PG content is responsible for the compressive behavior. In indentation geometry, the properties of the superficial tissue control its mechanical response [149]. In addition to the dynamic modulus, the superficial contrast agent content correlated also with the Young's modulus and thickness of the cartilage.

In study I, the immersion time required for contrast agent diffusion to reach equilibrium was found to exceed 8 h. According to Fick's laws of diffusion, the time to reach the diffusion equilibrium depends on the square of the thickness of the cartilage [54]. Human articular cartilage is typically thicker than bovine cartilage, which further increases the time required for reaching diffusion equilibrium. Long immersion times, like those used in the present studies, are obviously not applicable in clinical studies. *In vivo* the contrast agent intake in the cartilage may be enhanced by fluid flow associated with dynamic joint loading [37]. However, due to contrast agent washout from the joint, the peak contrast agent content in the cartilage is reached within few hours after an intravenous contrast agent injection [252]. In the case of intra-articular injection, the peak contrast agent content in cartilage may be reached even more rapidly which means that the Gibbs-Donnan equilibrium cannot be attained. Hence, direct quantification of the FCD and PG content may not be possible *in vivo*. Ioxaglate and gadopentetate are hypertonic contrast agents that in high concentrations diminish

the swelling pressure in cartilage and temporarily soften the tissue. Mechanical loading of softened cartilage may cause damage to the tissue and this risk will need to be considered carefully [261].

Depletion of proteoglycans has been reported to increase the diffusion of large neutral molecules, while diffusion of small neutral molecules remained unaffected [36,174,255]. This indicates that increased porosity due to PG cleavage increases the permeability of cartilage. If the partition of a contrast agent were to depend solely on the charge of the molecule, the electroneutral molecules should diffuse evenly into the water phase of cartilage. Experimental results, however, do not support this hypothesis [290]. Solutes ranging from free ions to large molecules have been reported to diffuse faster into degenerated cartilage [70,175]. Recent findings indicate that very small molecules, *e.g.* free iodine, penetrate quickly into the cartilage but are less sensitive to the integrity of cartilage [146]. Collagen and water contents and their distributions together with the tissue pore size and fixed charge density may effectively control the penetration of the contrast agent. Measurement of spatial contrast agent diffusion rate or flux could represent a feasible way to evaluate the integrity of the tissue. This might be a more feasible way to apply the CECT method *in vivo*, as it could be measured at early time points with no need to reach the Gibbs-Donnan equilibrium.

The present findings suggest that anionic contrast agents may not be optimal for quantitative spatial determination of PG concentration. However, they may be suitable for diagnosing cartilage degradation since there was significantly greater penetration of contrast agents into damaged tissue. In addition to the PG loss, also the loss of integrity of the cartilage structure and collagen network increase the penetration of the contrast agents [146]. Although further studies are needed to verify the *in vivo* feasibility of using CECT to assess the condition of articular cartilage, it is tempting to speculate that CECT could provide a cheap and minimally invasive means to simultaneously assess the integrity of articular cartilage and subchondral bone in patients with a suspected joint disease or an acute

cartilage injury.

Contrast agent enhanced pQCT is a minimally invasive method. The effective radiation dose of one pQCT cross-section is less than 2 μSv. However, intra-articular contrast agent injection would probably be needed to achieve a high enough contrast agent concentration into the cartilage. The related risks, for example infection, need to be low enough if the method is to gain acceptance as a cheap and straightforward means to assess the status of articular cartilage *in vivo*. The gadopentetate concentration applied in study I was about a hundred times higher than that used in clinical MRI with dGEMRIC, and would be too high for *in vivo* use. Ioxaglate, however, is a suitable contrast agent for *in vivo* CECT of articular cartilage as the maximum dose of 4 ml/kg would be more than enough if administered intra-articularly.

CT devices are already used clinically to measure BMD, morphology and thickness of cortical bone. Therefore, simultaneous measurement of articular cartilage and subchondral bone should be straightforward. The OA induced changes in the knee BMD have been reported to be detectable with a quantitative CT [19,124]. Modern clinical CT technology is capable of producing isotropic voxels down to 100 μm, which would allow three-dimensional visualization of the morphology and quantification of the properties of articular cartilage and subchondral bone.

9.2 SIMULTANEOUS ULTRASOUND ANALYSIS OF CARTILAGE AND BONE

Pulse-echo QUS measurement at 5 MHz was a feasible method to simultaneously assess the acoustic properties of articular cartilage and subchondral bone (study IV). The backscatter signal from the internal cartilage correlated with the water content, mechanical properties, thickness and especially with the collagen content of the cartilage (Table 8.2). This is in line with an earlier study using 50 MHz ultrasound [45]. Furthermore, ultrasound backscatter from the subchondral bone correlated with *BMD*, which is consistent

with the findings where ultrasound frequencies of up to 7.5 MHz were used [96, 110]. *URI* was related to water content, thickness and mechanical properties of the tissue. An association between *URI* and mechanical properties has been previously reported using 20 MHz ultrasound [231]. However, the presently reported *URI* values are larger than the values in the literature, probably due to the natural curvature of the samples. Inclination in the sample surface is known to lead to an overestimation of the *URI* [131].

AIB and *URI* seemed to be rather insensitive, while *IRC* is known to be highly sensitive, to the angle of incidence of the ultrasound pulse [131, 282]. The natural curvature of the samples may hence explain the lack of significant correlations between the reflection parameters and the reference parameters. Overall, the correlations in study IV are lower than those generally reported in the literature. In most of the previous *in vitro* studies, the cartilage surfaces have been carefully adjusted to be perpendicular to the incidence of the ultrasound beam. Such adjustment, however, was impossible in the present study due to the large sample size, scan length and natural curvature of the tibial plateau. The same problem can be seen in the bone ultrasound measurements. *In vitro* studies often include bone samples with perfectly flat surfaces and no cortical layer. *In vivo* ultrasound measurements, however, have to deal with uneven surfaces and a cortical layer of uneven thickness, which has been shown to reduce the accuracy of ultrasound measurements [159, 161, 287]. Uneven, non-parallel cartilage and bone surfaces compromise quantitative measurements. This fact needs to be carefully considered when designing clinical ultrasound measurements.

The present results provide signposts for the direction to which quantitative ultrasound techniques need to be developed. It is essential to eliminate the effects of overlying tissue layers and variation in the angles of incidence of the ultrasound pulse at reflecting interfaces if one wishes to make a reliable quantification of the reflection and backscatter parameters. Therefore, further studies and innovative approaches are needed to optimize the measurement

protocol and minimize the effect of overlying tissue layers. For example, application of a rotating ultrasound catheter [116, 266] or a convex array transducer could diminish some of the error sources related to the curvature of the structures. For such transducers, there would always be a point where the surface is perpendicular to the ultrasound beam. The ultrasound frequency (40 MHz) of the catheter used by Virén *et al.* (2009) is probably too high for ultrasound measurement of bone through a layer of cartilage. Fortunately, ultrasound catheters are commercially available, for example, at a 9 MHz frequency, which might be a more feasible frequency for use in the simultaneous measurement of articular cartilage and subchondral bone *in vivo*.

9.3 THE EFFECT OF BONE MARROW COMPOSITION ON ULTRASOUND PROPAGATION IN TRABECULAR BONE

The FDTD simulations (study III) revealed a major effect of bone marrow composition on the ultrasound propagation in trabecular bone (Table 8.3). In the simulations, *SOS* and *IRC* increased and ultrasound attenuation decreased when the fatty bone marrow was replaced with water. This result was expected because *SOS* is known to be lower and ultrasound attenuation higher in fat than in water. Further, *BUB* decreased and *IRC* increased when the bone marrow was replaced with water. In general, the contribution of bone marrow to the acoustic properties was stronger in those samples with a low bone volume fraction, apparently because of a larger volume of substituted bone marrow. The simulations agreed with an earlier experimental finding that the impact of bone marrow is especially strong in bone with low density and a low bone volume fraction [198]. A change in the composition of bone marrow did not affect the ability of the QUS parameters to predict *BMD* or bone volume fraction, but evoked systematic effects on the values of the QUS parameters. This may be explained by fixed properties of bone marrow in the simulations. In reality, significant site, disease, race, gender and individual-dependent variations exist in the prop-

erties of bone marrow. Obviously, the variation in the composition of bone marrow may reduce the ability of QUS measurements to predict BMD [198].

Earlier theoretical and experimental studies have demonstrated the nonlinearity between scattering, *BUA* and bone volume fraction [99, 109, 199, 238, 248, 259]. In the present study, this nonlinear behavior was, for the first time, verified with the FDTD model. Moreover, also *AA*, *AIB* and *BUB* seemed to exhibit a nonlinear relationship with the *BV/TV*. When the bone marrow was replaced with water, the change in *nBUA* and *AA* showed a nonlinear dependency with the *BV/TV*.

The selected voxel size of the FDTD mesh had a significant effect on the results of the simulations. Since the effect of downsampling varied between the QUS parameters, the sensitivity of the QUS parameters to structural changes may vary. *AA* and *nBUA* were the most sensitive parameters to detect small structural changes due to downsampling, while the change in *SOS* was minimal. In order to enable realistic requirements of memory usage and processor time, the voxel size cannot be as small as in the original microCT images. As the downsampled geometry does not perfectly match the real geometry, the simulations are not fully comparable with the experimental measurements of the same samples. Nonetheless, we believe that the investigation of the effect of bone marrow composition on the ultrasound properties is valid as the trabecular structure was kept constant. This is supported by the similar effect of bone marrow on the ultrasound parameters with voxel sizes of 72 and 90 μm. Furthermore, this approach is supported by the consistency of the present simulations with earlier experimental results [6, 198].

9.4 TOPOGRAPHICAL VARIATION IN THE PROPERTIES OF CARTILAGE AND BONE

The thickness, composition and mechanical properties of cartilage varied significantly across the tibial plateau (Tables 8.4 and 8.5). The thick cartilage near the center of the tibial plateau was me-

chanically softer, had higher water content and lower hydroxyproline and uronic acid contents than the thin cartilage near the edges of the joint. The *BMD* of the subchondral plate showed small but statistically significant variation while *BMD* of the subchondral trabecular bone varied more significantly. The *BMD* and the thickness of the subchondral plate exhibited a positive correlation (Table 8.2). Furthermore, the thickness of the subchondral plate was related to the dynamic modulus, superficial contrast agent content and thickness of the cartilage.

The present results seem to support the hypothesis of Noble and Alexander (1985). The part of the joint not covered by the meniscus had thick cartilage and a thick subchondral plate but the cartilage and subchondral plate were demonstrated to become thinner as the meniscus grew thicker. The subchondral trabecular bone was also more dense towards the middle of the plateau, which is in line with earlier findings [120]. The variation in loading conditions probably explains the detected topographical variation in the properties of cartilage and subchondral bone [3, 120, 209]. Measurement of the actual force distribution in the knee joint is difficult though it has been attempted with whole amputated knees [3]. In that study, the distribution of the load was found to vary individually, as did the relative size of the meniscus. The menisci are known to have a significant load-bearing function, transmitting at least 50% of the compressive load on the joint [3].

CECT revealed a significant variation in contrast agent partition across medial tibial plateau, especially in the superficial cartilage. The contrast agent content in the superficial layer of the thick and soft cartilage at the lateral side of the medial plateau was about 20% higher than that of the thin and stiff cartilage at the medial side. This variation and the significant correlations with the reference parameters indicate that the superficial contrast agent concentration depends on the composition and mechanical properties of cartilage and the CECT was able to detect this variation in the properties of cartilage.

Ultrasound backscatter and ultrasound roughness index varied

significantly across the medial tibial plateau. The *IRC* values of cartilage were lower than those reported in the literature, probably due to non-perpendicular incidence of the ultrasound pulse related to the natural curvature of the cartilage surface. The present IRC values resemble those reported for cartilage surfaces inclined by 5-7 degrees [131]. *URI* was largest at location 1 and significantly ($p = 0.046$) larger than that at location 3. Even though the structure and composition of the locations varied significantly ($p < 0.01$), *URI* was not able to detect the variation between locations 2, 3 and 4. This may be due to relatively low frequency of the applied ultrasound. Bone *IRC* and *AIB* varied significantly across the medial tibial condyle. The variation in bone ultrasound parameters, however, is probably partly due to variation in cartilage thickness. Thick cartilage attenuates ultrasound effectively, leading to an underestimation of bone ultrasound parameters. The same phenomenon would improve linear correlations between the bone ultrasound and cartilage reference parameters, if the thickness of the overlying cartilage was not taken into consideration. In this study, partial correlation analysis was used to adjust the measured ultrasound parameters with cartilage thickness and angles of incidence of the ultrasound pulse and tissue layers.

In comparison to the needle probe measurement of cartilage thickness, CECT underestimated and ultrasound overestimated the thickness. The underestimation seen with the CECT method, about 0.2 mm, is probably due to removal of the partial volume pixels. The overestimation of cartilage thickness with ultrasound may be partially explained by an excessively high predefined speed of sound in cartilage. If the predefined speed of sound in cartilage is optimized in order to obtain the best agreement between 30 MHz ultrasound and the needle probe measurement, 1503 m/s speed of sound, instead of 1602 m/s, should have been used in this study. However, 1503 m/s is an unrealistically low value for speed of sound in cartilage. Other factors such as the difference in the measurement locations or in the accuracy of the echo location may have contributed to the underestimation. Moreover, it is important to

note that even the needle probe technique may not represent a "gold standard" in measuring the thickness of cartilage.

9.5 COMPARISON OF THE CECT AND QUS METHODS

Contrast agent enhanced CT and QUS are promising methods for the simultaneous analysis of articular cartilage and subchondral bone. Earlier studies have revealed the potential of ultrasound, as the QUS parameters have been shown to correlate with the structure and composition of cartilage and bone. CECT, on the other hand, is inherently able to measure the BMD and morphology of subchondral bone, and the anionic contrast agent content in cartilage has been shown to correlate with the integrity and composition of the tissue. Both CECT and QUS are invasive methods. CECT requires intra-articular contrast agent injection and exposes the patient to ionizing radiation. QUS measurements, however, need to be conducted during an arthroscopy or open knee surgery.

In this study CECT was more sensitive than QUS at detecting the composition and mechanical properties of both cartilage and bone. CECT is based on the increase in X-ray attenuation due to the increased amount of contrast agent in degenerated cartilage. Interactions between X-rays and matter are well known and relatively straightforward. The challenge encountered in the *in vivo* application of the CECT is the contrast agent kinetics. As shown in a small animal model, a vasoconstrictive drug needs to be mixed in the contrast agent to slow down the washout of the contrast agent from the joint [219].

Ultrasound interactions in tissues and tissue interfaces are complex and difficult to predict. The QUS parameters are very sensitive to overlying tissue layers and the perpendicularity of the ultrasound pulse and the tissue interfaces, which is also demonstrated by the results of this study. This may be a problem in the *in vivo* application of QUS. If the technical challenges could be overcome, the ultrasound measurement of cartilage and subchondral bone could provide significant improvements *e.g.* in arthroscopic evaluation of

cartilage injuries and planning of repair surgery. Table 9.1 summarizes the advantages and disadvantages of the methods.

Table 9.1: Comparison of the CECT and QUS methods.

	CECT	**QUS**
Invasivity	· contrast agent injection · X-ray exposure	· arthroscopy or open surgery
Status	· pre-clinical · applicable *in vivo*	· clinical trials
Bone measurements	+ *BMD* values + sensitive to bone deformations - limited resolution	+ sensitive to structure and composition of trabecular bone - overlying tissues - perpendicularity requirement
Cartilage measurements	+ sensitive to integrity of superficial cartilage + sensitive to cartilage composition - limited resolution - contrast agent kinetics	+ sensitive to integrity of superficial cartilage + sensitive to cartilage composition - *in vivo* measurements technically challenging

10 Summary and conclusions

Quantitative ultrasound and contrast agent enhanced computed tomography showed significant clinical potential for diagnosis of degenerative cartilage diseases, such as OA. This thesis work established the basis of the contrast agent enhanced computed tomography of articular cartilage with a clinical pQCT instrument. Moreover, the thesis clarified the potential of the CT and ultrasound techniques for the simultaneous evaluation of articular cartilage and bone using experimental and numerical methods. The main conclusions of this thesis are summarized as follows:

1. Gadolinium and ioxaglate enhanced pQCT were both able to detect enzymatically induced proteoglycan depletion. However, the proteoglycan depletion had only a minor effect on the spatial distribution profiles of the contrast agents.

2. CECT was a feasible method for simultaneous analysis of cartilage integrity and mineral density of subchondral bone. The content of contrast agent in the superficial cartilage correlated with the composition and mechanical properties of the tissue.

3. Realistic three-dimensional FDTD simulations demonstrated the significant effect of bone marrow composition on the QUS parameters. Substitution of fatty bone marrow with water increased the speed of sound and ultrasound backscatter significantly, while ultrasound attenuation and reflection from the sample surface were significantly decreased.

4. The use of a 5 MHz pulse-echo ultrasound technique enabled simultaneous measurement of the acoustic properties of articular cartilage and subchondral bone. The acoustic properties of cartilage correlated with the composition and mechanical properties of the tissue. Ultrasound backscatter from the subchondral bone correlated with the *BMD* of the subchondral

plate. However, the uneven natural shape of the joint creates uncertainties in the QUS parameters and weakens the correlations. Moreover, ultrasound attenuation in the overlying cartilage layer leads to an underestimation of the ultrasound reflection from the bone surface and ultrasound backscatter from the subchondral bone.

In conclusion, the CECT method was more sensitive than QUS in evaluating the composition and mechanical properties of cartilage. Moreover, the measurements of the subchondral bone were more straightforward with the CECT. On the other hand, CECT applies ionizing radiation and suffers from limited resolution (~ 200 μm). Interestingly, the contrast agent content in the superficial cartilage was found to better reflect the properties of the cartilage than the full-thickness contrast agent content. For the QUS, the ultrasound roughness index and ultrasound backscatter from both cartilage and subchondral bone seemed to be the most sensitive parameters at reflecting the properties of cartilage and subchondral bone.

In principle, the CECT method is already clinically applicable. The pQCT device used in this thesis is an imaging device in clinical use and the contrast agent, ioxaglate, is an FDA approved drug which has been used for arthrographies. The QUS method is probably applicable only during a surgical procedure, for example during arthroscopy. Clinical IVUS devices have already been used in clinical trials to estimate the condition of cartilage and subchondral bone during arthroscopy.

Bibliography

[1] C. J. Adkins, *Equilibrium thermodynamics*, 3rd ed. (Cambridge University Press, Cambridge, UK, 1984).

[2] D. H. Agemura, J. O'Brien, W. D., J. E. Olerud, L. E. Chun, and D. E. Eyre, "Ultrasonic propagation properties of articular cartilage at 100 MHz," *J Acoust Soc Am* **87,** 1786–91 (1990).

[3] A. M. Ahmed and D. L. Burke, "*In vitro* measurement of static pressure distribution in synovial joints–Part I: Tibial surface of the knee," *J Biomech Eng* **105,** 216–25 (1983).

[4] A. M. Aisen, W. J. McCune, A. MacGuire, P. L. Carson, T. M. Silver, S. Z. Jafri, et al., "Sonographic evaluation of the cartilage of the knee," *Radiology* **153,** 781–4 (1984).

[5] R. D. Altman, "Overview of osteoarthritis," *Am J Med* **83,** 65–9 (1987).

[6] J. M. Alves, J. T. Ryaby, J. J. Kaufman, F. P. Magee, and R. S. Siffert, "Influence of marrow on ultrasonic velocity and attenuation in bovine trabecular bone," *Calcif Tissue Int* **58,** 362–7 (1996).

[7] C. G. Armstrong and V. C. Mow, "Variations in the intrinsic mechanical properties of human articular cartilage with age, degeneration, and water content," *J Bone Joint Surg Am* **64,** 88–94 (1982).

[8] G. A. Ateshian, "The role of interstitial fluid pressurization in articular cartilage lubrication," *J Biomech* **42,** 1163–76 (2009).

[9] D. Avci and G. A. Bachmann, "Osteoarthritis and osteoporosis in postmenopausal women: clinical similarities and differences," *Menopause* **11,** 615–21 (2004).

[10] A. J. Bailey, J. P. Mansell, T. J. Sims, and X. Banse, "Biochemical and mechanical properties of subchondral bone in osteoarthritis," *Biorheology* **41,** 349–58 (2004).

[11] P. N. Bansal, N. S. Joshi, V. Entezari, M. W. Grinstaff, and B. D. Snyder, "Contrast enhanced computed tomography can predict the glycosaminoglycan content and biomechanical properties of articular cartilage," *Osteoarthritis Cartilage* **18,** 184–91 (2010).

[12] P. N. Bansal, N. S. Joshi, V. Entezari, B. C. Malone, R. C. Stewart, B. D. Snyder, et al., "Cationic contrast agents improve quantification of glycosaminoglycan (GAG) content by contrast enhanced CT imaging of cartilage," *J Orthop Res* in press (2010).

[13] M. J. Barger-Lux and R. R. Recker, "Bone microstructure in osteoporosis: transilial biopsy and histomorphometry," *Top Magn Reson Imaging* **13,** 297–305 (2002).

[14] R. Barkmann, S. Dencks, P. Laugier, F. Padilla, K. Brixen, J. Ryg, et al., "Femur ultrasound (FemUS)–first clinical results on hip fracture discrimination and estimation of femoral BMD," *Osteoporos Int* **21,** 969–76 (2009).

[15] R. Barkmann, E. Kantorovich, C. Singal, D. Hans, H. K. Genant, M. Heller, et al., "A new method for quantitative ultrasound measurements at multiple skeletal sites: first results of precision and fracture discrimination," *J Clin Densitom* **3,** 1–7 (2000).

[16] R. Barkmann, P. Laugier, U. Moser, S. Dencks, F. Padilla, G. Haïat, et al., "A method for the estimation of femoral bone mineral density from variables of ultrasound transmission through the human femur," *Bone* **40,** 37–44 (2007).

[17] A. Bashir, M. L. Gray, and D. Burstein, "Gd-DTPA^{2-} as a measure of cartilage degradation," *Magn Reson Med* **36,** 665–73 (1996).

[18] A. Bedi, B. T. Feeley, and r. Williams, R. J., "Management of articular cartilage defects of the knee," *J Bone Joint Surg Am* **92,** 994–1009 (2010).

[19] K. L. Bennell, M. W. Creaby, T. V. Wrigley, and D. J. Hunter, "Tibial subchondral trabecular volumetric bone density in medial knee joint osteoarthritis using peripheral quantitative computed tomography technology," *Arthritis Rheum* **58,** 2776–85 (2008).

[20] A. Benninghoff, "Form und Bau der Gelenkknorpel in ihren Beziehungen zur Function. Erste Mitteilung: die modellierenden und formerhaltenden Faktoren des Knorpelreliefs.," *Z Anat* **76,** 43–63 (1925).

[21] M. A. Biot, "Theory of propagation of elastic waves in a fluid saturated porous solid I. Low frequency range," *J Acoust Soc Am* **28,** 168–78 (1956).

[22] W. Bloom and D. W. Fawcett, *A texbook of histology*, 9th ed. (W. B. Saunders Comp, Philadelphia, 1970).

[23] N. Blumenkrantz and G. Asboe-Hansen, "New method for quantitative determination of uronic acids," *Anal Biochem* **54,** 484–9 (1973).

[24] D. Bobinac, J. Spanjol, S. Zoricic, and I. Maric, "Changes in articular cartilage and subchondral bone histomorphometry in osteoarthritic knee joints in humans," *Bone* **32,** 284–90 (2003).

[25] M. Brittberg and C. S. Winalski, "Evaluation of cartilage injuries and repair," *J Bone Joint Surg Am* **85-A Suppl 2,** 58–69 (2003).

[26] P. M. Brooks, "Impact of osteoarthritis on individuals and society: how much disability? Social consequences and health economic implications," *Curr Opin Rheumatol* **14,** 573–7 (2002).

[27] C. P. Brown, S. W. Hughes, R. W. Crawford, and A. Oloyede, "Ultrasound assessment of articular cartilage: analysis of the frequency profile of reflected signals from naturally and artificially degraded samples," *Connect Tissue Res* **48,** 277–85 (2007).

[28] S. Brown, M. Worsfold, and C. Sharp, "Microplate assay for the measurement of hydroxyproline in acid-hydrolyzed tissue samples," *Biotechniques* **30,** 38–40, 42 (2001).

[29] J. A. Buckwalter and H. J. Mankin, "Articular cartilage: degeneration and osteoarthritis, repair, regeneration, and transplantation," *Instr Course Lect* **47,** 487–504 (1998).

[30] J. A. Buckwalter and H. J. Mankin, "Articular cartilage: tissue design and chondrocyte-matrix interactions," *Instr Course Lect* **47,** 477–86 (1998).

[31] J. A. Buckwalter and J. Martin, "Degenerative joint disease," *Clin Symp* **47,** 1–32 (1995).

[32] J. A. Buckwalter and J. A. Martin, "Osteoarthritis," *Adv Drug Deliv Rev* **58,** 150–67 (2006).

[33] J. A. Buckwalter, C. Saltzman, and T. Brown, "The impact of osteoarthritis: implications for research," *Clin Orthop Relat Res* S6-15 (2004).

[34] D. B. Burr, "The contribution of the organic matrix to bone's material properties," *Bone* **31,** 8–11 (2002).

[35] D. Burstein, A. Bashir, and M. L. Gray, "MRI techniques in early stages of cartilage disease," *Invest Radiol* **35,** 622–38 (2000).

[36] D. Burstein, M. L. Gray, A. L. Hartman, R. Gipe, and B. D. Foy, "Diffusion of small solutes in cartilage as measured by nuclear magnetic resonance (NMR) spectroscopy and imaging," *J Orthop Res* **11,** 465–78 (1993).

[37] D. Burstein, J. Velyvis, K. T. Scott, K. W. Stock, Y. J. Kim, D. Jaramillo, et al., "Protocol issues for delayed Gd(DTPA)$^{2-}$ enhanced MRI (dGEMRIC) for clinical evaluation of articular cartilage," *Magn Reson Med* **45,** 36–41 (2001).

[38] S. L. Carney and H. Muir, "The structure and function of cartilage proteoglycans," *Physiol Rev* **68,** 858–910 (1988).

[39] S. Chaffaï, F. Peyrin, S. Nuzzo, R. Porcher, G. Berger, and P. Laugier, "Ultrasonic characterization of human cancellous bone using transmission and backscatter measurements: relationships to density and microstructure," *Bone* **30,** 229–37 (2002).

[40] R. E. Challis and R. I. Kitney, "Biomedical signal processing (in four parts). Part 1. Time-domain methods," *Med Biol Eng Comput* **28,** 509–24 (1990).

[41] C. Chappard, F. Peyrin, A. Bonnassie, G. Lemineur, B. Brunet-Imbault, E. Lespessailles, et al., "Subchondral bone microarchitectural alterations in osteoarthritis: a synchrotron microcomputed tomography study," *Osteoarthritis Cartilage* **14,** 215–23 (2006).

[42] J. Charnley, "The lubrication of animal joints in relation to surgical reconstruction by arthroplasty," *Ann Rheum Dis* **19,** 10–9 (1960).

[43] S. R. Cherry, J. A. Sorenson, and M. E. Phelps, *Physics in nuclear medicine*, 3rd ed. (Saunders, Philadelphia, 2003).

[44] E. Chérin, A. Saïed, P. Laugier, P. Netter, and G. Berger, "Evaluation of acoustical parameter sensitivity to age-related and osteoarthritic changes in articular cartilage using 50-MHz ultrasound," *Ultrasound Med Biol* **24,** 341–54 (1998).

[45] E. Chérin, A. Saïed, B. Pellaumail, D. Loeuille, P. Laugier, P. Gillet, et al., "Assessment of rat articular cartilage maturation using 50-MHz quantitative ultrasonography," *Osteoarthritis Cartilage* **9,** 178–86 (2001).

[46] E. A. Chrischilles, C. D. Butler, C. S. Davis, and R. B. Wallace, "A model of lifetime osteoporosis impact," *Arch Intern Med* **151,** 2026–32 (1991).

[47] H. Chung, F. W. Wehrli, J. L. Williams, and S. D. Kugelmass, "Relationship between NMR transverse relaxation, trabecular bone architecture, and strength," *Proc Natl Acad Sci U S A* **90,** 10250–4 (1993).

[48] M. A. Cimmino and W. Grassi, "What is new in ultrasound and magnetic resonance imaging for musculoskeletal disorders?," *Best Pract Res Clin Rheumatol* **22,** 1141–8 (2008).

[49] J. A. Clowes, R. Eastell, and N. F. Peel, "The discriminative ability of peripheral and axial bone measurements to identify proximal femoral, vertebral, distal forearm and proximal humeral fractures: a case control study," *Osteoporos Int* **16,** 1794–802 (2005).

[50] M. D. Cockman, C. A. Blanton, P. A. Chmielewski, L. Dong, T. E. Dufresne, E. B. Hookfin, et al., "Quantitative imaging of proteoglycan in cartilage using a gadolinium probe and microCT," *Osteoarthritis Cartilage* **14,** 210–4 (2006).

[51] J. E. Compston, "Osteoporosis," *Clin Endocrinol* **33,** 653–82 (1990).

[52] C. Cooper, "Osteoporosis: disease severity and consequent fracture management," *Osteoporos Int* **21 Suppl 2,** S425–9 (2010).

[53] J. M. Coumas and W. E. Palmer, "Knee arthrography. Evolution and current status," *Radiol Clin North Am* **36,** 703–28 (1998).

[54] J. Crank, *The mathematics of diffusion*, 2nd ed. (Clarendon Press, Oxford, 1979).

[55] M. A. D'Agostino, P. Conaghan, M. Le Bars, G. Baron, W. Grassi, E. Martin-Mola, et al., "EULAR report on the use of ultrasonography in painful knee osteoarthritis. Part 1: prevalence of inflammation in osteoarthritis," *Ann Rheum Dis* **64,** 1703–9 (2005).

[56] P. P. Delsanto, R. S. Schechter, and R. B. Mignogna, "Connection machine simulation of ultrasonic wave propagation in materials III: The three-dimensional case," *Wave Motion* **26,** 329–339 (1997).

[57] D. W. Dempster and R. Lindsay, "Pathogenesis of osteoporosis," *Lancet* **341,** 797–801 (1993).

[58] J. Dequeker and O. Johnell, "Osteoarthritis protects against femoral neck fracture: the MEDOS study experience," *Bone* **14 Suppl 1,** S51–6 (1993).

[59] V. Detti, D. Kourtiche, and M. Nadi, "Acoustical characterization of bone using a cylindrical model and time of flight method: edge reconstruction and ultrasound velocity determination in cortical bone and in medullar marrow," *Physiol Meas* **23,** 313–24 (2002).

[60] M. Ding, A. Odgaard, and I. Hvid, "Changes in the three-dimensional microstructure of human tibial cancellous bone in early osteoarthritis," *J Bone Joint Surg Br* **85,** 906–12 (2003).

[61] D. G. Disler, E. Raymond, D. A. May, J. S. Wayne, and T. R. McCauley, "Articular cartilage defects: *in vitro* evaluation of accuracy and interobserver reliability for detection and grading with US," *Radiology* **215,** 846–51 (2000).

[62] E. Dogan and C. Posaci, "Monitoring hormone replacement therapy by biochemical markers of bone metabolism in menopausal women," *Postgrad Med J* **78,** 727–31 (2002).

[63] F. G. Donnan, "Theory of membrane equilibria," *Chem. Rev.* **1,** 73–79 (1924).

[64] I. A. Dontas and C. K. Yiannakopoulos, "Risk factors and prevention of osteoporosis-related fractures," *J Musculoskelet Neuronal Interact* **7,** 268–72 (2007).

[65] D. J. Dowsett, P. A. Kenny, and R. E. Johnston, *The physics of diagnostic imaging*, 2nd ed. (Hodder Arnold, London, 2006).

[66] G. N. Duda, A. Haisch, M. Endres, C. Gebert, D. Schroeder, J. E. Hoffmann, et al., "Mechanical quality of tissue engineered cartilage: results after 6 and 12 weeks *in vivo*," *J Biomed Mater Res* **53,** 673–7 (2000).

[67] P. J. Ehrlich and L. E. Lanyon, "Mechanical strain and bone cell function: a review," *Osteoporos Int* **13,** 688–700 (2002).

[68] Y. M. El Miedany, A. N. Mehanna, and M. A. El Baddini, "Altered bone mineral metabolism in patients with osteoarthritis," *Joint Bone Spine* **67,** 521–7 (2000).

[69] A. A. El-Sariti, J. A. Evans, and J. G. Truscott, "The temperature dependence of the speed of sound in bovine bone marrow at 750 kHz," *Ultrasound Med Biol* **32,** 985–9 (2006).

[70] R. C. Evans and T. M. Quinn, "Solute diffusivity correlates with mechanical properties and matrix density of compressed articular cartilage," *Arch Biochem Biophys* **442,** 1–10 (2005).

[71] D. Eyre, "Collagen of articular cartilage," *Arthritis Res* **4,** 30–5 (2002).

[72] D. R. Eyre, I. R. Dickson, and K. Van Ness, "Collagen cross-linking in human bone and articular cartilage. Age-related changes in the content of mature hydroxypyridinium residues," *Biochem J* **252,** 495–500 (1988).

[73] D. R. Eyre, J. J. Wu, and S. Apone, "A growing family of collagens in articular cartilage: identification of 5 genetically distinct types," *J Rheumatol* **14 Spec No,** 25–7 (1987).

[74] H. Fam, J. T. Bryant, and M. Kontopoulou, "Rheological properties of synovial fluids," *Biorheology* **44,** 59–74 (2007).

[75] D. T. Felson and T. Neogi, "Osteoarthritis: is it a disease of cartilage or of bone?," *Arthritis Rheum* **50,** 341–4 (2004).

[76] D. T. Felson and Y. Zhang, "An update on the epidemiology of knee and hip osteoarthritis with a view to prevention," *Arthritis Rheum* **41,** 1343–55 (1998).

[77] T. C. Fenter, M. J. Naslund, M. B. Shah, M. T. Eaddy, and L. Black, "The cost of treating the 10 most prevalent diseases in men 50 years of age or older," *Am J Manag Care* **12,** S90–8 (2006).

[78] H. Forster and J. Fisher, "The influence of loading time and lubricant on the friction of articular cartilage," *Proc Inst Mech Eng H* **210,** 109–19 (1996).

[79] H. Forster and J. Fisher, "The influence of continuous sliding and subsequent surface wear on the friction of articular cartilage," *Proc Inst Mech Eng H* **213,** 329–45 (1999).

[80] H. M. Frost, *Bone Biodynamics* (Little, Brown, Boston, 1964).

[81] L. P. Gartner and J. L. Hiatt, *Color textbook of histology*, 2nd ed. (W. B. Saunders Comp, Philadelphia, 2001).

[82] A. Gillis, A. Bashir, B. McKeon, A. Scheller, M. L. Gray, and D. Burstein, "Magnetic resonance imaging of relative glycosaminoglycan distribution in patients with autologous chondrocyte transplants," *Invest Radiol* **36,** 743–8 (2001).

[83] A. Gillis, M. Gray, and D. Burstein, "Relaxivity and diffusion of gadolinium agents in cartilage," *Magn Reson Med* **48,** 1068–71 (2002).

[84] J. P. Gleghorn, A. R. Jones, C. R. Flannery, and L. J. Bonassar, "Boundary mode lubrication of articular cartilage by recombinant human lubricin," *J Orthop Res* **27,** 771–7 (2009).

[85] C. C. Glüer, R. Eastell, D. M. Reid, D. Felsenberg, C. Roux, R. Barkmann, et al., "Association of five quantitative ultrasound devices and bone densitometry with osteoporotic vertebral fractures in a population-based sample: the OPUS Study," *J Bone Miner Res* **19,** 782–93 (2004).

[86] M. B. Goldring, "Update on the biology of the chondrocyte and new approaches to treating cartilage diseases," *Best Pract Res Clin Rheumatol* **20,** 1003–25 (2006).

[87] M. Gomez, F. Aguado, J. Manuel, J. M. Menendez, M. Revilla, L. F. Villa, et al., "Influence of soft tissue (fat and fat-free mass) on ultrasound bone velocity: an *in vivo* study," *Invest Radiol* **32,** 609–12 (1997).

[88] S. A. Goss, L. A. Frizzell, and F. Dunn, "Ultrasonic absorption and attenuation in mammalian tissues," *Ultrasound Med Biol* **5,** 181–6 (1979).

[89] K. F. Graff, *Wave motion in elastic solids* (The Clarendon Press, Oxford, 1975).

[90] H. Gray, *Anatomy of the Human Body*, 35th ed. (Lea & Febiger, Philadelphia, 1918).

[91] M. L. Gray, D. Burstein, and Y. Xia, "Biochemical (and functional) imaging of articular cartilage," *Semin Musculoskelet Radiol* **5,** 329–43 (2001).

[92] Q. Grimal, S. Haupert, D. Mitton, L. Vastel, and P. Laugier, "Assessment of cortical bone elasticity and strength: mechanical testing and ultrasound provide complementary data," *Med Eng Phys* **31,** 1140–7 (2009).

[93] S. Gupta, G. A. Hawker, A. Laporte, R. Croxford, and P. C. Coyte, "The economic burden of disabling hip and knee osteoarthritis (OA) from the perspective of individuals living with this condition," *Rheumatology (Oxford)* **44,** 1531–7 (2005).

[94] G. Haïat, F. Padilla, R. Barkmann, S. Kolta, C. Latremouille, C. C. Glüer, et al., "*In vitro* speed of sound measurement at intact human femur specimens," *Ultrasound Med Biol* **31,** 987–96 (2005).

[95] T. J. Haire and C. M. Langton, "Biot theory: a review of its application to ultrasound propagation through cancellous bone," *Bone* **24,** 291–5 (1999).

[96] M. A. Hakulinen, J. S. Day, J. Töyräs, M. Timonen, H. Kröger, H. Weinans, et al., "Prediction of density and mechanical properties of human trabecular bone *in vitro* by using ultrasound transmission and backscattering measurements at 0.2-6.7 MHz frequency range," *Phys Med Biol* **50,** 1629–42 (2005).

[97] M. A. Hakulinen, J. S. Day, J. Töyräs, H. Weinans, and J. S. Jurvelin, "Ultrasonic characterization of human trabecular bone microstructure," *Phys Med Biol* **51,** 1633–48 (2006).

[98] M. A. Hakulinen, J. Töyräs, S. Saarakkala, J. Hirvonen, H. Kröger, and J. S. Jurvelin, "Ability of ultrasound backscattering to predict mechanical properties of bovine trabecular bone," *Ultrasound Med Biol* **30,** 919–27 (2004).

[99] S. Han, J. Rho, J. Medige, and I. Ziv, "Ultrasound velocity and broadband attenuation over a wide range of bone mineral density," *Osteoporos Int* **6,** 291–6 (1996).

[100] T. E. Hardingham and H. Muir, "Hyaluronic acid in cartilage and proteoglycan aggregation," *Biochem J* **139,** 565–81 (1974).

[101] J. Harris, E. D., H. G. Parker, E. L. Radin, and S. M. Krane, "Effects of proteolytic enzymes on structural and mechanical properties of cartilage," *Arthritis Rheum* **15,** 497–503 (1972).

[102] E. M. Hasler, W. Herzog, J. Z. Wu, W. Müller, and U. Wyss, "Articular cartilage biomechanics: theoretical models, material properties, and biosynthetic response," *Crit Rev Biomed Eng* **27,** 415–88 (1999).

[103] K. Hattori, K. Mori, T. Habata, Y. Takakura, and K. Ikeuchi, "Measurement of the mechanical condition of articular cartilage with an ultrasonic probe: quantitative evaluation using wavelet transformation," *Clin Biomech (Bristol, Avon)* **18,** 553–7 (2003).

[104] C. W. Hayes, D. A. Jamadar, G. W. Welch, M. L. Jannausch, L. L. Lachance, D. C. Capul, et al., "Osteoarthritis of the knee: comparison of MR imaging findings with radiographic severity measurements and pain in middle-aged women," *Radiology* **237,** 998–1007 (2005).

[105] W. C. Hayes, L. M. Keer, G. Herrmann, and L. F. Mockros, "A mathematical analysis for indentation tests of articular cartilage," *J Biomech* **5,** 541–51 (1972).

[106] T. Hildebrand and P. Rüegsegger, "A new method for the model-independent assessment of thickness in three-dimensional images.," *J Microsc* **185,** 67–75 (1997).

[107] M. C. Hochberg, M. Lethbridge-Cejku, J. Scott, W. W., C. C. Plato, and J. D. Tobin, "Obesity and osteoarthritis of the hands in women," *Osteoarthritis Cartilage* **1,** 129–35 (1993).

[108] R. Hodgskinson and J. D. Currey, "The effect of variation in structure on the Young's modulus of cancellous bone: a comparison of human and non-human material," *Proc Inst Mech Eng H* **204,** 115–21 (1990).

[109] R. Hodgskinson, C. F. Njeh, M. A. Whitehead, and C. M. Langton, "The non-linear relationship between BUA and porosity in cancellous bone," *Phys Med Biol* **41,** 2411–20 (1996).

[110] B. K. Hoffmeister, D. P. Johnson, J. A. Janeski, D. A. Keedy, B. W. Steinert, A. M. Viano, et al., "Ultrasonic characterization of human cancellous bone *in vitro* using three different apparent backscatter parameters in the frequency range 0.6-15.0 MHz," *IEEE Trans Ultrason Ferroelectr Freq Control* **55,** 1442–52 (2008).

[111] B. K. Hoffmeister, r. Jones, C. I., G. J. Caldwell, and S. C. Kaste, "Ultrasonic characterization of cancellous bone using apparent integrated backscatter," *Phys Med Biol* **51,** 2715–27 (2006).

[112] B. K. Hoffmeister, S. A. Whitten, S. C. Kaste, and J. Y. Rho, "Effect of collagen and mineral content on the high-frequency ultrasonic properties of human cancellous bone," *Osteoporos Int* **13,** 26–32 (2002).

[113] B. K. Hoffmeister, S. A. Whitten, and J. Y. Rho, "Low-megahertz ultrasonic properties of bovine cancellous bone," *Bone* **26,** 635–42 (2000).

[114] A. Hosokawa and T. Otani, "Ultrasonic wave propagation in bovine cancellous bone," *J Acoust Soc Am* **101,** 558–62 (1997).

[115] K. Hu, P. Radhakrishnan, R. V. Patel, and J. J. Mao, "Regional structural and viscoelastic properties of fibrocartilage upon dynamic nanoindentation of the articular condyle," *J Struct Biol* **136,** 46–52 (2001).

[116] Y. P. Huang and Y. P. Zheng, "Intravascular Ultrasound (IVUS): A Potential Arthroscopic Tool for Quantitative Assessment of Articular Cartilage," *Open Biomed Eng J* **3,** 13–20 (2009).

[117] M. Huber, S. Trattnig, and F. Lintner, "Anatomy, biochemistry, and physiology of articular cartilage," *Invest Radiol* **35,** 573–80 (2000).

[118] E. R. Hughes, T. G. Leighton, G. W. Petley, and P. R. White, "Ultrasonic propagation in cancellous bone: a new stratified model," *Ultrasound Med Biol* **25,** 811–21 (1999).

[119] J. Huopio, H. Kröger, R. Honkanen, J. Jurvelin, S. Saarikoski, and E. Alhava, "Calcaneal ultrasound predicts early postmenopausal fractures as well as axial BMD. A prospective study of 422 women," *Osteoporos Int* **15,** 190–5 (2004).

[120] I. Hvid and S. L. Hansen, "Trabecular bone strength patterns at the proximal tibial epiphysis," *J Orthop Res* **3,** 464–72 (1985).

[121] H. Isaksson, J. Töyräs, M. Hakulinen, A. S. Aula, I. Tamminen, P. Julkunen, et al., "Structural parameters of normal and osteoporotic human trabecular bone are affected differently by microCT image resolution," *Osteoporos Int* (2010).

[122] G. D. Jay, J. R. Torres, M. L. Warman, M. C. Laderer, and K. S. Breuer, "The role of lubricin in the mechanical behavior of synovial fluid," *Proc Natl Acad Sci U S A* **104,** 6194–9 (2007).

[123] F. Jenson, F. Padilla, and P. Laugier, "Prediction of frequency-dependent ultrasonic backscatter in cancellous bone using statistical weak scattering model," *Ultrasound Med Biol* **29,** 455–64 (2003).

[124] J. D. Johnston, B. A. Masri, and D. R. Wilson, "Computed tomography topographic mapping of subchondral density (CT-TOMASD) in osteoarthritic and normal knees: methodological development and preliminary findings," *Osteoarthritis Cartilage* **17,** 1319–26 (2009).

[125] G. A. Joiner, E. R. Bogoch, K. P. Pritzker, M. D. Buschmann, A. Chevrier, and F. S. Foster, "High frequency acoustic parameters of human and bovine articular cartilage following experimentally-induced matrix degradation," *Ultrason Imaging* **23,** 106–16 (2001).

[126] K. M. Jordan, N. K. Arden, M. Doherty, B. Bannwarth, J. W. Bijlsma, P. Dieppe, et al., "EULAR Recommendations 2003: an evidence based approach to the management of knee osteoarthritis: Report of a Task Force of the Standing Committee for International Clinical Studies Including Therapeutic Trials (ESCISIT)," *Ann Rheum Dis* **62,** 1145–55 (2003).

[127] D. Joseph, W. Y. Mao, W. M. Lai, and V. C. Mow, "True density of normal and enzymatically treated bovine articular cartilage," *Trans Orthop Res Soc* **24,** 642 (1999).

[128] L. C. Junqueira, J. Carneiro, and R. O. Kelley, *Basic histology, 7th edition* (Appleton & Lange, Norwalk, 1992).

[129] J. S. Jurvelin, T. Räsänen, P. Kolmonen, and T. Lyyra, "Comparison of optical, needle probe and ultrasonic techniques for the measurement of articular cartilage thickness," *J Biomech* **28,** 231–5 (1995).

[130] A. C. Kak and M. Slaney, *Principles of Computerized Tomographic Imaging* (IEEE Press, New York, 1988).

[131] E. Kaleva, S. Saarakkala, J. S. Jurvelin, T. Virén, and J. Töyräs, "Effects of ultrasound beam angle and surface roughness on the quantitative ultrasound parameters of articular cartilage," *Ultrasound Med Biol* **35,** 1344–51 (2009).

[132] E. Kaleva, T. Virén, S. Saarakkala, J. Sahlman, J. Sirola, J. Puhakka, et al., "Arthroscopic Ultrasound Assessment of Articular Cartilage in Human Knee Joint: A Potential Diagnostic Method," *Cartilage* in press (2010).

[133] C. Kang, M. Paley, R. Ordidge, and R. Speller, "*In vivo* MRI measurements of bone quality in the calcaneus: a comparison with DXA and ultrasound," *Osteoporos Int* **9,** 65–74 (1999).

[134] J. A. Kanis, "Diagnosis of osteoporosis and assessment of fracture risk," *Lancet* **359,** 1929–36 (2002).

[135] F. S. Kaplan, W. C. Hayes, T. M. Keaveny, A. Boskey, T. A. Einhorn, and J. P. Iannotti, "Form and Function of Bone," in *Orthopaedic Basic Science*, 2nd ed., S. R. Simon, ed. (American Academy of Orthopaedic Surgeons, Rosemont, 1994).

[136] J. Karjalainen, J. Töyräs, O. Riekkinen, and M. A. Hakulinen, "Ultrasound backscattering outperforms the clinically used ultrasound parameters in discrimination of osteoporotic-like human trabecular bone samples," in *World congress on medical and biomedical engineering*, Vol. 25/2 (2009), pp. 94–97.

[137] J. P. Karjalainen, J. Töyräs, O. Riekkinen, M. Hakulinen, and J. S. Jurvelin, "Ultrasound backscatter imaging provides frequency-dependent information on structure, composition and mechanical properties of human trabecular bone," *Ultrasound Med Biol* **35,** 1376–84 (2009).

[138] J. J. Kaufman, G. Luo, and R. S. Siffert, "Ultrasound simulation for 3D-axisymmetric models," in *IEEE ultrasonics symposium*, Vol. 2 (2003), pp. 2065–2068.

[139] J. J. Kaufman, G. Luo, and R. S. Siffert, "A portable real-time ultrasonic bone densitometer," *Ultrasound Med Biol* **33,** 1445–52 (2007).

[140] H. I. Keen and P. G. Conaghan, "Usefulness of ultrasound in osteoarthritis," *Rheum Dis Clin North Am* **35,** 503–19 (2009).

[141] J. H. Kellgren and J. S. Lawrence, "Radiological assessment of osteo-arthrosis," *Ann Rheum Dis* **16,** 494–502 (1957).

[142] I. Kiviranta, J. Jurvelin, M. Tammi, A. M. Säämänen, and H. J. Helminen, "Microspectrophotometric quantitation of glycosaminoglycans in articular cartilage sections stained with Safranin O," *Histochemistry* **82,** 249–55 (1985).

[143] P. Kiviranta, E. Lammentausta, J. Töyräs, I. Kiviranta, and J. S. Jurvelin, "Indentation diagnostics of cartilage degeneration," *Osteoarthritis Cartilage* **16,** 796–804 (2008).

[144] P. Kiviranta, J. Rieppo, R. K. Korhonen, P. Julkunen, J. Töyräs, and J. S. Jurvelin, "Collagen network primarily controls Poisson's ratio of bovine articular cartilage in compression," *J Orthop Res* **24,** 690–9 (2006).

[145] P. Kiviranta, J. Töyräs, M. T. Nieminen, M. S. Laasanen, S. Saarakkala, H. J. Nieminen, et al., "Comparison of novel clinically applicable methodology for sensitive diagnostics of cartilage degeneration," *Eur Cell Mater* **13,** 46–55 (2007).

[146] H. T. Kokkonen, J. S. Jurvelin, and J. Töyräs, "Detection of acute mechanical injury of articular cartilage using contrast enhanced computed tomography," *Trans Orthop Res Soc* **35,** 1362 (2010).

[147] R. K. Korhonen, P. Julkunen, J. Rieppo, R. Lappalainen, Y. T. Konttinen, and J. S. Jurvelin, "Collagen network of articular cartilage modulates fluid flow and mechanical stresses in chondrocyte," *Biomech Model Mechanobiol* **5,** 150–9 (2006).

[148] R. K. Korhonen, M. S. Laasanen, J. Töyräs, R. Lappalainen, H. J. Helminen, and J. S. Jurvelin, "Fibril reinforced poroelastic model predicts specifically mechanical behavior of normal, proteoglycan depleted and collagen degraded articular cartilage," *J Biomech* **36,** 1373–9 (2003).

[149] R. K. Korhonen, M. Wong, J. Arokoski, R. Lindgren, H. J. Helminen, E. B. Hunziker, et al., "Importance of the superficial tissue layer for the indentation stiffness of articular cartilage," *Med Eng Phys* **24,** 99–108 (2002).

[150] K. A. Kulmala, R. K. Korhonen, P. Julkunen, J. S. Jurvelin, T. M. Quinn, H. Kröger, et al., "Diffusion coefficients of articular cartilage for different CT and MRI contrast agents," *Med Eng Phys* **32,** 878–82 (2010).

[151] J. E. Kurkijärvi, L. Mattila, R. O. Ojala, A. I. Vasara, J. S. Jurvelin, I. Kiviranta, et al., "Evaluation of cartilage repair in the distal femur after autologous chondrocyte transplantation using T_2 relaxation time and dGEMRIC," *Osteoarthritis Cartilage* **15,** 372–8 (2007).

[152] J. E. Kurkijärvi, M. J. Nissi, I. Kiviranta, J. S. Jurvelin, and M. T. Nieminen, "Delayed gadolinium-enhanced MRI of cartilage (dGEMRIC) and T_2 characteristics of human knee articular cartilage: topographical variation and relationships to mechanical properties," *Magn Reson Med* **52,** 41–6 (2004).

[153] M. S. Laasanen, S. Saarakkala, J. Töyräs, J. Rieppo, and J. S. Jurvelin, "Site-specific ultrasound reflection properties and superficial collagen content of bovine knee articular cartilage," *Phys Med Biol* **50,** 3221–33 (2005).

[154] M. S. Laasanen, J. Töyräs, A. Vasara, S. Saarakkala, M. M. Hyttinen, I. Kiviranta, et al., "Quantitative ultrasound imaging of spontaneous repair of porcine cartilage," *Osteoarthritis Cartilage* **14,** 258–63 (2006).

[155] Y. M. Lai, L. Qin, H. Y. Yeung, K. K. Lee, and K. M. Chan, "Regional differences in trabecular BMD and micro-architecture of weight-bearing bone under habitual gait loading–a pQCT and microCT study in human cadavers," *Bone* **37,** 274–82 (2005).

[156] A. Laib and P. Rüegsegger, "Calibration of trabecular bone structure measurements of *in vivo* three-dimensional peripheral quantitative computed tomography with 28-microm-resolution microcomputed tomography," *Bone* **24,** 35–9 (1999).

[157] E. Lammentausta, T. S. Silvast, J. Narvainen, J. S. Jurvelin, M. T. Nieminen, and O. H. Gröhn, "T_2, Carr-Purcell T_2 and $T_{1\rho}$ of fat and water as surrogate markers of trabecular bone structure," *Phys Med Biol* **53,** 543–55 (2008).

[158] C. M. Langton and C. F. Njeh, "The measurement of broadband ultrasonic attenuation in cancellous bone–a review of the science and technology," *IEEE Trans Ultrason Ferroelectr Freq Control* **55,** 1546–54 (2008).

[159] C. M. Langton, C. F. Njeh, R. Hodgskinson, and J. D. Currey, "Prediction of mechanical properties of the human calcaneus by broadband ultrasonic attenuation," *Bone* **18,** 495–503 (1996).

[160] C. M. Langton, S. B. Palmer, and R. W. Porter, "The measurement of broadband ultrasonic attenuation in cancellous bone," *Eng Med* **13,** 89–91 (1984).

[161] C. M. Langton and M. Subhan, "Computer and experimental simulation of a cortical end-plate phase cancellation artefact in the measurement of BUA at the calcaneus," *Physiol Meas* **22,** 581–7 (2001).

[162] J. S. Lawrence, J. M. Bremner, and F. Bier, "Osteo-arthrosis. Prevalence in the population and relationship between symptoms and x-ray changes," *Ann Rheum Dis* **25,** 1–24 (1966).

[163] H. A. Leddy and F. Guilak, "Site-specific molecular diffusion in articular cartilage measured using fluorescence recovery after photobleaching," *Ann Biomed Eng* **31,** 753–60 (2003).

[164] B. Li and R. M. Aspden, "Composition and mechanical properties of cancellous bone from the femoral head of patients with osteoporosis or osteoarthritis," *J Bone Miner Res* **12,** 641–51 (1997).

[165] B. Li and R. M. Aspden, "Material properties of bone from the femoral neck and calcar femorale of patients with osteoporosis or osteoarthritis," *Osteoporos Int* **7,** 450–6 (1997).

[166] B. Li and R. M. Aspden, "Mechanical and material properties of the subchondral bone plate from the femoral head of patients with osteoarthritis or osteoporosis," *Ann Rheum Dis* **56,** 247–54 (1997).

[167] L. P. Li, J. Soulhat, M. D. Buschmann, and A. Shirazi-Adl, "Nonlinear analysis of cartilage in unconfined ramp compression using a

fibril reinforced poroelastic model," *Clin Biomech (Bristol, Avon)* **14,** 673–82 (1999).

[168] W. Lin, Y. X. Qin, and C. Rubin, "Ultrasonic wave propagation in trabecular bone predicted by the stratified model," *Ann Biomed Eng* **29,** 781–90 (2001).

[169] E. Losina, R. P. Walensky, C. L. Kessler, P. S. Emrani, W. M. Reichmann, E. A. Wright, et al., "Cost-effectiveness of total knee arthroplasty in the United States: patient risk and hospital volume," *Arch Intern Med* **169,** 1113–21; discussion 1121–2 (2009).

[170] T. Lyyra-Laitinen, M. Niinimäki, J. Töyräs, R. Lindgren, I. Kiviranta, and J. S. Jurvelin, "Optimization of the arthroscopic indentation instrument for the measurement of thin cartilage stiffness," *Phys Med Biol* **44,** 2511–24 (1999).

[171] C. H. MacLean, K. Knight, H. Paulus, R. H. Brook, and P. G. Shekelle, "Costs attributable to osteoarthritis," *J Rheumatol* **25,** 2213–8 (1998).

[172] A. F. Mak, W. M. Lai, and V. C. Mow, "Biphasic indentation of articular cartilage–I. Theoretical analysis," *J Biomech* **20,** 703–14 (1987).

[173] A. Maroudas, "Physicochemical properties of cartilage in the light of ion exchange theory," *Biophys J* **8,** 575–95 (1968).

[174] A. Maroudas, "Distribution and diffusion of solutes in articular cartilage," *Biophys J* **10,** 365–79 (1970).

[175] A. Maroudas, "Biophysical chemistry of cartilaginous tissues with special reference to solute and fluid transport," *Biorheology* **12,** 233–48 (1975).

[176] A. Maroudas, M. T. Bayliss, and M. F. Venn, "Further studies on the composition of human femoral head cartilage," *Ann Rheum Dis* **39,** 514–23 (1980).

[177] A. Maroudas and P. Bullough, "Permeability of articular cartilage," *Nature* **219,** 1260–1 (1968).

[178] A. Maroudas and R. Schneiderman, ""Free" and "exchangeable" or "trapped" and "non-exchangeable" water in cartilage," *J Orthop Res* **5,** 133–8 (1987).

[179] C. W. McCutchen, "The frictional properties of animal joints," *Wear* **5,** 1–17 (1962).

[180] C. A. McKenzie, A. Williams, P. V. Prasad, and D. Burstein, "Three-dimensional delayed gadolinium-enhanced MRI of cartilage (dGEMRIC) at 1.5T and 3.0T," *J Magn Reson Imaging* **24,** 928–33 (2006).

[181] G. Meachim, "Age-related degeneration of patellar articular cartilage," *J Anat* **134,** 365–71 (1982).

[182] E. Mittra, C. Rubin, B. Gruber, and Y. X. Qin, "Evaluation of trabecular mechanical and microstructural properties in human calcaneal bone of advanced age using mechanical testing, microCT, and DXA," *J Biomech* **41,** 368–75 (2008).

[183] A. Moayyeri, S. Kaptoge, N. Dalzell, S. Bingham, R. N. Luben, N. J. Wareham, et al., "Is QUS or DXA better for predicting the 10-year absolute risk of fracture?," *J Bone Miner Res* **24,** 1319–25 (2009).

[184] P. Moilanen, "Ultrasonic guided waves in bone," *IEEE Trans Ultrason Ferroelectr Freq Control* **55,** 1277–86 (2008).

[185] V. C. Mow, D. C. Fithian, and M. A. Kelly, "Fundamentals of articular cartilage and meniscus biomechanics," in *Articular cartilage and knee joint function: basic science and arthroscopy*, J. W. Ewing, ed. (Raven Press Ltd., New York, 1990).

[186] V. C. Mow and X. E. Guo, "Mechano-electrochemical properties of articular cartilage: their inhomogeneities and anisotropies," *Annu Rev Biomed Eng* **4,** 175–209 (2002).

[187] V. C. Mow, M. H. Holmes, and W. M. Lai, "Fluid transport and mechanical properties of articular cartilage: a review," *J Biomech* **17,** 377–94 (1984).

[188] V. C. Mow, S. C. Kuei, W. M. Lai, and C. G. Armstrong, "Biphasic creep and stress relaxation of articular cartilage in compression? Theory and experiments," *J Biomech Eng* **102,** 73–84 (1980).

[189] V. C. Mow, A. Ratcliffe, and A. R. Poole, "Cartilage and diarthrodial joints as paradigms for hierarchical materials and structures," *Biomaterials* **13,** 67–97 (1992).

[190] W. C. Mow, W. Zhu, and A. Ratcliffe, "Structure and function of articular cartilage and meniscus," in *Basic orthopaedic biomechanics*, W. C. Mow and W. C. Hayes, eds. (Raven Press, Ltd, New York, 1991).

[191] H. Muir, "The chondrocyte, architect of cartilage. Biomechanics, structure, function and molecular biology of cartilage matrix macromolecules," *Bioessays* **17,** 1039–48 (1995).

[192] H. Muir, P. Bullough, and A. Maroudas, "The distribution of collagen in human articular cartilage with some of its physiological implications," *J Bone Joint Surg Br* **52,** 554–63 (1970).

[193] M. Muller, D. Mitton, P. Moilanen, V. Bousson, M. Talmant, and P. Laugier, "Prediction of bone mechanical properties using QUS and pQCT: study of the human distal radius," *Med Eng Phys* **30,** 761–7 (2008).

[194] S. L. Murphy, D. M. Strasburg, A. K. Lyden, D. M. Smith, J. F. Koliba, D. P. Dadabhoy, et al., "Effects of activity strategy training on pain and physical activity in older adults with knee or hip osteoarthritis: a pilot study," *Arthritis Rheum* **59,** 1480–7 (2008).

[195] S. L. Myers, K. Dines, D. A. Brandt, K. D. Brandt, and M. E. Albrecht, "Experimental assessment by high frequency ultrasound of articular cartilage thickness and osteoarthritic changes," *J Rheumatol* **22,** 109–16 (1995).

[196] E. Nägele, V. Kuhn, H. Vogt, T. M. Link, R. Müller, E. M. Lochmüller, et al., "Technical considerations for microstructural analysis of human trabecular bone from specimens excised from various skeletal sites," *Calcif Tissue Int* **75,** 15–22 (2004).

[197] P. H. Nicholson and R. Alkalay, "Quantitative ultrasound predicts bone mineral density and failure load in human lumbar vertebrae," *Clin Biomech (Bristol, Avon)* **22,** 623–9 (2007).

[198] P. H. Nicholson and M. L. Bouxsein, "Bone marrow influences quantitative ultrasound measurements in human cancellous bone," *Ultrasound Med Biol* **28,** 369–75 (2002).

[199] P. H. Nicholson, R. Strelitzki, R. O. Cleveland, and M. L. Bouxsein, "Scattering of ultrasound in cancellous bone: predictions from a theoretical model," *J Biomech* **33,** 503–6 (2000).

[200] H. J. Nieminen, S. Saarakkala, M. S. Laasanen, J. Hirvonen, J. S. Jurvelin, and J. Töyräs, "Ultrasound attenuation in normal and spontaneously degenerated articular cartilage," *Ultrasound Med Biol* **30,** 493–500 (2004).

[201] H. J. Nieminen, J. Töyräs, J. Rieppo, M. T. Nieminen, J. Hirvonen, R. Korhonen, et al., "Real-time ultrasound analysis of articular cartilage degradation *in vitro*," *Ultrasound Med Biol* **28,** 519–25 (2002).

[202] M. T. Nieminen, J. Rieppo, J. Silvennoinen, J. Töyräs, J. M. Hakumäki, M. M. Hyttinen, et al., "Spatial assessment of articular cartilage proteoglycans with Gd-DTPA-enhanced T_1 imaging," *Magn Reson Med* **48,** 640–8 (2002).

[203] M. T. Nieminen, J. Töyräs, M. S. Laasanen, J. Silvennoinen, H. J. Helminen, and J. S. Jurvelin, "Prediction of biomechanical properties of articular cartilage with quantitative magnetic resonance imaging," *J Biomech* **37,** 321–8 (2004).

[204] M. J. Nissi, J. Töyräs, M. S. Laasanen, J. Rieppo, S. Saarakkala, R. Lappalainen, et al., "Proteoglycan and collagen sensitive MRI evaluation of normal and degenerated articular cartilage," *J Orthop Res* **22,** 557–64 (2004).

[205] C. F. Njeh, D. Hans, T. Fuerst, C. C. Glüer, and H. K. Genant, *Quantitative Ultrasound: Assessment of Osteoporosis and Bone Status*, Vol. 70, (Martin Dunitz Ltd., London, 1999).

[206] C. F. Njeh, R. Hodgskinson, J. D. Currey, and C. M. Langton, "Orthogonal relationships between ultrasonic velocity and material properties of bovine cancellous bone," *Med Eng Phys* **18,** 373–81 (1996).

[207] C. F. Njeh, C. W. Kuo, C. M. Langton, H. I. Atrah, and C. M. Boivin, "Prediction of human femoral bone strength using ultrasound velocity and BMD: an *in vitro* study," *Osteoporos Int* **7,** 471–7 (1997).

[208] C. F. Njeh, I. Saeed, M. Grigorian, D. L. Kendler, B. Fan, J. Shepherd, et al., "Assessment of bone status using speed of sound at multiple anatomical sites," *Ultrasound Med Biol* **27,** 1337–45 (2001).

[209] J. Noble and K. Alexander, "Studies of tibial subchondral bone density and its significance," *J Bone Joint Surg Am* **67,** 295–302 (1985).

[210] F. Padilla, L. Akrout, S. Kolta, C. Latremouille, C. Roux, and P. Laugier, "*In vitro* ultrasound measurement at the human femur," *Calcif Tissue Int* **75,** 421–30 (2004).

[211] F. Padilla, E. Bossy, G. Haïat, F. Jenson, and P. Laugier, "Numerical simulation of wave propagation in cancellous bone," *Ultrasonics* **44,** e239–43 (2006).

[212] F. Padilla, F. Jenson, V. Bousson, F. Peyrin, and P. Laugier, "Relationships of trabecular bone structure with quantitative ultrasound parameters: *in vitro* study on human proximal femur using transmission and backscatter measurements," *Bone* **42,** 1193–202 (2008).

[213] A. W. Palmer, R. E. Guldberg, and M. E. Levenston, "Analysis of cartilage matrix fixed charge density and three-dimensional morphology via contrast-enhanced microcomputed tomography," *Proc Natl Acad Sci U S A* **103,** 19255–60 (2006).

[214] A. M. Parfitt, "Trabecular bone architecture in the pathogenesis and prevention of fracture," *Am J Med* **82,** 68–72 (1987).

[215] A. M. Parfitt, M. K. Drezner, F. H. Glorieux, J. A. Kanis, H. Malluche, P. J. Meunier, et al., "Bone histomorphometry: standardization of nomenclature, symbols, and units. Report of the ASBMR Histomorphometry Nomenclature Committee," *J Bone Miner Res* **2,** 595–610 (1987).

[216] S. G. Patil, Y. P. Zheng, J. Y. Wu, and J. Shi, "Measurement of depth-dependence and anisotropy of ultrasound speed of bovine articular cartilage *in vitro*," *Ultrasound Med Biol* **30,** 953–63 (2004).

[217] B. Pellaumail, A. Watrin, D. Loeuille, P. Netter, G. Berger, P. Laugier, et al., "Effect of articular cartilage proteoglycan depletion on high frequency ultrasound backscatter," *Osteoarthritis Cartilage* **10,** 535–41 (2002).

[218] K. Pinker, P. Szomolanyi, G. C. Welsch, T. C. Mamisch, S. Marlovits, A. Stadlbauer, et al., "Longitudinal evaluation of cartilage composition of matrix-associated autologous chondrocyte transplants with 3-T delayed gadolinium-enhanced MRI of cartilage," *AJR Am J Roentgenol* **191,** 1391–6 (2008).

[219] T. M. Piscaer, J. H. Waarsing, N. Kops, P. Pavljasevic, J. A. Verhaar, G. J. van Osch, et al., "*In vivo* imaging of cartilage degeneration using microCT-arthrography," *Osteoarthritis Cartilage* **16,** 1011–7 (2008).

[220] A. R. Poole, T. Kojima, T. Yasuda, F. Mwale, M. Kobayashi, and S. Laverty, "Composition and structure of articular cartilage: a template for tissue repair," *Clin Orthop Relat Res* S26-33 (2001).

[221] G. Poór, E. J. Atkinson, W. M. O'Fallon, and L. J. Melton 3rd, "Determinants of reduced survival following hip fractures in men," *Clin Orthop Relat Res* 260-5 (1995).

[222] P. Qvist, A. C. Bay-Jensen, C. Christiansen, E. B. Dam, P. Pastoureau, and M. A. Karsdal, "The disease modifying osteoarthritis drug (DMOAD): Is it in the horizon?," *Pharmacol Res* **58,** 1–7 (2008).

[223] E. L. Radin, F. de Lamotte, and P. Maquet, "Role of the menisci in the distribution of stress in the knee," *Clin Orthop Relat Res* 290-4 (1984).

[224] O. Riekkinen, M. A. Hakulinen, M. J. Lammi, J. S. Jurvelin, A. Kallioniemi, and J. Töyräs, "Acoustic properties of trabecular bone–relationships to tissue composition," *Ultrasound Med Biol* **33,** 1438–44 (2007).

[225] O. Riekkinen, M. A. Hakulinen, M. Timonen, J. Töyräs, and J. S. Jurvelin, "Influence of overlying soft tissues on trabecular bone acoustic measurement at various ultrasound frequencies," *Ultrasound Med Biol* **32,** 1073–83 (2006).

[226] O. Riekkinen, M. A. Hakulinen, J. Töyräs, and J. S. Jurvelin, "Dual-frequency ultrasound–new pulse-echo technique for bone densitometry," *Ultrasound Med Biol* **34,** 1703–8 (2008).

[227] E. M. Roos and L. Dahlberg, "Positive effects of moderate exercise on glycosaminoglycan content in knee cartilage: a four-month, randomized, controlled trial in patients at risk of osteoarthritis," *Arthritis Rheum* **52,** 3507–14 (2005).

[228] J. Rothfuss, W. Mau, H. Zeidler, and M. H. Brenner, "Socioeconomic evaluation of rheumatoid arthritis and osteoarthritis: a literature review," *Semin Arthritis Rheum* **26,** 771–9 (1997).

[229] C. Roux, V. Roberjot, R. Porcher, S. Kolta, M. Dougados, and P. Laugier, "Ultrasonic backscatter and transmission parameters at the os calcis in postmenopausal osteoporosis," *J Bone Miner Res* **16,** 1353–62 (2001).

[230] S. Saarakkala, P. Julkunen, P. Kiviranta, J. Mäkitalo, J. S. Jurvelin, and R. K. Korhonen, "Depth-wise progression of osteoarthritis in human articular cartilage: investigation of composition, structure and biomechanics," *Osteoarthritis Cartilage* **18,** 73–81 (2010).

[231] S. Saarakkala, M. S. Laasanen, J. S. Jurvelin, and J. Töyräs, "Quantitative ultrasound imaging detects degenerative changes in articular cartilage surface and subchondral bone," *Phys Med Biol* **51,** 5333–46 (2006).

[232] S. Saarakkala, J. Töyräs, J. Hirvonen, M. S. Laasanen, R. Lappalainen, and J. S. Jurvelin, "Ultrasonic quantitation of superficial degradation of articular cartilage," *Ultrasound Med Biol* **30,** 783–92 (2004).

[233] A. Saïed, E. Chérin, H. Gaucher, P. Laugier, P. Gillet, J. Floquet, et al., "Assessment of articular cartilage and subchondral bone: subtle and progressive changes in experimental osteoarthritis using 50 MHz echography *in vitro*," *J Bone Miner Res* **12,** 1378–86 (1997).

[234] J. T. Samosky, D. Burstein, W. Eric Grimson, R. Howe, S. Martin, and M. L. Gray, "Spatially-localized correlation of dGEMRIC-measured GAG distribution and mechanical stiffness in the human tibial plateau," *J Orthop Res* **23,** 93–101 (2005).

[235] M. Schoenberg, "Wave propagation in alternating solid and fluid layers," *Wave Motion* **6,** 303–320 (1984).

[236] D. G. Seeley, W. S. Browner, M. C. Nevitt, H. K. Genant, J. C. Scott, and S. R. Cummings, "Which fractures are associated with low appendicular bone mass in elderly women? The Study of Osteoporotic Fractures Research Group," *Ann Intern Med* **115,** 837–42 (1991).

[237] D. A. Senzig, F. K. Forster, and J. E. Olerud, "Ultrasonic attenuation in articular cartilage," *J Acoust Soc Am* **92,** 676–81 (1992).

[238] L. Serpe and J. Y. Rho, "The nonlinear transition period of broadband ultrasound attenuation as bone density varies," *J Biomech* **29,** 963–6 (1996).

[239] D. E. Shepherd and B. B. Seedhom, "The 'instantaneous' compressive modulus of human articular cartilage in joints of the lower limb," *Rheumatology (Oxford)* **38,** 124–32 (1999).

[240] D. E. Shepherd and B. B. Seedhom, "Thickness of human articular cartilage in joints of the lower limb," *Ann Rheum Dis* **58,** 27–34 (1999).

[241] P. J. Shull and B. R. Tittmann, "Ultrasound," in *Nondestructive Evaluation: Theory, Techniques, and Applications*, P. J. Shull, ed. (Marcel Dekker Inc., New York, USA, 2002).

[242] T. S. Silvast, J. S. Jurvelin, M. J. Lammi, and J. Töyräs, "pQCT study on diffusion and equilibrium distribution of iodinated anionic contrast agent in human articular cartilage–associations to matrix composition and integrity," *Osteoarthritis Cartilage* **17,** 26–32 (2009).

[243] M. Sode, A. J. Burghardt, R. A. Nissenson, and S. Majumdar, "Resolution dependence of the non-metric trabecular structure indices," *Bone* **42,** 728–36 (2008).

[244] G. J. Stanisz and R. M. Henkelman, "Gd-DTPA relaxivity depends on macromolecular content," *Magn Reson Med* **44,** 665–7 (2000).

[245] A. Stevens and J. Lowe, *Human histology*, 2nd ed. (Mosby, London, 1997).

[246] A. Stewart, V. Kumar, and D. M. Reid, "Long-term fracture prediction by DXA and QUS: a 10-year prospective study," *J Bone Miner Res* **21,** 413–8 (2006).

[247] K. L. Stone, D. G. Seeley, L. Y. Lui, J. A. Cauley, K. Ensrud, W. S. Browner, et al., "BMD at multiple sites and risk of fracture of multiple types: long-term results from the Study of Osteoporotic Fractures," *J Bone Miner Res* **18,** 1947–54 (2003).

[248] R. Strelitzki, P. H. Nicholson, and V. Paech, "A model for ultrasonic scattering in cancellous bone based on velocity fluctuations in a binary mixture," *Physiol Meas* **19,** 189–96 (1998).

[249] M. Talmant, S. Kolta, C. Roux, D. Haguenauer, I. Vedel, B. Cassou, et al., "*In vivo* performance evaluation of bi-directional ultrasonic axial transmission for cortical bone assessment," *Ultrasound Med Biol* **35,** 912–9 (2009).

[250] U. Tarantino, G. Cannata, D. Lecce, M. Celi, I. Cerocchi, and R. Iundusi, "Incidence of fragility fractures," *Aging Clin Exp Res* **19,** 7–11 (2007).

[251] C. Tiderius, M. Hori, A. Williams, L. Sharma, P. V. Prasad, M. Finnell, et al., "dGEMRIC as a function of BMI," *Osteoarthritis Cartilage* **14,** 1091–7 (2006).

[252] C. J. Tiderius, R. Jessel, Y. J. Kim, and D. Burstein, "Hip dGEMRIC in asymptomatic volunteers and patients with early osteoarthritis: the influence of timing after contrast injection," *Magn Reson Med* **57,** 803–5 (2007).

[253] C. J. Tiderius, L. E. Olsson, H. de Verdier, P. Leander, O. Ekberg, and L. Dahlberg, "Gd-DTPA^{2-}-enhanced MRI of femoral knee cartilage: a dose-response study in healthy volunteers," *Magn Reson Med* **46,** 1067–71 (2001).

[254] C. J. Tiderius, L. E. Olsson, P. Leander, O. Ekberg, and L. Dahlberg, "Delayed gadolinium-enhanced MRI of cartilage (dGEMRIC) in early knee osteoarthritis," *Magn Reson Med* **49,** 488–92 (2003).

[255] P. A. Torzilli, J. M. Arduino, J. D. Gregory, and M. Bansal, "Effect of proteoglycan removal on solute mobility in articular cartilage," *J Biomech* **30,** 895–902 (1997).

[256] S. Trattnig, S. Marlovits, S. Gebetsroither, P. Szomolanyi, G. H. Welsch, E. Salomonowitz, et al., "Three-dimensional delayed gadolinium-enhanced MRI of cartilage (dGEMRIC) for *in vivo* evaluation of reparative cartilage after matrix-associated autologous chondrocyte transplantation at 3.0T: Preliminary results," *J Magn Reson Imaging* **26,** 974–82 (2007).

[257] J. Töyräs, M. S. Laasanen, S. Saarakkala, M. J. Lammi, J. Rieppo, J. Kurkijärvi, et al., "Speed of sound in normal and degenerated bovine articular cartilage," *Ultrasound Med Biol* **29,** 447–54 (2003).

[258] J. Töyräs, T. Lyyra-Laitinen, M. Niinimäki, R. Lindgren, M. T. Nieminen, I. Kiviranta, et al., "Estimation of the Young's modulus of articular cartilage using an arthroscopic indentation instrument and ultrasonic measurement of tissue thickness," *J Biomech* **34,** 251–6 (2001).

[259] J. Töyräs, M. T. Nieminen, H. Kröger, and J. S. Jurvelin, "Bone mineral density, ultrasound velocity, and broadband attenuation predict mechanical properties of trabecular bone differently," *Bone* **31,** 503–7 (2002).

[260] J. Töyräs, J. Rieppo, M. T. Nieminen, H. J. Helminen, and J. S. Jurvelin, "Characterization of enzymatically induced degradation of articular cartilage using high frequency ultrasound," *Phys Med Biol* **44,** 2723–33 (1999).

[261] J. Töyräs, M. Turunen, M. Lammi, J. S. Jurvelin, and R. K. Korhonen, "Hyperosmolaric Contrast Agents in Cartilage Tomography May Expose Cartilage to Overload-Induced Cell Death," *Trans Orthop Res Soc* **34,** 1155 (2009).

[262] M. Venn and A. Maroudas, "Chemical composition and swelling of normal and osteoarthrotic femoral head cartilage. I. Chemical composition," *Ann Rheum Dis* **36,** 121–9 (1977).

[263] L. M. Verbrugge and D. L. Patrick, "Seven chronic conditions: their impact on US adults' activity levels and use of medical services," *Am J Public Health* **85,** 173–82 (1995).

[264] N. Verzijl, J. DeGroot, S. R. Thorpe, R. A. Bank, J. N. Shaw, T. J. Lyons, et al., "Effect of collagen turnover on the accumulation of advanced glycation end products," *J Biol Chem* **275,** 39027–31 (2000).

[265] T. Virén, S. Saarakkala, J. S. Jurvelin, H. J. Pulkkinen, V. Tiitu, P. Valonen, et al., "Quantitative evaluation of spontaneously and surgically repaired rabbit articular cartilage using intra-articular ultrasound method *in situ*," *Ultrasound Med Biol* **36,** 833–9 (2010).

[266] T. Virén, S. Saarakkala, E. Kaleva, H. J. Nieminen, J. S. Jurvelin, and J. Töyräs, "Minimally invasive ultrasound method for intra-articular diagnostics of cartilage degeneration," *Ultrasound Med Biol* **35,** 1546–54 (2009).

[267] H. K. Väänänen, "Pathogenesis of osteoporosis," *Calcif Tissue Int* **49 Suppl,** S11–4 (1991).

[268] J. H. Waarsing, J. S. Day, and H. Weinans, "An improved segmentation method for *in vivo* microCT imaging," *J Bone Miner Res* **19,** 1640–50 (2004).

[269] S. Wallach, J. D. Feinblatt, J. Carstens, J. H., and L. V. Avioli, "The bone "quality" problem," *Calcif Tissue Int* **51,** 169–72 (1992).

[270] C. C. Wang, N. O. Chahine, C. T. Hung, and G. A. Ateshian, "Optical determination of anisotropic material properties of bovine articular cartilage in compression," *J Biomech* **36,** 339–53 (2003).

[271] S. Z. Wang, Y. P. Huang, S. Saarakkala, and Y. P. Zheng, "Quantitative assessment of articular cartilage with morphologic, acoustic and mechanical properties obtained using high-frequency ultrasound," *Ultrasound Med Biol* **36,** 512–27 (2010).

[272] X. Wang, R. A. Bank, J. M. TeKoppele, and C. M. Agrawal, "The role of collagen in determining bone mechanical properties," *J Orthop Res* **19,** 1021–6 (2001).

[273] R. D. Wasnich, "Epidemiology of osteoporosis," in *Osteoporosis. Fundamentals of clinical practice*, M. J. Favus, ed. (Lippincott-Raven Publishers, Philadelphia, 1997).

[274] A. Watanabe, T. Obata, H. Ikehira, T. Ueda, H. Moriya, and Y. Wada, "Degeneration of patellar cartilage in patients with recurrent patellar dislocation following conservative treatment: evaluation with delayed gadolinium-enhanced magnetic resonance imaging of cartilage," *Osteoarthritis Cartilage* **17,** 1546–53 (2009).

[275] A. Watanabe, Y. Wada, T. Obata, T. Ueda, M. Tamura, H. Ikehira, et al., "Delayed gadolinium-enhanced MR to determine glycosaminoglycan concentration in reparative cartilage after autologous chondrocyte implantation: preliminary results," *Radiology* **239,** 201–8 (2006).

[276] K. A. Wear, "Frequency dependence of ultrasonic backscatter from human trabecular bone: theory and experiment," *J Acoust Soc Am* **106,** 3659–64 (1999).

[277] K. A. Wear and B. S. Garra, "Assessment of bone density using ultrasonic backscatter," *Ultrasound Med Biol* **24,** 689–95 (1998).

[278] S. Webb, *From the watching of shadows: the origins of radiological tomography* (Adam Hilger, Bristol, 1990).

[279] P. N. T. Wells, *Physical principles of ultrasonic diagnostics* (Academic Press, London, 1969).

[280] P. N. T. Wells, *Biomedical Ultrasonics* (Academic Press, London, 1977).

[281] E. Wiener, K. Woertler, G. Weirich, E. J. Rummeny, and M. Settles, "Contrast enhanced cartilage imaging: Comparison of ionic and non-ionic contrast agents," *Eur J Radiol* **63,** 110–9 (2007).

[282] J. E. Wilhjelm, P. C. Pedersen, and S. M. Jacobsen, "The influence of roughness, angle, range, and transducer type on the echo signal from planar interfaces," *IEEE Trans Ultrason Ferroelectr Freq Control* **48,** 511–21 (2001).

[283] A. Williams, A. Gillis, C. McKenzie, B. Po, L. Sharma, L. Micheli, et al., "Glycosaminoglycan distribution in cartilage as determined by delayed gadolinium-enhanced MRI of cartilage (dGEMRIC): potential clinical applications," *AJR Am J Roentgenol* **182,** 167–72 (2004).

[284] A. Williams, L. Sharma, C. A. McKenzie, P. V. Prasad, and D. Burstein, "Delayed gadolinium-enhanced magnetic resonance imaging of cartilage in knee osteoarthritis: findings at different radiographic stages of disease and relationship to malalignment," *Arthritis Rheum* **52,** 3528–35 (2005).

[285] J. Wolff, *The law of bone remodelling* (Springer, New York, 1986).

[286] J. J. Wu, P. E. Woods, and D. R. Eyre, "Identification of cross-linking sites in bovine cartilage type IX collagen reveals an antiparallel type II-type IX molecular relationship and type IX to type IX bonding," *J Biol Chem* **267,** 23007–14 (1992).

[287] Y. Xia, W. Lin, and Y. X. Qin, "The influence of cortical end-plate on broadband ultrasound attenuation measurements at the human calcaneus using scanning confocal ultrasound," *J Acoust Soc Am* **118,** 1801–7 (2005).

[288] L. Xie, A. S. Lin, R. E. Guldberg, and M. E. Levenston, "Nondestructive assessment of sGAG content and distribution in normal and degraded rat articular cartilage via EPIC-microCT," *Osteoarthritis Cartilage* **18,** 65–72 (2010).

[289] L. Xie, A. S. Lin, M. E. Levenston, and R. E. Guldberg, "Quantitative assessment of articular cartilage morphology via EPIC-microCT," *Osteoarthritis Cartilage* **17,** 313–20 (2009).

[290] L. Zhang and A. Z. Szeri, "Transport of neutral solute in articular cartilage: effect of microstructure anisotropy," *J Biomech* **41,** 430–7 (2008).

[291] Y. Zhang, J. Niu, M. Kelly-Hayes, C. E. Chaisson, P. Aliabadi, and D. T. Felson, "Prevalence of symptomatic hand osteoarthritis and its impact on functional status among the elderly: The Framingham Study," *Am J Epidemiol* **156,** 1021–7 (2002).

[292] Z. M. Zhang, Z. C. Li, L. S. Jiang, S. D. Jiang, and L. Y. Dai, "Micro-CT and mechanical evaluation of subchondral trabecular bone structure between postmenopausal women with osteoarthritis and osteoporosis," *Osteoporos Int* **21,** 1383–1390 (2009).